

Phenol Gasification in Supercritical Water: Chemistry, Byproducts, and Toxic Impacts

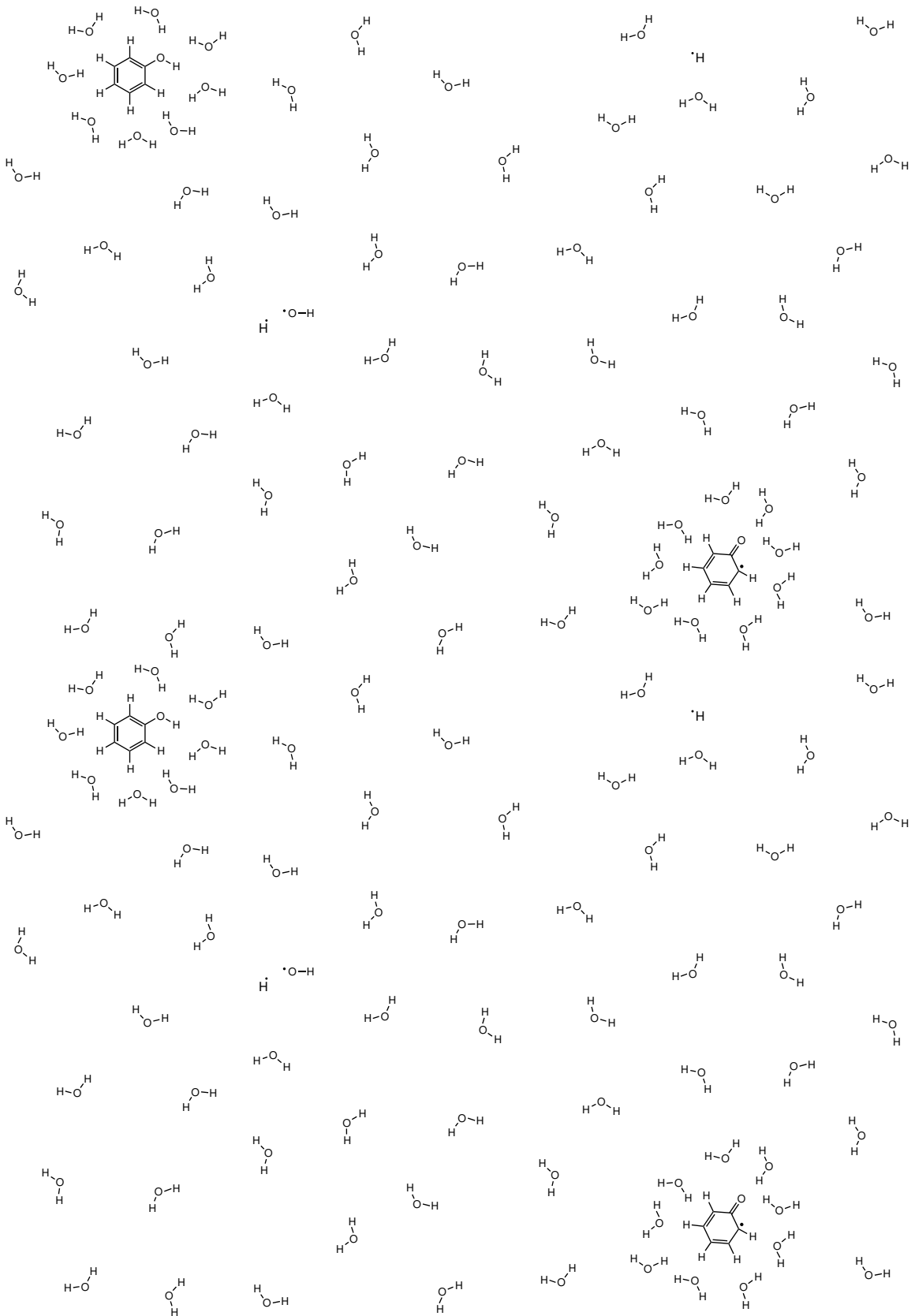
by

Chad Michael Huelsman

A dissertation submitted in partial fulfillment
of the requirements for the degree of
Doctor of Philosophy
(Chemical Engineering)
in the University of Michigan
2014

Doctoral Committee:

Professor Phillip E. Savage, Chair
Professor Zhan Chen
Professor H. Scott Fogler
Assistant Professor Charles W. Monroe



© Chad Michael Huelsman

All rights reserved.
2014

A. M. D. G.

A C K N O W L E D G M E N T S

My years at the University of Michigan have given me some of the most rewarding and memorable experiences in my life, and there are many people to thank.

First, I would like to thank all my early teachers who helped cultivate my affinity for science and problem-solving. I am grateful to the University of Dayton for its commitment to well rounded undergraduate education. Particular undergraduate mentors include Tony Saliba, John Graham, Ed Gatzke, and Mike Elsass.

At the University of Michigan, I had the opportunity to mentor quite a few undergraduate students myself: Zuleika Oquendo, Jongyoon Bae, Zachary Markin, Tyler Cialek, Sukhjit Sidhu, and Erin Branton. I am not only grateful for all the tangible ways in which these students contributed to this work, but also for the lessons they taught me about how to be a good mentor.

I consider myself lucky to have shared a lab with many wonderful current and former members of the Savage research group. In particular, I thank Fernando Resende for helping me find my way as a first-year student and Natalie Rebacz for her humor and vigilance in maintaining a high standard of lab practice. It was also a pleasure working alongside Tanawan Pinnarat, Changi Shujauddin, Bobby Levine, Dongil Kang, Jake Dickinson, Peter Valdez, Allison Franck, Thomas Yeh, Julia Faeth, and Tiffany Mo.

I thank glassblower Harald Eberhart for offering his expertise and assistance.

Perhaps my most lasting accomplishment will have been the friendships I forged while in Ann Arbor. There are too many to list here, but in particular I will thank Min Kim, Elizabeth Stewart, Aaron Shinkle, and Matt Morabito for their friendship and encouragement.

I owe everything to my parents, Mike and Becky Huelsman, who have been a constant source of love and support in my life. You have given me the invaluable gift of knowing what is truly important in this world.

I thank my doctoral committee members for their guidance over the years. I especially thank my advisor, Phil Savage. I could not have asked for a better mentor. I always left his office with a clearer picture of my work than when I entered.

I gratefully acknowledge my funding sources. This work has been supported by the National Science Foundation (NSF) under Grant No. 0755617, by STAR Fellowship Assistance Agreement No. FP917340 awarded by the U.S. Environmental Protection Agency (EPA), and by the University of Michigan Rackham Graduate School. It has not been formally reviewed by either the NSF or the EPA.

TABLE OF CONTENTS

Dedication	ii
Acknowledgments	iii
List of Figures	vi
List of Tables	ix
List of Code	x
List of Appendices	xi
Abstract	xii
Chapter	
1 Introduction	1
1.1 Background and motivation	1
1.2 Properties of supercritical water	2
1.3 Biomass, model compounds, and phenol	4
2 Literature Review	5
2.1 Hydrothermal gasification of biomass	5
2.1.1 Gas phase reactions and kinetics	7
2.1.2 Regimes in hydrothermal gasification	10
2.1.3 Hydrothermal gasification chemistry	14
2.1.4 Economic and technological outlook	21
2.2 Supercritical water gasification of phenol	23
2.2.1 Insights from pyrolysis literature	23
2.2.2 Insights from SCWO literature	28
2.2.3 Survey of published work	31
2.2.4 Limitations of previous work	34
3 Experimental Methods	36
3.1 Materials	36
3.2 Reaction procedure	36
3.3 Sample recovery and analytical procedure	39

4 Effect of Reaction Conditions on Products	42
4.1 Intermediate products and byproducts	42
4.2 Effect of temperature	47
4.3 Effect of water density	51
4.4 Effect of initial concentration	55
5 Kinetics of Phenol Conversion	59
5.1 Modeling of water density effects	59
5.2 Modeling of initial concentration effects	65
5.3 Data-fitting procedure and results	68
5.4 Discussion	71
6 Reaction Pathways	73
6.1 Primary products	73
6.2 Dibenzofuran SCWG	75
6.3 Benzene SCWG	82
6.4 Reaction network for gas and primary products	83
7 Kinetic Model for Phenol SCWG Pathways	86
7.1 Reaction engineering	86
7.2 Equilibria calculations with ASPEN	89
7.3 Data-fitting with MATLAB	90
7.4 Results and discussion	92
7.5 Rate analysis	96
8 Toxic Byproducts Characterization	103
8.1 Importance of toxicity characterization	104
8.2 Additional experiments and results	107
8.3 USEtox model	109
8.3.1 Environmental fate	111
8.3.2 Exposure pathways	115
8.3.3 Toxicological effects	116
8.3.4 Characterization factors	119
8.4 Results and discussion	121
9 Conclusions and Future Work	126
9.1 Conclusions	126
9.2 Future Work	130
Appendices	132
Bibliography	143

LIST OF FIGURES

1.1	Effect of temperature on physical properties of water at a pressure of 25 MPa	3
2.1	Calculated equilibrium gas yields for hydrothermal gasification of wood sawdust as a function of temperature	10
2.2	Reaction pathways for cellulose decomposition in supercritical water . .	16
2.3	Reaction pathways for lignin decomposition in supercritical water . . .	17
2.4	Kinetic model for phenol pyrolysis	24
2.5	Molar yields reported by DiLeo for homogeneous phenol SCWG (600 °C, 0.079 g/cm ³ water density, 5 wt. % phenol loading)	33
4.1	Quartz reactor with char on the inner wall	44
4.2	Total ion chromatogram for liquid sample obtained from phenol SCWG (60 min, 600 °C, 0.12 g/cm ³ water density, 0.1 mol/L phenol concentration)	45
4.3	Effect of temperature on gas yields from phenol SCWG (30 min, 0.079 g/cm ³ water density, 0.095 mol/L phenol concentration)	48
4.4	Effect of temperature on yields of representative liquid phase intermediates from phenol SCWG (30 min, 0.079 g/cm ³ water density, 0.095 mol/L phenol concentration)	49
4.5	Effect of water density on gas yields from phenol SCWG (60 min, 600 °C, 0.100 mol/L phenol concentration)	52
4.6	Effect of water density on yields of major liquid phase intermediates from phenol SCWG (60 min, 600 °C, 0.100 mol/L phenol concentration)	53
4.7	Effect of water density on yields of minor liquid phase intermediates from phenol SCWG (60 min, 600 °C, 0.100 mol/L phenol concentration)	54
4.8	Effect of water density on conversion from phenol SCWG (60 min, 600 °C, 0.100 mol/L phenol concentration)	54
4.9	Effect of phenol concentration on gas yields from phenol SCWG (60 min, 600 °C, 0.120 g/cm ³ water density)	57
4.10	Effect of phenol concentration on yields of major liquid phase intermediates from phenol SCWG (60 min, 600 °C, 0.120 g/cm ³ water density)	57
4.11	Effect of phenol concentration on yields of minor liquid phase intermediates from phenol SCWG (60 min, 600 °C, 0.120 g/cm ³ water density)	58
4.12	Effect of phenol concentration on conversion from phenol SCWG (60 min, 600 °C, 0.120 g/cm ³ water density)	58

5.1	Proposed schematic of <i>in situ</i> structures for phenol in SCW	67
5.2	Comparison of experimental and predicted concentration values for phenol SCWG	70
6.1	Delplots for dibenzofuran and benzene from phenol SCWG at 500, 600, and 700 °C	76
6.2	Effect of temperature on yields of the reactant, benzene, and carbon from dibenzofuran SCWG and phenol SCWG (30 min, 0.18 g/cm ³ water density, 1.2 mol/L atomic carbon concentration)	78
6.3	Effect of temperature on moles of H ₂ , CH ₄ , and CO ₂ formed per mole of initial carbon from dibenzofuran SCWG and phenol SCWG (30 min, 0.18 g/cm ³ water density, 1.2 mol/L atomic carbon concentration)	80
6.4	Effect of temperature on yields of phenol, biphenyl, and 2-phenylphenol from dibenzofuran SCWG (30 min, 0.18 g/cm ³ water density, 0.10 mol/L dibenzofuran concentration)	81
6.5	Effect of temperature on yields of fluorene, anthracene/phenanthrene, pyrene, triphenylene, and naphthalene from dibenzofuran SCWG (30 min, 0.18 g/cm ³ water density, 0.10 mol/L dibenzofuran concentration)	82
6.6	Phenol SCWG reaction network	85
7.1	Comparison of experimental data and kinetic model at 500, 600, and 700 °C for H ₂ , phenol, dibenzofuran, and benzene (0.18 g/cm ³ water density, 0.10 mol/L phenol concentration)	94
7.2	Comparison of experimental and calculated concentration values for benzene, phenol, dibenzofuran, H ₂ , CO, CH ₄ , and CO ₂ from phenol SCWG (0.18 g/cm ³ water density)	95
7.3	Delplots for dibenzofuran and benzene obtained from the kinetic model for phenol SCWG at temperatures of 500, 600, and 700 °C, a water density of 0.18 g/cm ³ , and the same phenol concentrations as in Figure 6.1	97
7.4	Rates of H ₂ formation and consumption due to water-gas shift, reverse water-gas shift, gasification, and steam reforming at 500, 600, and 700 °C (0.18 g/cm ³ water density, 0.10 mol/L phenol concentration)	100
7.5	Rates of phenol formation and consumption due to phenol+phenol combination, dibenzofuran decomposition, dehydroxylation, and phenol+benzene combination at 500, 600, and 700 °C (0.18 g/cm ³ water density, 0.10 mol/L phenol concentration)	101
7.6	Rates of dibenzofuran formation and consumption due to phenol+phenol combination, decomposition, and gasification at 600 °C (0.18 g/cm ³ water density, 0.10 mol/L phenol concentration)	102
7.7	Rates of benzene formation and consumption due to phenol dehydroxylation, benzene+benzene combination, phenol+benzene combination, and dibenzofuran decomposition at 600 °C (0.18 g/cm ³ water density, 0.10 mol/L phenol concentration)	102

8.1	Effect of temperature and time on mass yields of benz[a]anthracene and benzo[a]pyrene from phenol SCWG (0.18 g/cm ³ water density, 0.10 mol/L phenol concentration)	110
8.2	Effect of temperature on ecotoxic impact due to emission of byproducts into freshwater (60 min, 0.18 g/cm ³ water density, 0.10 mol/L phenol concentration)	123
8.3	Effect of temperature on non-carcinogenic impact due to emission of byproducts into freshwater (60 min, 0.18 g/cm ³ water density, 0.10 mol/L phenol concentration)	123
8.4	Effect of temperature on carcinogenic impact due to emission of byproducts into freshwater (60 min, 0.18 g/cm ³ water density, 0.10 mol/L phenol concentration)	124

LIST OF TABLES

4.1	Experimental conditions, phenol conversions, and gas mole fractions . .	43
4.2	Identified liquid phase intermediate compounds from phenol SCWG (60 min, 600 °C, 0.12 g/cm ³ water density, 0.1 mol/L phenol concentration)	46
4.3	Fraction of initial carbon in quantified products from phenol SCWG (30 min, 0.079 g/cm ³ water density, 0.095 mol/L phenol concentration) . . .	49
5.1	Kinetic parameters for phenol disappearance	70
6.1	Conversion and major product yields from benzene SCWG (30 min, 600 °C, 0.18 g/cm ³ water density, 0.10 mol/L benzene concentration) . .	83
7.1	Kinetic parameters for the phenol SCWG network	92
8.1	Polycyclic aromatic hydrocarbons regulated by the U.S. EPA as priority pollutants	106
8.2	Environmental fate generated by USEtox for select compounds emitted into freshwater	114
8.3	Human intake fraction generated by USEtox for select compounds emitted into freshwater	117
8.4	Toxicity characterization factors generated by USEtox for byproducts from phenol SCWG emitted into freshwater	121
A.1	Experimental conditions, conversions, and major product yields from dibenzofuran SCWG (30 min, 0.18 g/cm ³ water density, 0.10 mol/L dibenzofuran concentration)	132
A.2	Experimental conditions, conversions, and major product yields from toxicity experiments (0.18 g/cm ³ water density, 0.10 mol/L phenol concentration)	133
A.3	Carcinogenic, non-carcinogenic, and ecotoxic impacts of byproducts from phenol SCWG emitted into freshwater (0.18 g/cm ³ water density, 0.10 mol/L phenol concentration)	134

LIST OF CODE

B.1	ResidualSum.m	136
B.2	PointDiffSolver.m	140
B.3	myfun.m	141

LIST OF APPENDICES

A Additional Experimental Data	132
B MATLAB Code	135

ABSTRACT

Phenol Gasification in Supercritical Water: Chemistry, Byproducts, and Toxic Impacts

by

Chad Michael Huelsman

Chair: Phillip E. Savage

In order to better understand the chemistry underlying supercritical water gasification (SCWG) of biomass, phenol was processed with supercritical water in quartz reactors while systematically varying the temperature, water density, reactant concentration, and reaction time. Both the gas and liquid phases were analyzed post-reaction to identify and quantify the reaction intermediates and products, including H₂, CO, CH₄, and CO₂ in the gas phase and many different compounds—mainly polycyclic aromatic hydrocarbons (PAHs)—in the liquid phase. Higher temperatures promoted gasification and resulted in a product gas rich in H₂ and CH₄ (33% and 29%, respectively, at 700 °C), but char yields increased as well. Dibenzofuran and other identified phenolic dimers were implicated as precursor molecules for char formation pathways, which can be driven by free radical polymerization at high temperatures. Two different reaction pathways emerged from the kinetic modeling of phenol conversion: a water-inhibited

thermal pathway in which $\text{rate} \propto [\text{phenol}]^{1.73}[\text{water}]^{-16.60}$ and a water-accelerated hydrothermal pathway in which $\text{rate} \propto [\text{phenol}]^{0.92}[\text{water}]^{1.39}$. Benzene and dibenzofuran form directly from phenol and account for nearly all phenol consumption during SCWG at 500–700 °C. Experiments with dibenzofuran as the starting reactant generated the same array of products—typically in comparable quantities—as that observed with phenol as the reactant. When benzene was the reactant, biphenyl was the main product and some H₂ formed. Information about the reaction pathways obtained from these experiments served as the basis for constructing and optimizing a kinetic model that describes the reaction rates of phenol and its primary and gaseous products in supercritical water. Arrhenius parameters are reported, and the formation and consumption rates for each species as calculated by the model are analyzed. Since many of the identified PAHs are EPA priority pollutants and have known human health and environmental effects, the UNEP/SETAC toxicity model, “USEtox,” was employed to characterize the human toxic and ecotoxic impacts due to a hypothetical emission of this byproduct stream into freshwater. Total toxic impact increased with gasification temperature up to a maximum at 650 °C but then decreased at 700°C.

CHAPTER 1

Introduction

1.1 Background and motivation

Humans have been using plant biomass as a primary energy resource for millennia. The use of leaves, grasses, and wood as a fuel for heating predates civilization itself, with earliest archeological evidence of a cooked diet dating from 1.9 million years ago [1] and that of controlled use of fire dating from 1 million years ago [2]. Prior to the late 19th Century, wood fuel was the largest source of primary energy in the U.S., and wood continues to be the largest biomass energy resource today [3]. The U.S. Energy Information Administration's Annual Energy Outlook forecasts an annual growth rate of 0.9% for grid-connected biomass power generation and 2.9% for industry generated biomass power through 2040 [4]. As global demand for energy continues to increase despite growing public concern over depleting fossil fuels and greenhouse gas emissions, plant biomass remains the focus of extensive investigation as a clean and sustainable energy alternative because it is renewable, potentially carbon neutral, and widely available.

A common feature of all plant biomass is its significant moisture content, which

ranges from 10–60 wt. % for lignocellulosic biomass and even higher for aquatic biomass such as microalgae. This moisture poses an obstacle to the thermal efficiency of many biomass valorization processes, such as conventional gasification and fast pyrolysis, because energy inputs that could otherwise be applied directly toward the conversion of biomass are instead diverted to the heat-up and phase-change of water [5]. Interest in obviating a drying step and the capital, energy, and time investment it entails has led many investigators to study and develop hydrothermal processes for biomass valorization. Such processes include the possibility of heat integration and efficient energy recovery. Hydrothermal processing, or the application of heat and pressure to biomass in an aqueous medium, mimics the processes that converted ancient plant material into the crude oil and natural gas reservoirs we rely upon today.

1.2 Properties of supercritical water

Water has unique properties at elevated temperatures and pressures which hydrothermal processes exploit. Under supercritical conditions, wherein distinct liquid and vapor phases cease to exist, supercritical water (SCW) exhibits both liquid-like (*e.g.*, high thermal conductivity [6]) and gas-like (*e.g.*, high diffusivity [7]) characteristics. Above the critical point (374 °C and 22.1 MPa), the density, dielectric constant, and ion product of water decrease dramatically with increasing temperature at fixed pressure, as shown in Figure 1.1. Thus, even non-polar organic compounds become completely miscible in supercritical water, providing

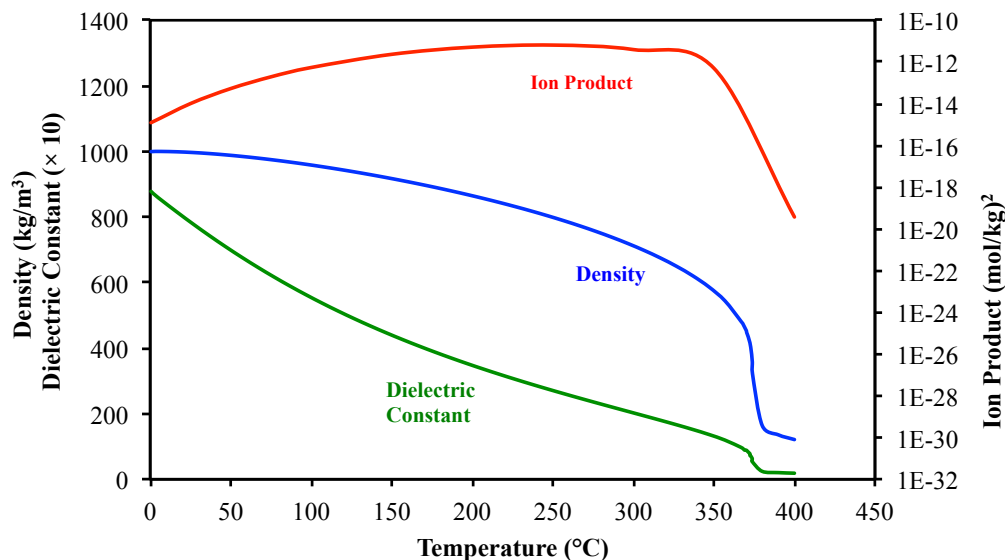


Figure 1.1: Effect of temperature on physical properties of water at a pressure of 25 MPa.

a homogeneous single-phase medium for organic reactions to occur [8]. Moreover, the properties of supercritical water are also dependent upon water density and therefore can be tuned by adjusting reactor temperature, size, and water loading [9]. Hydrothermal processing under these supercritical conditions is commonly termed supercritical water gasification (SCWG), because, as in conventional gasification, the chief product is a gas mixture comprising H_2 , CH_4 , CO_2 , and CO along with tar and char byproducts. Gasification reactions carried out in a homogeneous supercritical phase, however, proceed more rapidly and produce less tar and char because the water molecules serve as both solvent and reactant, even contributing substantially to H_2 production [10, 11, 12]. H_2 - and CH_4 -rich gas is a versatile form of stored energy that offers direct pathways to both electricity (*e.g.*, *via* fuel cells) and liquid fuels (*e.g.*, *via* steam reforming and Fischer-Tropsch synthesis).

1.3 Biomass, model compounds, and phenol

Plant biomass comprises cellulose, hemicellulose, and lignin as major polymeric constituents [13], with lignin, in particular, being made up of phenolic structures. It is natural, therefore, to select phenol as a model compound for the lignin in biomass. In SCWG, phenol originates not only from lignin, however, but also from gasification of cellulose and glucose [14, 15, 16, 17, 18], microalgae [19, 20, 21], whole biomass [18, 22, 23, 24, 25], other lignin model compounds [26, 27, 28], and even C₄ compounds [29]. The lattermost result indicates that phenol forms during SCWG even when no aromatic structure is initially present. Furthermore, phenol is a well-documented organic pollutant in industrial wastewater effluents, for which SCWG has been advanced as a wastewater treatment technology [30]. Phenols have been described as one of the last hurdles to complete gasification of biomass, because they are such ubiquitous and long-lived intermediates in SCWG [29, 31]. Their having been implicated as possible intermediates for undesirable char formation pathways [32] and their relative inertness in supercritical water compared to other biomass derivatives make them a prime candidate for further study. Thus, understanding the underlying chemistry of phenol SCWG is crucial for maximizing gas yield and minimizing byproduct formation in this complex hydrothermal process. A detailed study of the byproducts is also important for environmental reasons. As biomass valorization processes are developed, it is essential that any potential byproducts with adverse environmental consequences be identified and their formation and disappearance pathways be elucidated.

CHAPTER 2

Literature Review

This chapter features a review of relevant literature. The first section provides a contextual overview of hydrothermal gasification of biomass and includes some literature highlights at the time this work was first undertaken. The second section focuses more closely on phenol chemistry and goes into greater detail. After surveying hydrothermal biomass gasification literature, phenol pyrolysis and oxidation literature, and previous phenol SCWG literature, the chapter concludes with a summary of current gaps in scientific understanding.

2.1 Hydrothermal gasification of biomass

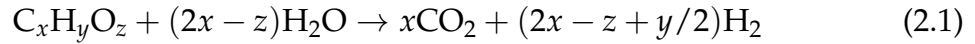
Wet biomass can be gasified at low temperatures ($\sim 300\text{--}400\text{ }^{\circ}\text{C}$) to make primarily CH_4 or at higher temperatures ($\sim 600\text{--}700\text{ }^{\circ}\text{C}$) to make primarily H_2 . As previously mentioned, hydrothermal gasification has distinct advantages over conventional gasification of wet biomass and more quickly converts wet organic materials to fuel gases than biomethanation processes (*i.e.*, anaerobic digestion) [33]. Moreover, hydrothermal gasification is a highly efficient and economically attractive

biomass and waste valorization technology [34]. Recently, a life cycle assessment of low-temperature hydrothermal gasification of waste biomass (20% solids manure or wood) to synthetic natural gas (SNG) demonstrated that 60–70% of the feedstock energy content was converted to SNG [35]. The fertilizer co-product reduced greenhouse gas (GHG) emissions by 0.6 kg_{eq.} CO₂/MJ SNG, accounting for 97% of the beneficial impact. Not surprisingly, the major environmental impact for hydrothermal gasification is the CO₂ that is separated from CH₄ during treatment of the product gas. A large number of excellent review articles pertaining to hydrothermal gasification have appeared recently [5, 31, 36, 37, 38, 39, 40, 41, 42, 43, 44].

Hydrothermal gasification was first described by Modell in 1985, who processed sawdust in SCW [45]. Since then, a substantial amount of work has been done to develop this technology by studying the effects of different feedstocks, reaction conditions, and catalysts on product yield and composition. Despite such attention, SCWG remains a chemically complex process that is not fully understood. This is due, in part, to the structural complexity of biomass, which makes it difficult to reduce the process to a network of reaction pathways with well-defined steps. Furthermore, research in this area tends to take a pragmatic approach that focuses on maximizing gas yields rather than elucidating and characterizing the mechanisms that constitute the underlying chemistry. In this section, the chemistry of hydrothermal gasification, including known reaction pathways, catalysis, and the influence of different process variables on product yields and composition will be discussed.

2.1.1 Gas phase reactions and kinetics

The overall process that takes place during SCWG to produce H₂ can be summarized by the following endothermic reaction:

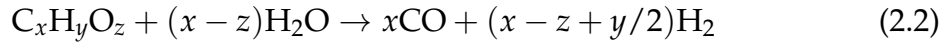


The elemental composition of the biomass (x , y , and z ; see equation 2.1) governs the composition of the gas mixture that forms at equilibrium. Typically, a feedstock with higher H content will result in increased gasification yields. Importantly, water is not only the reaction medium, but also a reactant and source of hydrogen. The presence of water in SCWG leads to hydrolysis reactions that help decompose the biomass feedstock into intermediate compounds [36].

Recently, [Resende and Savage](#) developed a kinetics model of cellulose and lignin conversion in uncatalyzed SCWG, which provided insight into the dominant intermediate reactions [46]. The model incorporates 11 reactions, including hydrolysis, steam-reforming, thermal decomposition, water-gas shift, and methanation. Due to the complexity of the feedstock, reaction intermediate species were not tracked individually; rather, they were considered together as a single pseudo-component. Nevertheless, the model predicted gas yields at biomass loadings and water densities different from those used in its construction, and simulations at long times produced equilibrium predictions that agreed with thermodynamic calculations.

In this model, biomass-derived intermediate compounds participate in steam

reforming to generate syngas, a mixture of CO and H₂ (equation 2.2).



This endothermic reaction is the workhorse for generating H₂, and is particularly dominant at short times, when little gasification has taken place [46]. CO participates in two important reversible, exothermic gas-phase reactions: water-gas shift (equation 2.3) and methanation (equation 2.4).



These gas interconversion reactions, particularly water-gas shift, are most dominant at long reaction times when a majority of product gases have already been released [46].

Pyrolytic reactions also contribute to hydrothermal gasification, particularly at high temperatures. Pyrolysis cleaves bonds in biomass intermediate compounds directly, leading to the formation of H₂, CH₄, CO, and CO₂ gases as well as tar and char. Solids production represents an effective loss of gas and is undesirable. One of the advantages of gasification in water is that char formation is suppressed [47], except at slow heating rates [12]. The Resende model showed that H₂ is primarily produced *via* steam-reforming (equation 2.2) at short times and water-gas shift (equation 2.3) at long times, whereas CO₂, CO, and CH₄ form predominantly from

intermediate species *via* hydrothermal pyrolysis reactions [46]. This type of modeling analysis can serve as a foundation for future studies with other feedstocks and at other reaction conditions. Other than previous work in quartz reactors from this lab [48, 49] and that of Buhler *et al.* in a metal reactor [50], there were no published articles that reported SCWG kinetics of biomass model compounds when the present work was undertaken.

In an effort to eliminate confounding catalytic effects due to metal reactor walls, quartz capillary reactors have been used to study SCWG of several biomass model compounds: phenol and guaiacol (lignin model compounds) [49], glycine [51], and methanol [48]. In these works, the effects of temperature, water density, reactant loading, and the presence of catalytic Ni wire on the yields and kinetics of liquid- and gas-phase reaction products were examined. Experiments with phenol led to rapid gasification at temperatures of 600 and 700 °C, and the presence of Ni increased the water-gas shift reaction rate, resulting in higher H₂ yields than reactions without catalyst. Glycine experiments resulted in char formation, and although the presence of Ni catalyst did not promote gasification to completion, it did increase H₂ and CO₂ formation *via* the water-gas shift reaction. Notably, gasification of methanol at 500 and 550 °C did not approach completion without the addition of Ni catalyst, and the major gas product was H₂.

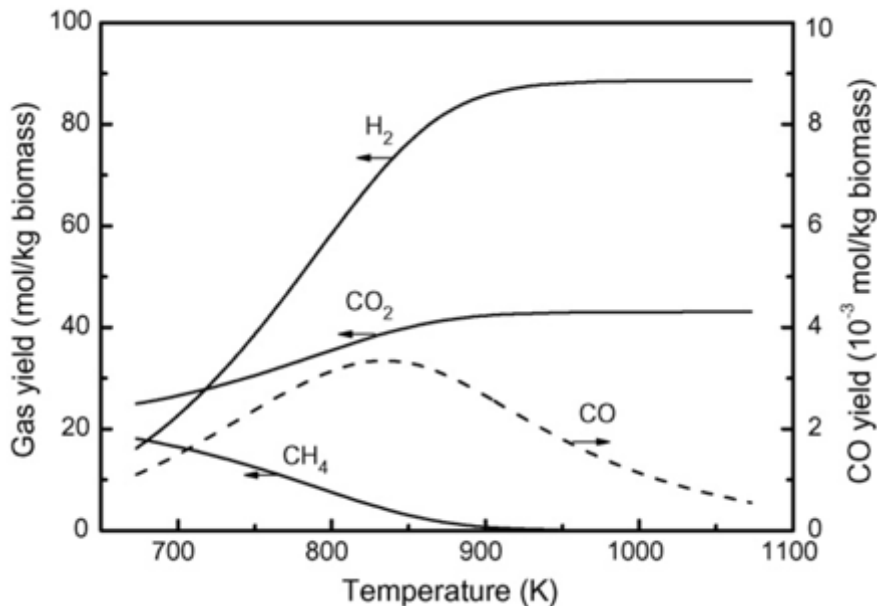


Figure 2.1: Calculated equilibrium gas yields for hydrothermal gasification of wood sawdust as a function of temperature. Dry biomass concentration is 5 wt. % and pressure is 250 bar [52].

2.1.2 Regimes in hydrothermal gasification

In general, lower temperatures (350–500 °C) favor CH₄ production while higher temperatures (400–600 °C) result in greater H₂ production (*c.f.* Figure 2.1) [52]. Except at high temperatures (>600 °C) or long reaction times, uncatalyzed hydrothermal gasification of biomass does not approach complete conversion, and measured gas yields tend to be far from their equilibrium values [46]. As a result, catalysis has been a major focus of research efforts to improve gas yields. Due to the different product yields and catalytic demands of each process, a distinction has emerged between low-temperature (near or supercritical water) catalytic gasification to obtain CH₄-rich gas and high-temperature SCWG to obtain H₂-rich gas.

2.1.2.1 Low-Temperature Catalytic Gasification

Low-temperature hydrothermal gasification generally ranges from approximately 350 to 500 °C and always involves catalysis [37]. Consequently, catalyst activity and stability is a major research focus. Early work demonstrated the effectiveness of Ni metal at promoting hydrothermal gasification of biomass at 350–450 °C and 20 MPa [53]. Consistent with the overall thermodynamics, CH₄ is predominant at these temperatures. These initial findings suggested that employing metal catalysts in a high-pressure aqueous environment could compensate for operation at lower temperatures.

Additional work showed that many commercial base and noble metal catalysts are inactive or present stability issues stemming from carbon deposition, oxidation, and sintering in a hot pressurized water environment [54]. Only Ni, Ru, and Rh were reported to have a significant effect on hydrothermal gasification at 350 °C and 20 MPa. Although Ru showed long-term stability, Ni suffered from rapid sintering but could be stabilized by another metal [55]. The stability of common support materials in hot water was also investigated; some reacted with water or lost their physical integrity (*e.g.*, γ -alumina), while carbon, monoclinic zirconia, and rutile titania were stable [55]. Results have been promising in subsequent studies with nickel and ruthenium catalyst formulations [37, 15, 56]. Alkali salts have also been studied as homogeneous catalysts for low temperature hydrothermal gasification [57, 15, 14, 58, 59, 60, 61, 62, 63]. These catalysts, which are naturally present in real biomass, lower the onset temperature for cellulose degradation,

depress char formation, and increase H₂ and CO₂ production by promoting the water-gas shift reaction [64, 65]. The activity of alkalis has been postulated to arise from their ability to suppress dehydration reactions that form furfural and 5-hydroxymethylfurfural (5-HMF), which are tar and char precursors, and from their ability to capture CO₂ as a metal carbonate in order to enhance the water-gas shift reaction and promote H₂ formation [63].

2.1.2.2 High Temperature SCWG

In high-temperature gasification (500–800 °C), free radical mechanisms dominate [50]. Pyrolysis reactions that directly release gases and the water-gas shift reaction (equation 2.3) are heavily promoted, leading to high yields of H₂-rich gaseous product. Lee et al. gasified glucose in SCW at 480–750 °C and 28 MPa [10]. The H₂ yield increased sharply with increasing temperature above 660 °C, while the CO yield peaked at this temperature and decreased at higher temperatures. This effect can be attributed to the very high rate of the water-gas shift reaction at these high temperatures (~700 °C). Although the water-gas shift reaction is exothermic and thermodynamically less favorable with increasing temperature, the overall H₂ yield at equilibrium remains high in this range due to high water concentrations (*c.f.* Figure 2.1).

Heterogeneous metal catalysts are often avoided at SCWG conditions due to degradation and deactivation [66], but activated carbon and alkali have been employed as catalysts to aid high temperature gasification. Carbon gasification efficiencies near 100% were achieved for glucose gasification in supercritical water at

600 °C and 34.5 MPa with activated carbon [67]. Similar experiments with more complex biomass feedstocks resulted in reduced reaction rates with higher temperatures (650–715 °C) required to achieve high conversions [66]. Deactivation of the carbon was observed after several hours in both cases. Significantly, activated carbon catalyst can be recovered and separated from the ash produced by SCWG of biomass [68]. Recovery of catalyst and removal of ash will be necessary in large-scale continuous processes. Homogeneous alkali catalysts have also been employed to improve high temperature gasification. In experiments at 600–700 °C and 20–40 MPa, KOH as a catalyst increased H₂ and CO₂ yields and decreased CO yield by accelerating the water-gas shift reaction [62]. Moreover, carbohydrates, aromatics, glycine, and real biomass were completely gasified to a H₂-rich product gas at 550–600 °C and 25 MPa with the addition of KOH and K₂CO₃ [47].

Lee and Ihm gasified glucose in SCW with Ni and activated carbon as heterogeneous catalysts [69]. SEM was used to characterize the catalysts, demonstrating that although they were effective, combined Ni/activated carbon catalysts suffered from coke deposition at low temperatures and Ni sintering, both of which inhibit catalytic activity by increasing pore size and reducing surface area. Catalysts with mesosize pores (2–50 nm) may be preferred for minimizing mass transport limitations when gasifying glucose in SCW.

Resende and Savage reported on the non-catalytic gasification of lignin and cellulose in SCW [70]. Batch reactions were carried out in quartz reactors to avoid catalytic wall effects. The influence of different process variables on gasification yield and composition was systematically studied. The apparent activation ener-

gies suggested that H₂ and CO₂ form *via* different pathways, but these pathways are similar for both lignin and cellulose feedstocks.

2.1.3 Hydrothermal gasification chemistry

The chemical compositions of different biomass feedstocks are complex and vary depending on the source. For this reason, model compounds that are structurally similar to the components of biomass are often selected for study to obtain insight about their chemical behavior when undergoing hydrothermal gasification. Cellulose and lignin are commonly selected as biomass model compounds. Derivatives of biomass are also commonly used; glucose, xylose, and other monosaccharides form when cellulose and hemicellulose undergo hydrolysis. Phenols and aromatics result when lignin breaks down under hydrothermal conditions. Much of the previous work with simple model compounds has been exploratory, with little attention paid to the identities and yields of intermediate products in the liquid phase and along reaction pathways.

2.1.3.1 Cellulose

The glycosidic bonds in cellulose and hemicellulose hydrolyze very quickly in high temperature water. Bio-macromolecule monomers can form a bio-oil (at low temperatures) or be gasified (at higher temperatures). Reaction schemes for different temperature regimes have been proposed. At temperatures near 300 °C, glucose and oligosaccharides react much faster than cellulose hydrolyzes, resulting in a low yield of these hydrolysis products [71]. Mostly char is formed, unless catalysts

are used to promote low-temperature gasification. Above the critical point, however, the cellulose hydrolysis rate jumps more than an order of magnitude and it becomes faster than the glucose decomposition rate, leading to an accumulation of hydrolysis products in the liquid phase. This phenomenon has been studied in a diamond anvil cell [71, 72, 73], which led to a mapping of the main reaction pathways [74] (*c.f.* Figure 2.2). Furthermore, gas formation is favored at higher temperatures as the main reaction mechanism shifts from ionic to free radical, as mentioned earlier.

2.1.3.2 Lignin

Lignin decomposes in a hydrothermal environment to form low molecular weight phenolic compounds such as syringols, guaiacols, and catechols (*c.f.* Figure 2.3). Elimination reactions simultaneously produce formaldehyde, which immediately instigates condensation reactions with these alkylphenols [76, 77]. As a result, the alkylphenols polymerize to form higher molecular weight compounds with formaldehyde acting as a cross-linking agent [75]. In short, without the addition of catalysts, hydrothermal gasification of lignin leads to substantial char formation and, therefore, low gas yields [74]. Ru and Rh with γ -alumina and carbon supports have been shown to be very effective catalysts for gasifying alkylphenols in water at 500 °C and 0.3 g/cm³, whereas Pt and Pd were not effective [78]. However, char formation was suppressed by the presence of many of these noble metal catalysts. In experiments with lignin at 500 °C and 0.35 g/cm³, zirconia and NaOH increased the H₂ yield by a factor of two and four, respectively, by inhibiting char

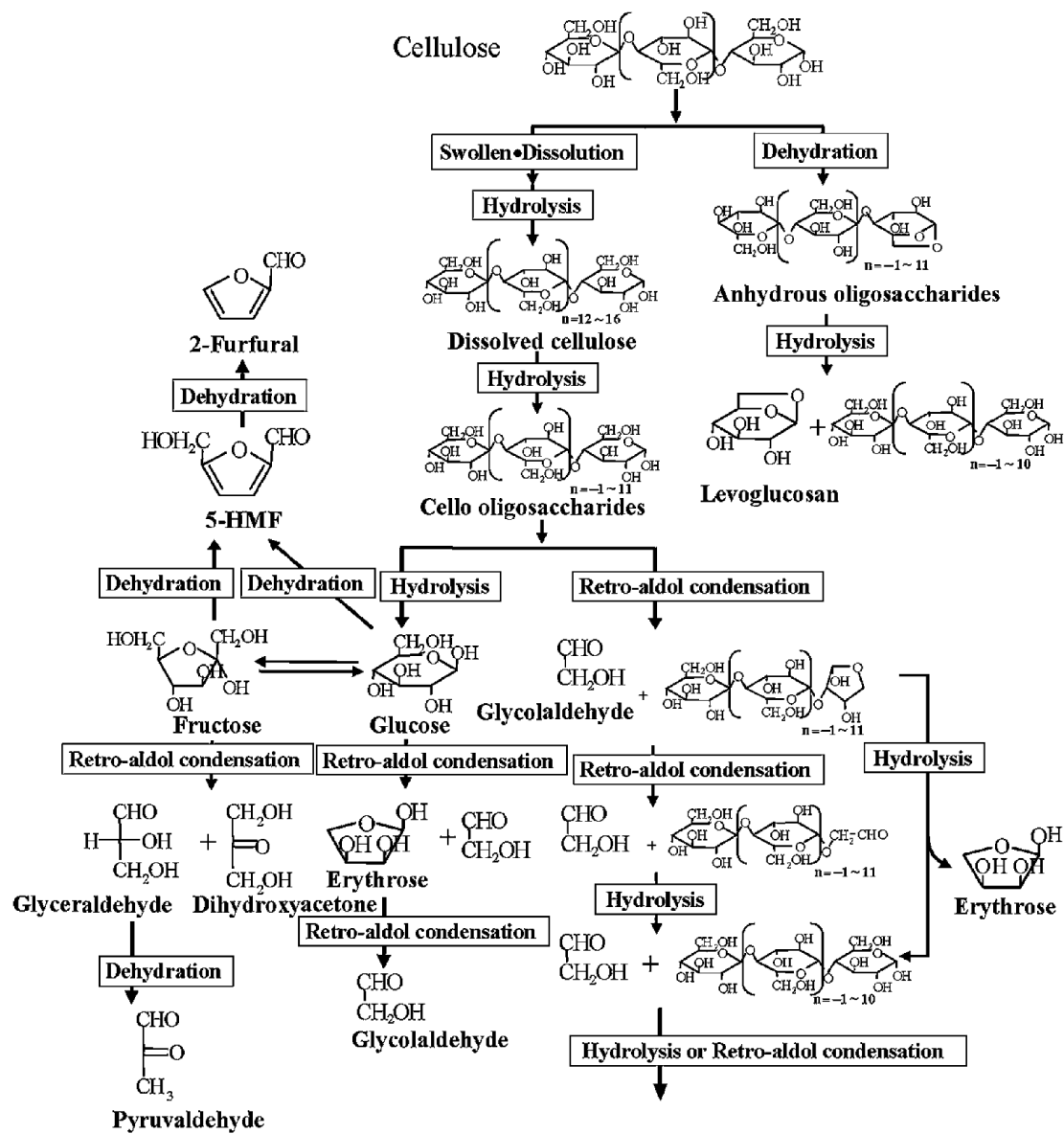


Figure 2.2: Reaction pathways for cellulose in supercritical water (around 500 °C) [75].

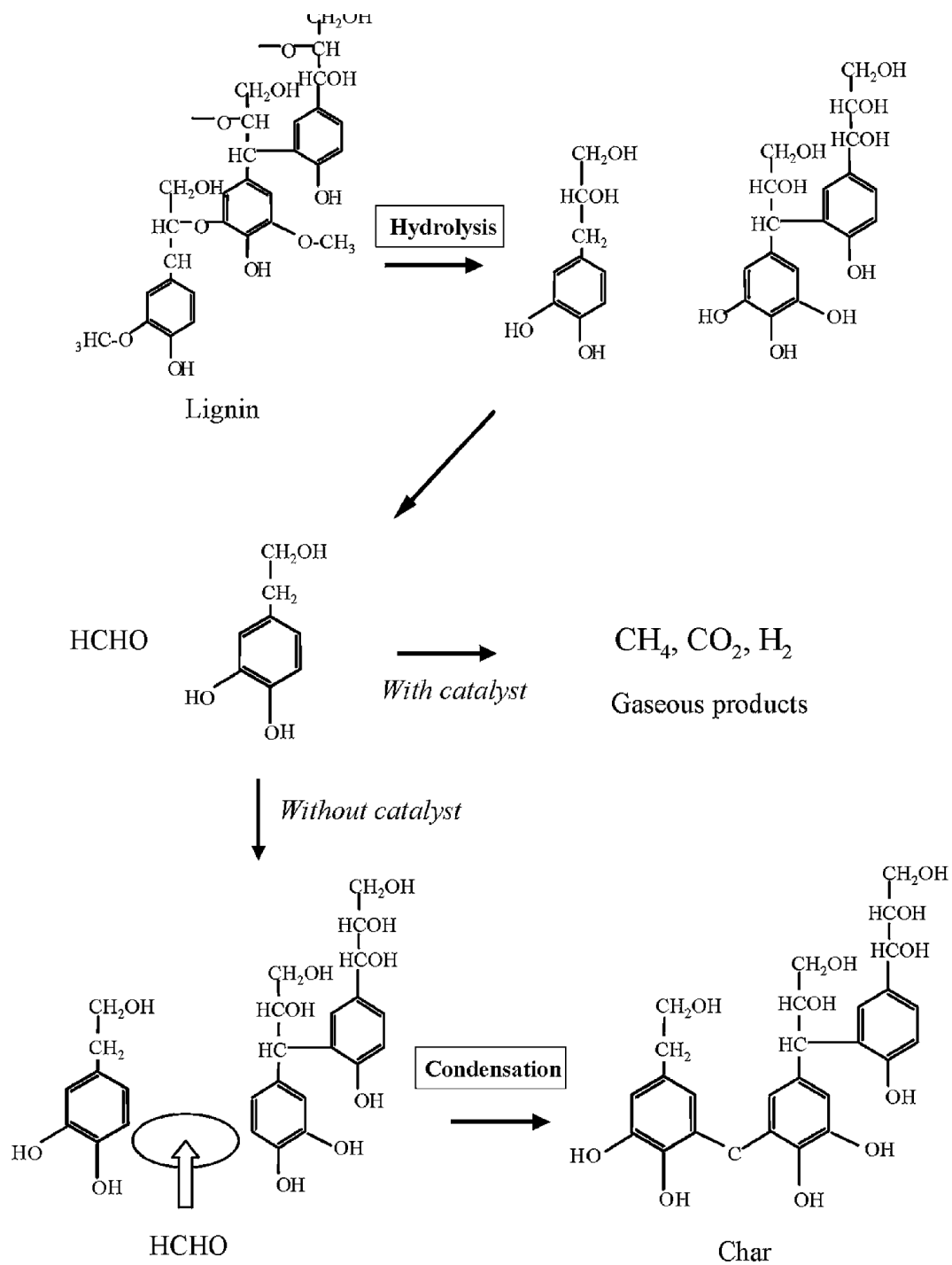


Figure 2.3: Reaction pathways for lignin in supercritical water (around 500 °C) [75].

formation [79]. Some char formation was observed with NaOH and Ni catalysts when gasifying lignin in water at 400 °C and 0.33 g/cm³ water density, but the H₂ yield was still greater than without a catalyst [80]. No char and a high CH₄ yield were obtained with Ru.

2.1.3.3 Protein

Studies of protein-containing biomass resulted in lower than expected gasification yields [81]. Experiments with glucose, alanine, and KHCO₃ as models for cellulose, protein, and natural salts, respectively, confirmed that the presence of the amino acid decreases gas yields significantly and increases the dissolved organic carbon content [61]. It was discovered that, under hydrothermal conditions, Maillard reactions take place between the amines produced by protein degradation and the sugars produced by carbohydrate degradation to form nitrogen-containing cyclic organic compounds. These N-heterocyclic compounds form stable free radical cations, which also behave as free radical scavengers. Too stable to start free radical chains on their own, these scavengers readily react with the less stable free radicals that are important for gas formation. Consequently, proteins inhibit the free radical chain reactions that lead to gasification, resulting in lower gas yields. The presence of alkali salts has been found to counteract this inhibitory effect [61].

2.1.3.4 Interactions Between Model Compounds

In an effort to understand the mechanisms of hydrothermal gasification, we must move beyond the reaction pathways of individual feedstock components and in-

investigate their interactions. [Yoshida and Matsumura](#) studied the hydrothermal gasification of mixtures of cellulose, xylan, and lignin to represent the three main components of terrestrial biomass and determined that they do not collectively behave as a sum of the degradation reactions for the individual components [82]. Cellulose and hemicellulose mixtures produced gas distributions and yields similar to a weighted average of the expectation for each individual component, indicating the behavior of these two components is additive and no significant interaction exists. However, introducing lignin into a mixture with either cellulose or hemicellulose greatly suppressed H₂ production [65]. It was concluded that the degradation intermediates from cellulose and xylan react with lignin, perhaps donating H atoms *via* hydrogenation, resulting in decreased H₂ formation. [Goodwin and Rorrer](#) observed similar results and arrived at the same conclusion by studying hydrothermal gasification of mixtures of phenol and xylose, which are model compounds for lignin and hemicellulose, respectively [83]. [Weiss-Hortala et al.](#) suggested phenol might behave as a free radical scavenger in order to explain lower gas yields when adding a small amount of phenol to the SCWG of glucose (a cellulose model compound) [84]. The chemistry behind this behavior is still unclear.

2.1.3.5 Aquatic Feedstocks

In addition to lignocellulosics, catalytic hydrothermal gasification at sub-critical temperatures for the production of CH₄-rich gaseous fuels has been explored for macroalgae [37] and microalgae [85, 86] and is now being tested at a pilot scale [87].

Its usefulness in on-farm waste management has also been explored [88]. Minowa and Sawayama used a 50% Ni on silica-alumina catalyst and reacted harvested *Chlorella vulgaris* (87% moisture, 7% N, 6% ash, 49% C) at 350 °C and 18 MPa for ~1 hr [86]. Higher catalyst loading led to increased conversion to gas (max 70% at 0.5 g catalyst/g wet algae) and increased the proportion of CH₄. Notably, nutrients (e.g., N) recovered in the aqueous phase can be recycled for continued algal growth, though questions of its suitability remain due to catalyst (Ni) contamination [86, 89].

SCWG has been explored with microalgae, with a focus on decreasing catalyst loss by precipitating N, S, and P as salts under SCW conditions in the appropriate pH range prior to the catalytic reactor [90]. In the conceptual process design, a dewatered algae slurry (~20% solids) would be pumped to ~30 MPa and preheated to 300–350 °C. Salts would then be precipitated and removed continuously from the fluid stream, which then flows to a hydrothermal methanation reactor at ~400 °C. Salt-based complications in SCW processing, which may be particularly acute in marine biomass, have been explored in continuously stirred tank reactors [59] and were recently studied in situ with neutron radiography to visualize salt buildup [91]. The continuous flow process was designed to be thermally self-sufficient, with heat demands met by methane combustion or heat recovery. Ruthenium on activated coconut carbon (Ru/C) and ruthenium on zirconia (Ru/ZrO₂) were used for batch experiments without salt precipitation and showed promising results.

Brown et al. converted the marine microalga *Nannochloropsis sp.* into a crude

bio-oil product and a gaseous product *via* hydrothermal processing from 200 to 500 °C and a batch holding time of 60 min [19]. The total yield and energy content of the gas were found to increase with temperature. CO₂ was always the most abundant gas product. H₂ was the second most abundant gas at all temperatures other than 500 °C, where its yield was surpassed by that of CH₄. The activation energies for gas formation suggested that neither water-gas shift (equation 2.3) nor steam-reforming (equation 2.2) was the sole dominant pathway for H₂ and CO₂ formation.

2.1.4 Economic and technological outlook

Hydrothermal gasification of biomass shows promise as a clean and renewable energy conversion technology. Though SCWG is still not fully understood, many studies have revealed important aspects of the underlying chemistry. The main pathways for the hydrothermal gasification reactions that convert relatively low-value natural biomass to high-value synthetic fuel gas have been elucidated. Specifically, numerous model compound studies have clarified the role played by individual biomass components, such as cellulose, lignin, proteins, and salts. The influence of process variables such as temperature, pressure, water density, and biomass concentration are well understood. Work in the area of catalysis has revealed some of the reactions that are catalyzed by different metals, activated carbon, and alkali salts and under which conditions these catalysts are stable.

Nevertheless, there are still many areas where research is needed before com-

mercial plants that gasify biomass in water can become economical. Biomass feedstocks are very complex, and so too is the chemistry needed to convert them to gases. A more fundamental mechanistic understanding of this chemistry is needed if detailed kinetic models are to be developed for process optimization and if catalytic opportunities are to be fully realized. However, while model compounds will continue to be useful for evincing reaction pathways of individual biomass components, the interactions between these pathways are not currently well understood and must be investigated. Eventually, the detailed reaction network must be built into a model that explains the hydrothermal gasification of whole biomass. Understanding how feedstocks other than lignocellulosics behave under hydrothermal gasification conditions will be important too. Recent work with aquatic biomass [90] and wastes [34, 68] has demonstrated the importance of extending this technology beyond traditional renewable feedstocks. In particular, these studies have begun addressing some of the challenges this technology faces regarding feedstock ash content, catalyst deactivation, and product separation and recovery. A host of other technological issues must be considered as well: feedstock transport, solids handling, heat exchange efficiencies, and the need for robust, specialized equipment to maintain high pressures and temperatures. Many of these problems are currently being investigated at the pilot scale [92, 93] and recent work in computational fluid dynamics is improving reactor design to enhance gasification and improve process efficiency [94].

2.2 Supercritical water gasification of phenol

In this second section of Chapter 2, the focus of the discussion of previous work narrows to investigations that were primarily concerned with the fate of phenol at high temperatures. This will provide a foundation for the proposal of reaction pathways in phenol SCWG.

2.2.1 Insights from pyrolysis literature

As mentioned in section 2.1.1, pyrolytic reactions are an integral part of gasification in supercritical water. Pyrolysis is all that remains if the complexity of water is removed from the picture of SCWG. It is therefore suspected that many of the mechanisms in phenol SCWG can be attributed to the interplay of free radicals, which are created when high temperatures induce homolytic cleavage in phenol and its intermediates. Examining the modest body of phenol pyrolysis literature should provide insights into the expected chemistry in phenol SCWG.

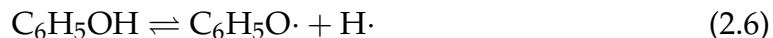
Shock-tube experiments with phenol at 1177–1377 °C led [Horn et al. \(1998\)](#) to propose a reaction mechanism for the pyrolysis of phenol [95], summarized in Figure 2.4. Included are kinetic parameters obtained from data. Phenol pyrolysis initiates with direct molecular elimination of CO to form cyclopentadiene (equation 2.5) or thermolysis to yield phenoxy radicals and H atoms (equation 2.6).



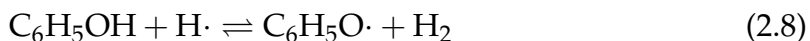
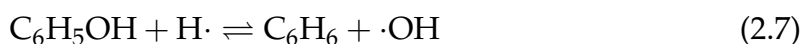
Figure 2.4: Kinetic model for phenol pyrolysis [95].

	reactions considered	A	b	E
1	$C_6H_5OH = C_5H_6 + CO$	1.00×10^{12}	0.0	60 740.0
2	$C_6H_5OH = C_6H_5O + H$	3.20×10^{15}	0.0	81 500.0
3	$C_6H_5OH + H = C_6H_6 + OH$	2.20×10^{13}	0.0	8 000.0
4	$C_6H_5OH + H = C_6H_5O + H_2$	1.15×10^{14}	0.0	12 400.0
5	$C_6H_5OH + H = C_6H_5O + H_2O$	6.00×10^{14}	0.0	0.0
6	$C_6H_5O = C_5H_5 + CO$	7.40×10^{11}	0.0	43 800.0
7	$C_5H_6 = C_5H_5 + H$	4.00×10^{14}	0.0	77 000.0
8	$C_5H_6 + H = C_5H_5 + H_2$	2.80×10^{13}	0.0	2 260.0
9	$C_5H_6 + H = C_3H_5 + C_2H_2$	6.60×10^{14}	0.0	12 310.0
10	$C_5H_5 = C_5H_5(L)$	7.50×10^{11}	1.0	77 000.0
11	$C_5H_5(L) = C_3H_3 + C_2H_2$	3.70×10^{11}	0.0	30 000.0
12	$2C_5H_5 = C_{10}H_8 + 2H$	2.00×10^{13}	0.0	4 000.0
13	$2C_3H_3 = C_6H_5 + H$	1.00×10^{13}	0.0	0.0
14	$C_3H_3 + H = C_3H_4$	5.00×10^{13}	0.0	0.0
15	$C_3H_4 + H = C_3H_3 + H_2$	5.00×10^7	2.0	5 000.0
16	$C_3H_4 + H = CH_3 + C_2H_2$	1.00×10^{14}	0.0	4 000.0
17	$C_6H_5 = C_6H_5(L)$	2.50×10^{13}	0.0	70 500.0
18	$C_6H_5(L) = C_4H_3 + C_2H_2$	7.90×10^{62}	-14.7	57 000.0
19	$C_4H_3 = C_4H_2 + H$	1.60×10^{43}	-9.3	43 100.0

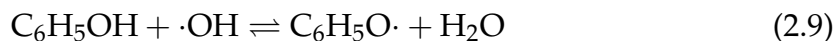
^a A is in units of mol·cm³·s·K; E is in units of cal/mol. $k = AT^b \exp(-E/RT)$.



Reaction 2.5 is dominant, whereas the rate coefficient for reaction 2.6 was found to have an upper limit of $0.15k_{2.5}$. Following initiation, H atoms attack phenol to displace OH and form benzene (equation 2.7) or to evolve H₂ gas and form additional phenoxy radicals (equation 2.8).



The hydroxyl radicals produced in the displacement reaction will readily abstract H atoms from phenol to form water (equation 2.9).

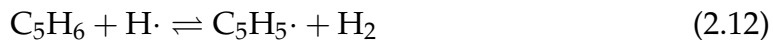


Phenoxy radicals produced in reactions 2.6, 2.8, and 2.9 will unimolecularly decompose into CO gas and cyclopentadienyl radicals (equation 2.10).

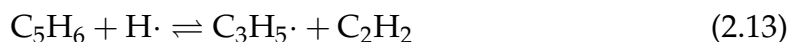


Cyclopentadienyl radicals are also produced from the cyclopentadiene generated in reaction 2.5, either by direct cleavage of H atoms (equation 2.11) or by evolution of H₂ (equation 2.12).

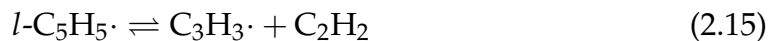




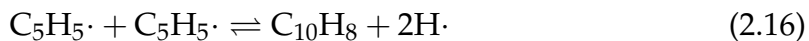
Decomposition of cyclopentadiene can be instigated by the addition of H atoms, resulting in allyl radicals and acetylene *via* ring-opening (equation 2.13).



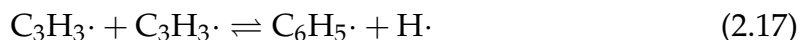
Cyclopentadienyl radical rings can spontaneously open to yield linear pent-1-en-4-yn-3-yl radicals (equation 2.14), which then decompose into propargyl radicals and acetylene (equation 2.15).



Linear radicals are distinguished here from cyclic radicals by the the notation “*l*.” Two cyclopentadienyl radicals may also dimerize to form naphthalene (equation 2.16).



Recombination of two propargyl radicals produces phenyl radicals (equation 2.17).

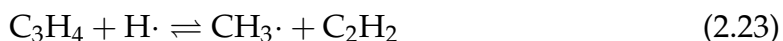
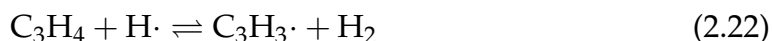


Like cyclopentadienyl radicals, phenyl radicals will spontaneously undergo ring-

opening (equation 2.18) and decompose into acetylene (equation 2.19) and diacetylene (equation 2.20).



Alternatively, propargyl radicals can react with H atoms to form propyne or allenes (equation 2.21). Subsequent H additions result in the reconstitution of propargyl radicals with the evolution of H₂ gas (equation 2.22) or decomposition into methyl radicals and acetylene (equation 2.23).



The phenoxy and cyclopentadienyl radicals predicted by the Horn model are known to play a significant role in ring formation and the growth of polycyclic aromatic hydrocarbons (PAHs) that leads to soot (*i.e.*, char) [96]. These radicals were experimentally detected by [Khachatryan et al.](#) in a later study that further validated the Horn mechanisms [97]. Their analysis suggested that phenoxy radical concentration is most sensitive to the rates of reactions 2.6 and 2.10, and cyclopentadienyl radical concentration is most sensitive to the rate of reaction 2.6. Cyclopentadienyl

is the dominant persistent free radical above 700 °C and is observed at temperatures as low as 400 °C [97].

In the same year as the Horn model, Brezinsky et al. reported similar pyrolysis experiments with phenol at 900 °C [98]. Major reaction products were CO and cyclopentadiene, with benzene, acetylene, naphthalene, methane, and methylcyclopentadiene present in lesser amounts. The mechanisms proposed to explain these results were largely congruent with the Horn model, which predicts all species except for methylcyclopentadiene. Accordingly, Brezinsky et al. suggested methylcyclopentadiene and its radical may form *via* reaction of cyclopentadienyl and methyl radicals (equation 2.24), a mechanism which also implies an additional benzene formation route (equation 2.25).



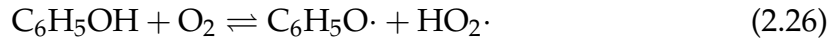
This mechanism is supported by experiments at similar temperatures, wherein pyrolysis of cyclopentadiene yielded primarily benzene [98].

2.2.2 Insights from SCWO literature

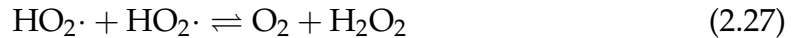
Supercritical water oxidation (SCWO) involves the oxidation of organic materials in the dual presence of supercritical water and one or more oxidizing agents. Thornton investigated the reaction kinetics and pathways of SCWO, primarily as

a hazardous waste treatment technology, using phenol as a model pollutant for industrial aqueous streams [100, 101, 99, 102, 103, 104]. Gopalan and Savage extended this work into a detailed reaction mechanism and kinetic model for phenol SCWO [106, 107, 105]. SCWG is not always completely devoid of oxygen, especially at short times when atmospheric O₂ may be present in a reactor headspace. Phenol SCWG is therefore expected to encompass some phenol SCWO chemistry, so a brief review of this chemistry is appropriate.

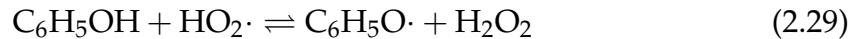
According to the Gopalan model, phenol SCWO is initiated when phenol is oxidized to form phenoxy and hydroperoxyl radicals (equation 2.26).



Hydroperoxyl radicals react to reform oxygen and produce hydrogen peroxide (equation 2.27), which readily decomposes into hydroxyl radicals (equation 2.28).



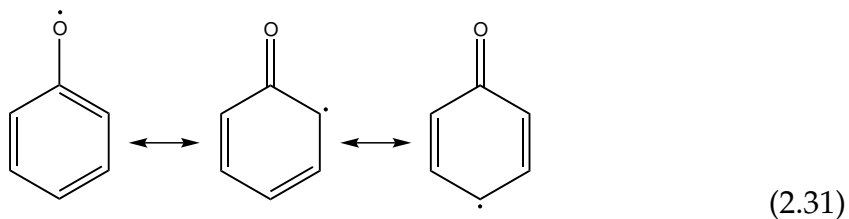
Both hydroperoxyl and hydroxyl radicals can react with phenol to form additional phenoxy radicals (equations 2.29 and 2.30).





Thus, phenoxy radicals are prevalent in SCWO, as in pyrolysis, but are attributable to different mechanisms, and they also react to form different products.

The main reaction products detected in phenol SCWO experiments carried out at 380–480 °C were CO, CO₂, dibenzofuran, 2-phenoxyphenol, 4-phenoxyphenol, and 2,2'-biphenol [101, 105]. These compounds can be explained by the chemistry of phenoxy radicals. The phenoxy radical is resonance-stabilized and therefore reactive at not just the O radical site, but also at the ortho and para position (equation 2.31).



The chief pathways available to the phenoxy radical are ring-coupling (*i.e.*, dimerization), ring-opening, and hydroxylation to a benzenediol [106]. The dimers 2-phenoxyphenol, 4-phenoxyphenol, and 2,2'-biphenol can be explained by the ortho-O coupling, para-O coupling, and ortho-ortho coupling, respectively, of phenoxy radicals. Dibenzofuran is a secondary product that may form by intramolecular dehydration of 2,2'-biphenol [108]. Pyrolytic ring-opening mechanisms discussed in section 2.2.1 are available to phenoxy radicals in SCWO *via* reactions 2.10 and 2.14. Additionally, attack by hydroperoxyl or hydroxyl radicals may instigate phenoxy ring-opening. Once a ring has been opened, further degradation can lead to CO and CO₂ production.

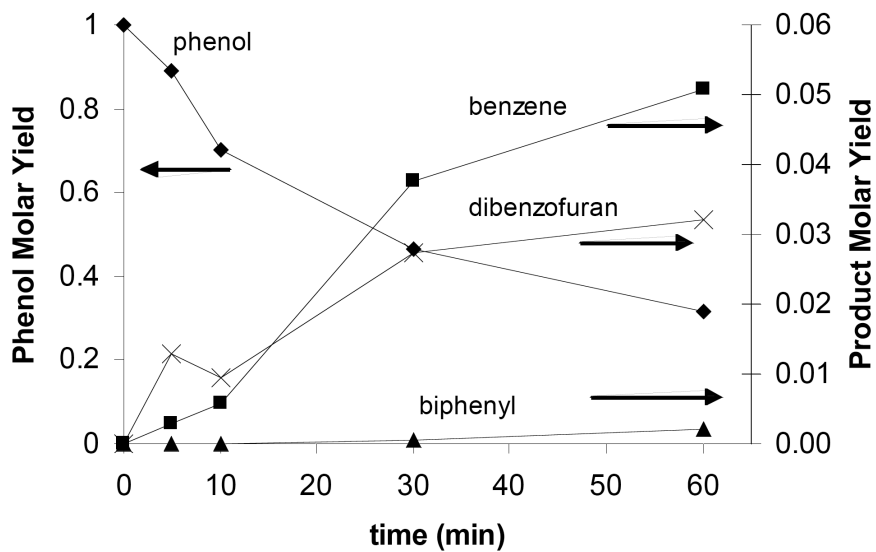
2.2.3 Survey of published work

Previous research on phenol SCWG is limited to a handful of individual studies reported in the literature [67, 83, 84, 109, 110, 111] and the thesis work by DiLeo [49, 51, 112]. In 1996, Xu et al. performed a single experiment to gasify phenol as a DoD waste representative compound at 600 °C and 34.5 MPa in the presence of activated carbon catalyst [67]. Products detected were H₂, CO, CO₂, CH₄, and benzene. Two studies investigated SCWG of phenol in the presence of another compound in flow reactors. Goodwin and Rorrer (2009) confirmed the difficulty of gasifying phenol but found the addition of xylose (a hemicellulose model compound) improved SCWG reaction rates at 750 °C and 25 MPa [83]. They also identified H₂, CO, CO₂, CH₄, and benzene as phenol SCWG reaction products. Weiss-Hortala et al. (2010) conducted a similar study with phenol and glucose at 400–500 °C and 25 MPa but did not obtain results for phenol-only SCWG [84]. In all of these studies, the effect of process variables (*e.g.*, temperature, water density, phenol loading) was not considered, catalysis was present, and no kinetics analysis was performed.

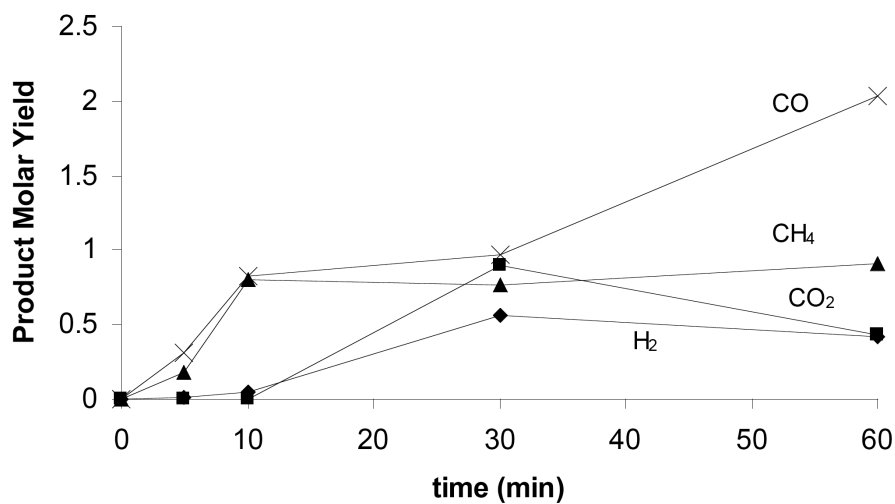
DiLeo's thesis work (2007) was unique in that it avoided reactor wall catalysis by using quartz capillary reactors in order to clearly define the performance difference between homogeneous and metal-catalyzed phenol SCWG reactions. H₂, CO, CO₂, and CH₄ were reported as gas products and benzene, biphenyl, and dibenzofuran were the only detected liquid-phase intermediate products. Char was not observed in these experiments. Notably, DiLeo examined the effects of

temperature (600 and 700 °C), water density (0.064, 0.079, and 0.159 g/cm³), phenol loading (2 and 5 wt. %), and the presence of catalytic Ni wire on the yields of all SCWG products. Among other things, he concluded that higher temperatures favor H₂ formation, Ni catalysis increases the reaction rate and H₂ selectivity, and phenol conversion is fastest at an intermediate water density. Figure 2.5 presents the uncatalyzed “base case” results from DiLeo’s work. The kinetics analysis was limited to a simple global rate law that presumed first-order kinetics to model the disappearance of phenol, and no additional insight into the reaction pathways was reported. This presents a significant opportunity for future research. Another limitation of this work was a critical assumption made in calculating the gas product yields. Because no char or other solids were visually observed after reaction, DiLeo relied upon a carbon balance to determine the amount of gas that formed. If the assumption is incorrect, the gas yields may be overpredicted dramatically.

Two groups recently investigated the effect of added O₂ on Na₂CO₃-catalyzed phenol SCWG in nickel alloy flow reactors. [Xu et al.](#) identified benzene, dibenzofuran, biphenols, and 2-phenoxyphenol in the liquid phase, and they also found C₂ light gases in the gas phase [109]. [Guan et al.](#) identified oxalic and maleic acid (ring-opening products) and dibenzofuran, phenoxyphenols, and biphenol (dimerization products) in the liquid phase [110]. Both studies suggest added O₂ can increase the phenol conversion *via* partial oxidation. [Guan et al.](#) followed up this work with a kinetic model for partial oxidation of phenol in supercritical water consisting of nine reaction pathways (six oxidation reactions, two hydrothermal gasification reactions, and the water-gas shift reaction) [111]. The modeling con-



(a) Liquid-phase products.



(b) Gas-phase products.

Figure 2.5: Molar yields reported by DiLeo for homogeneous phenol SCWG (600 °C, 0.079 g/cm³ water density, 5 wt. % phenol loading) [112].

firmed that added O₂ assists in the degradation of phenol, but leads to decreased H₂ yield.

2.2.4 Limitations of previous work

An attempt to summarize the gaps in literature dealing with phenol SCWG is necessarily also a summation of the main gaps in all biomass SCWG literature. The preponderance of work done in biomass SCWG is exploratory and pays little attention to the identities and yields of the liquid-phase intermediates that form. The goal has been to maximize the amount of gas produced through empirical means, rather than to develop an understanding of the underlying kinetics and pathways for the SCWG reactions that take place. Typically, reaction parameters such as time, temperature, water density, and concentration are varied, and the effect this has on the gas yield is reported. However, most studies have not taken a systematic approach. Consequently, there is a deficiency in our understanding of the chemistry that underlies SCWG of biomass, and it must be addressed if we are to advance SCWG as an economically viable technology for renewable energy production.

As mentioned already, one weakness affecting the research in this area is the prevalence of reactor wall catalysis. The vast majority of SCWG work with biomass and biomass model compounds has been carried out in metal reactors, and the results from these studies were influenced by the catalytic activity of the metal walls. The nature and extent of the role the reactor wall plays is not usually characterized by the researchers, and, as a result, the degree to which SCWG may be

attributed to heterogeneous reactions is not clear at this time. This makes it difficult to draw meaningful conclusions about the underlying chemistry involved in SCWG. Moreover, the uncertainty of wall catalysis prevents the comparison of results from studies at different laboratories and even at the same laboratories if the conditions are not carefully replicated.

Finally, aside from greenhouse gas considerations, concerns over potential environmental impacts of a scaled up process are nonexistent in biomass SCWG literature. For example, a consequence of the overemphasis on only yields of desired products (*i.e.*, gas) is that a blind eye is turned toward undesired byproducts. Nongaseous byproducts of SCWG generally consist of char and tars that, like their fossil fuel analogs, can be harmful to human and environmental health.

This dissertation represents the culmination of a systematic attempt to address the gaps in current phenol SCWG literature highlighted above. The investigation begins with identification and quantification of heretofore unknown reaction intermediates and products. It continues with the isolation of the influence of individual process variables on product yields and phenol conversions. These data permit development of the first rate equation for phenol disappearance in SCW, and they pave the way for a more thorough understanding of phenol SCWG chemistry. Reaction pathways are elucidated, primary products are identified and studied, and a reaction network is constructed. The elucidated pathways and experimental kinetic data inform the development of a kinetic model that can predict primary product and gas yields. Finally, potentially harmful byproducts are identified and characterized by their carcinogenic, non-carcinogenic, and ecotoxic impacts.

CHAPTER 3

Experimental Methods

3.1 Materials

Phenol (99+% purity), dibenzofuran (99+% purity, sometimes abbreviated herein as “DBF”), and benzene (99.9% purity) were purchased from Sigma-Aldrich or Fisher Scientific and used as received. Reagent-grade or better acetone was used in the work-up procedure. An analytical liquid standard comprising 16 EPA priority PAHs (product no. Z-014G) was purchased from AccuStandard, and all other chemicals were purchased from Fisher Scientific or Sigma-Aldrich in high purity and used as received. Helium and argon (99.997% purity) were obtained from Cryogenic Gases, and analytical gas standards were obtained from Air Liquide Specialty Gases.

3.2 Reaction procedure

Mini-batch reactors approximately 14 cm in length were fashioned from quartz capillary tubing (2 mm I.D., 2 mm wall thickness) from GM Associates, Inc. us-

ing a flame-sealing process. The reactors had an internal volume of ~ 0.4 mL. Stock solutions of phenol in deionized water were prepared in varying concentrations and loaded into the reactors prior to sealing. Reactor loading varied with the reaction condition to be used, such that the concentrations at reaction conditions spanned 0.0–0.2 mmol phenol/mL and 4.4–10.0 mmol water/mL. Multiplying water concentration by the molar mass of water gives the corresponding water density range: 0.080–0.180 g/cm³. These concentrations ensured an excess of water and a sufficiently high water density to maintain a single supercritical phase during the reactions at the lowest temperature studied (*i.e.*, 500 °C). In some experiments, dibenzofuran or benzene were used as reactants, requiring different loading procedures. Dibenzofuran was weighed out and loaded in solid form, and deionized water was then injected into the reactor using a syringe. Liquid benzene was injected directly using a syringe, and deionized water was then added. Reactant loading was dictated by the desired concentration at reaction conditions, and water loading was dictated by the desired water density (water was always in excess and supercritical at the lowest reaction temperature).

For reactions carried out at 600 °C or below, the reactor was suspended in a Techne SBL-2 isothermal fluidized sand bath. For reactions above this temperature, the reactor was placed within a Barnstead Thermolyne 21100 isothermal tube furnace. The heat up time for a reactor in the sand bath is about 30 s at 600 °C, and the heat up time for a reactor in the furnace is about 2 min at 700 °C. These heat up times were measured using a thermocouple sheathed in the same quartz capillary tubing used for reactor construction. Heat up is faster in the sand bath because the

fluidized sand is a better heat transfer mechanism than the heating coils in the tube furnace. Although the sand bath temperature was a function of depth, the temperature was uniform radially, and the reactor was placed horizontally at a fixed depth. Temperature within the tube furnace varied up to 10 °C along the axis, but spatial temperature differences in the furnace or sand bath were equalized within the quartz capillary tubing enclosure, since the conductive heat transfer within quartz exceeds the convective heat transfer for quartz-air and quartz-sand interfaces.¹ Heat and mass transfer within the reactor was facilitated by the unique properties of supercritical water mentioned previously. After the desired reaction time had elapsed, the reactor was removed and placed in front of a fan for rapid cool down, reaching room temperature within 2 min. Quartz is slightly soluble in supercritical water, but at 600 °C, only about 0.04% of the reactor material would be leached out even if equilibrium were achieved [113]. If quartz dissolution occurred, it did not compromise the structural integrity of the reactors. Replicate reactions were carried out for at least one of the reaction times at every condition investigated (temperature, phenol concentration, and water concentration), to determine representative standard deviations in the experimental results.

Due to the inherent risks of carrying out reactions at high temperatures and pressures, safety precautions were taken to avoid injury. Quartz reactors would shatter on occasion. This would typically happen within the first minute of heat

¹Faster heat transfer within the quartz than at the quartz-sand interface would ensure a uniform temperature in the axial dimension of the reactor itself when placed in the sand bath. An axial variation in temperature within the tube furnace would have even less effect, since heat transfer is slower in the furnace. One may envision a steady state in which, for example, a quartz reactor at 695 °C sits within an axial furnace gradient that is 690 °C on each end and 700 °C in the center.

up, such that the effects of explosion could be contained either within the sand bath or the enclosed furnace walls. However, loading or removing quartz reactors from the sand bath or furnace was always executed with an abundance of personal protective equipment: safety glasses, a face shield, and high temperature arm gloves.

3.3 Sample recovery and analytical procedure

Recovery of products in both the gas phase and liquid phase was not feasible with a single reactor, so two nominally identical sets of experiments were conducted at each set of reaction conditions, but with different sample recovery and analysis procedures. Reaction products in the liquid phase were recovered for analysis by first scoring each quartz reactor and carefully breaking it in half. A long-needle syringe was then used to fill each half with acetone to dissolve the water, unconverted phenol, and any products. Multiple syringe plunges facilitated mixing and dissolution, and the resulting solution was transferred into a 2 mL sample vial. This acetone wash process was repeated twice more for each half-reactor. Afterward, the contents of the vial were diluted to a final volume of 1.5 mL and retained for analysis. Liquid sample components were identified on an Agilent 6890N gas chromatograph and 5973N mass spectrometer (GC-MS) equipped with an HP-5 ms capillary column (50 m \times 0.20 mm I.D., 0.33 μ m film thickness) using helium as the carrier gas. They were quantified on an Agilent 6890 GC equipped with an identical column using a flame ionization detector (GC-FID). Identical tempera-

ture programs were used on both instruments: 50 °C for 5 min, 25 °C/min ramp, 250 °C for 25 min. Peaks were identified by matching retention times with GC-MS analysis. Three sets of external standards, prepared using known concentrations of identified compounds, were analyzed and used to construct calibration curves relating peak area and concentration.

To recover and analyze reaction products in the gas phase, each quartz reactor was scored and placed within a pressurization chamber consisting of a stainless steel tube (20 cm × 1/2 in O.D., 0.065 in wall thickness) with a Swagelok cap on one end and a needle valve on the other. The pressurization chamber was then connected to a helium cylinder at the valve, pressurized to 10 psi, and removed from the cylinder. Forceful striking of the pressurized chamber shattered the quartz reactor within, releasing its gaseous contents. After releasing these product gases, the chamber contents were not immediately well-mixed, so an experimentally determined rest time of 45 minutes was required prior to analysis so the gas sample could equilibrate by diffusion. Afterward, the chamber was connected to a gas-sampling valve and the pressurized sample was injected onto an Agilent 6890 GC equipped with a Supelco 60/80 mesh Carboxen 1000 packed column (15 ft × 1/8 in O.D.) using argon as the carrier gas. Quantification was performed with a thermal conductivity detector (GC-TCD). The GC temperature program was as follows: 35 °C for 5 min, 20 °C/min ramp, 225 °C for 5 min. Analytical gas standards of known composition were used to construct calibration curves relating peak area and mole %. The absolute amount of each gas component was calculated using the known amount of N₂ in the chamber (from air initially in the reactor, the

pressurization chamber, and the cylinder connections) as an internal standard. To eliminate carryover from one sample to the next, the pressurization chamber was purged with air for about five minutes between runs.

Alternate methods were employed to ensure that no key compounds were overlooked in the standard procedure described above. If they formed, molecules in the weight range between single-carbon gases (*e.g.*, CO, CH₄, and CO₂) and benzene would serve as important chemical links between phenol, aromatic intermediates, and desired fuel gas molecules. We conducted experiments that incorporated dilution avoidance, liquid-liquid extraction, and the use of larger reactors to improve detectability by increasing sample recovery and analyte concentration. Freeze drying was used to remove water from liquid samples to eliminate the large water peak in the chromatographic analysis that could mask the presence of potential low molecular weight compounds. GC-MS analysis of freeze-dried samples revealed no new compounds in the water elution region. A gas sampling technique was developed for GC-MS analysis (using the HP-5 ms capillary column) in order to identify compounds in gas samples, and an analytical gas standard of C₂–C₆ alkane gases was run to verify such gases would be detected if they were present. The only new gas phase constituent detected in phenol SCWG samples was benzene vapor. The detection of nothing between single-carbon gases and benzene in the gas chromatography is strong evidence that no species in the C₂–C₆ range are being overlooked.

CHAPTER 4

Effect of Reaction Conditions on Products

This chapter presents the results from phenol SCWG experiments conducted at the conditions listed in Table 4.1. Experiments were designed to survey a large parameter space, with phenol conversion spanning 0–100% due to the range of temperatures used. Various water densities and phenol concentrations were studied to isolate the effect of the molecular availability of each of these species. The range of reaction times allows important kinetic information to be extracted and phenol disappearance to be modeled using a rate equation in Chapter 5.

4.1 Intermediate products and byproducts

Phenol SCWG produced H_2 , CO, CH_4 , and CO_2 and many higher molecular weight compounds in the liquid phase. Twenty of these liquid phase products were identified, most for the first time. Table 4.2 presents these results, which include all the species that were identified in multiple experiments, but it is not exhaustive. Compounds larger than those in Table 4.2 were not identified or detected, but it is likely that such compounds formed and ultimately lead to the char that is observed

Table 4.1: Experimental conditions, phenol conversions, and gas mole fractions.

T (°C)	t (min)	Water Density (g/cm ³)	Phenol Conc. (mol/L)	Phenol Conversion (fractional)	Carbon Recovery (fractional)	Gas Mole Fraction (dry basis)			
						H ₂	CO	CH ₄	CO ₂
500	8	0.079	0.044	0.05	1.02	0.02	0.48	0.00	0.50
500	15	0.079	0.044	0.00	1.04	0.01	0.29	0.00	0.70
500	30	0.079	0.044	0.05 ± 0.08	1.03 ± 0.04	0.02	0.60	0.00	0.39
500	60	0.079	0.044	0.01	1.07	0.03	0.52	0.00	0.45
500	8	0.180	0.101	0.00	1.15	0.06	0.31	0.00	0.62
500	15	0.180	0.101	0.00	1.08	0.04	0.42	0.00	0.54
500	30	0.180	0.101	0.01 ± 0.03	1.06 ± 0.02	0.11	0.37	0.00	0.52
500	60	0.180	0.101	0.00	1.08	0.19	0.29	0.00	0.53
500	8	0.079	0.095	0.02	1.06	0.02	0.44	0.00	0.54
500	15	0.079	0.095	0.08	0.97	0.04	0.32	0.00	0.64
500	30	0.079	0.095	0.05 ± 0.05	1.02 ± 0.06	0.05	0.43	0.00	0.52
500	60	0.079	0.095	0.09	0.95	0.06	0.37	0.00	0.58
500	8	0.180	0.216	0.00	1.14	0.06	0.26	0.00	0.68
500	15	0.180	0.216	0.00	1.07	0.06	0.23	0.00	0.71
500	30	0.180	0.216	0.01 ± 0.05	1.05 ± 0.05	0.11	0.17	0.03	0.70
500	60	0.180	0.216	0.00	1.05	0.15	0.23	0.00	0.63
600	8	0.079	0.044	0.00	1.10	0.05	0.46	0.05	0.44
600	15	0.079	0.044	0.21	0.91	0.09	0.32	0.08	0.52
600	30	0.079	0.044	0.28 ± 0.07	0.87 ± 0.04	0.14	0.33	0.11	0.42
600	60	0.079	0.044			0.24	0.26	0.21	0.29
600	8	0.180	0.101	0.00	1.12	0.27	0.15	0.12	0.45
600	15	0.180	0.101	0.23	0.92	0.29	0.13	0.18	0.40
600	30	0.180	0.101	0.35 ± 0.08	0.77 ± 0.04	0.32	0.10	0.25	0.32
600	60	0.180	0.101	0.51	0.65	0.35	0.08	0.30	0.26
600	8	0.079	0.095	0.07	0.97	0.13	0.49	0.06	0.33
600	15	0.079	0.095	0.15	0.93	0.23	0.37	0.10	0.31
600	30	0.079	0.095	0.47 ± 0.07	0.70 ± 0.10	0.26	0.32	0.12	0.30
600	60	0.079	0.095			0.28	0.27	0.21	0.25
600	8	0.180	0.216	0.00	1.08	0.34	0.30	0.09	0.27
600	15	0.180	0.216	0.19	0.91	0.38	0.19	0.14	0.29
600	30	0.180	0.216	0.31 ± 0.03	0.81 ± 0.13	0.36	0.12	0.21	0.31
600	60	0.180	0.216	0.64 ± 0.10	0.77 ± 0.20	0.26	0.05	0.30	0.39
600	60	0	0.101	0.35 ± 0.03	0.82 ± 0.02	0.29	0.44	0.17	0.10
600	60	0.080	0.101	0.60 ± 0.03	0.72 ± 0.09	0.21	0.21	0.22	0.36
600	60	0.100	0.100	0.28 ± 0.05	0.87 ± 0.03	0.29	0.26	0.11	0.34
600	60	0.120	0.100	0.24 ± 0.07	0.89 ± 0.04	0.35	0.16	0.17	0.32
600	60	0.140	0.100	0.51 ± 0.13	0.70 ± 0.12	0.34	0.19	0.17	0.30
600	60	0.160	0.100	0.53 ± 0.14	0.70 ± 0.10	0.37	0.00	0.22	0.41
600	60	0.120	0.020	0.50 ± 0.03	0.72 ± 0.02	0.21	0.31	0.07	0.41
600	60	0.120	0.050	0.41 ± 0.12	0.76 ± 0.11	0.37	0.00	0.15	0.48
600	60	0.120	0.150	0.32 ± 0.06	0.80 ± 0.15	0.40	0.13	0.20	0.28
600	60	0.120	0.200	0.53 ± 0.16	0.75 ± 0.13	0.31	0.12	0.28	0.29
700	8	0.079	0.044	0.88	0.44	0.26	0.31	0.21	0.22
700	15	0.079	0.044	0.97	0.36	0.31	0.19	0.24	0.27
700	30	0.079	0.044	1.00 ± 0.00	0.27 ± 0.02	0.35	0.07	0.25	0.32
700	60	0.079	0.044	1.00	0.23	0.37	0.03	0.27	0.33
700	8	0.180	0.101	1.00	0.31	0.25	0.07	0.30	0.38
700	15	0.180	0.101	1.00	0.39	0.24	0.02	0.34	0.41
700	30	0.180	0.101	1.00 ± 0.00	0.29 ± 0.002	0.25	0.01	0.36	0.38
700	60	0.180	0.101	1.00	0.27	0.25	0.01	0.37	0.37
700	8	0.079	0.095	0.95	0.41	0.26	0.31	0.24	0.18
700	15	0.079	0.095	0.99	0.32	0.29	0.18	0.27	0.26
700	30	0.079	0.095	1.00 ± 0.00	0.26 ± 0.02	0.33	0.06	0.29	0.32
700	60	0.079	0.095	1.00	0.23	0.31	0.02	0.33	0.33
700	8	0.180	0.216	0.98	0.37	0.23	0.08	0.33	0.36
700	15	0.180	0.216	1.00	0.28	0.23	0.01	0.37	0.39
700	30	0.180	0.216	1.00 ± 0.00	0.28 ± 0.04	0.22	0.01	0.41	0.36
700	60	0.180	0.216	1.00 ± 0.00	0.21 ± 0.01	0.20	0.01	0.44	0.35

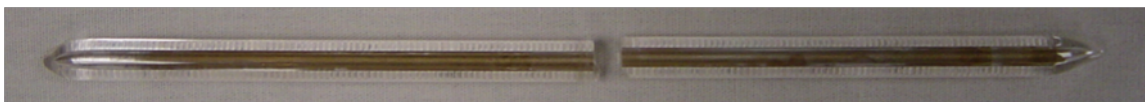


Figure 4.1: Quartz reactor with char on the inner wall.

on reactor walls, as seen in Figure 4.1. Note that char deposition occurred along the entire length of the reactor, which suggests a uniform, homogeneous supercritical fluid phase existed throughout the reactor. This homogeneous phase was visible immediately after the quartz reactors were removed from the heat source, and distinct gas and liquid phases emerged only after several seconds of cooling. Control experiments confirmed that none of the detected species are contaminants from water or reactor materials, nor are they byproducts from reactor sealing or heating procedures. The polycyclic aromatic hydrocarbons (PAHs) in Table 4.2 represent likely char precursor molecules, and they are also known carcinogens. Understanding the formation pathways for these molecules can provide insight into how to suppress their formation and char and also how to improve gas yield through process optimization and catalysis.

Figure 4.2 shows a typical total ion chromatogram for the liquid phase recovered from phenol SCWG at 600 °C. Benzene (peak 1) and dibenzofuran (peak 14) are by far the most abundant products in the liquid phase. The predominance of these compounds suggests they form directly from phenol (peak 4), *via* a deoxygenation reaction in the case of benzene and dimerization in the case of dibenzofuran. In high temperature SCWG (500–800 °C), free radical mechanisms dominate [50]. Pyrolytic studies with phenol indicate resonance-stabilized phenoxy radicals readily form and play a key role in phenol decomposition [114, 95, 98].

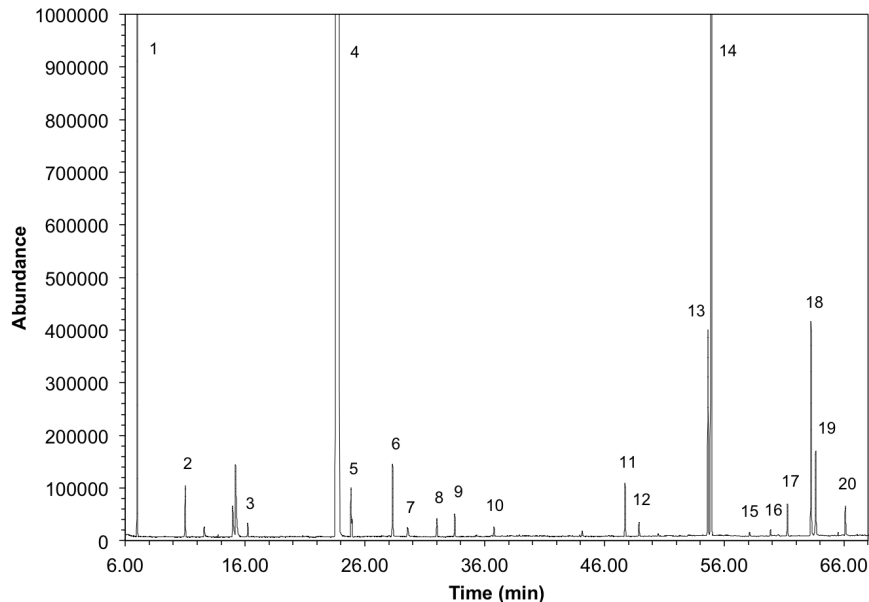
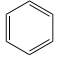
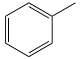
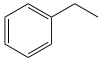
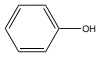
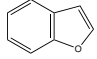
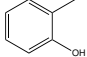
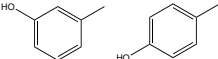
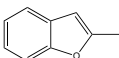
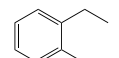
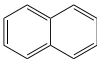
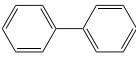
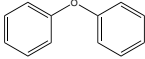
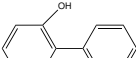
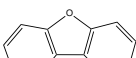
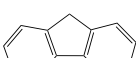
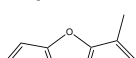
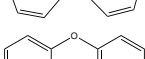
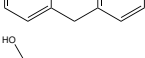
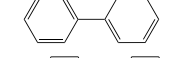
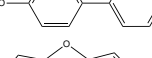


Figure 4.2: Total ion chromatogram for liquid sample obtained from phenol SCWG (60 min, 600 °C, 0.12 g/cm³ water density, 0.1 mol/L phenol concentration). Peak labels correspond to identities in Table 4.2. Unlabeled peaks are either known contaminants or unidentified compounds.

Combination of phenol with a phenoxy radical at the *ortho* position followed by an intramolecular dehydration could explain the formation of dibenzofuran [108]. Furthermore, benzene is a major product of phenol pyrolysis and results from a displacement of the hydroxyl group by an H atom liberated in the creation of other free radicals, such as phenoxy [95, 98, 115]. Simple mechanisms such as these are the most plausible since benzene and dibenzofuran accumulate very rapidly in this system. Other intermediates in Table 4.2, although present in lower concentrations, likely also result from the same free radical chemistry using phenoxy and other radicals as building blocks.

Table 4.2: Identified liquid phase intermediate compounds from phenol SCWG (60 min, 600 °C, 0.12 g/cm³ water density, 0.1 mol/L phenol concentration).

Peak I.D. in Figure 4.2	Compound	Structure	Peak Area %	R.T. (min)
1	benzene		7.13	7.00
2	toluene		0.28	11.01
3	ethylbenzene		0.10	16.23
4	phenol		73.61	23.86
5	benzofuran		0.12	24.92
6	o-cresol		0.50	28.32
7	m-/p-cresol		0.12	29.56
8	2-methylbenzofuran		0.15	32.01
9	2-ethylphenol		0.15	33.50
10	naphthalene		0.08	36.78
11	biphenyl		0.40	47.72
12	diphenyl ether		0.11	48.89
13	2-phenylphenol		1.40	54.64
14	dibenzofuran		13.19	54.92
15	fluorene		0.03	58.13
16	4-methyl- dibenzofuran		0.05	59.87
17	xanthene		0.23	61.27
18	3-phenylphenol		1.48	63.24
19	4-phenylphenol		0.65	63.63
20	dibenzofuran-2-ol		0.24	66.10

4.2 Effect of temperature

Experimental data were obtained for phenol SCWG at three different temperatures—500, 600, and 700 °C—with very different results. Figure 4.3 shows that the molar yields (defined as moles product per mole initial phenol) of all gas species increase dramatically with temperature due to increasing phenol conversion. Only about 5 mol % phenol has been converted at 500 °C, but the conversion is 47% at 600 °C, and complete conversion is achieved at 700 °C (30 min, 0.079 g/cm³ water density, 0.095 mol/L phenol concentration). At 500 °C, the gas mainly consists of CO and CO₂, suggesting there is insufficient thermal energy for H₂ and CH₄ formation after 30 min at this temperature. As temperature increases, the bonds in phenol or intermediate compounds are more easily broken, and the molecular transformations that result in H₂ and CH₄ (*e.g.*, steam reforming and methanation) are more likely to occur. This explanation is consistent with the increasing mole fractions of H₂ and CH₄ at higher temperatures (33% and 29%, respectively, at 700 °C compared to 5% and 0% at 500 °C; *c.f.* Table 4.1 at the conditions of Figure 4.3).

Taking the molar yield of a gas species at some fixed time to be proportional to its average rate of formation over that time interval allows the activation energies for gas formation to be calculated from the data in Figure 4.3. The apparent activation energies are 170 kJ/mol for H₂, 53 kJ/mol for CO, 248 kJ/mol for CH₄, and 96 kJ/mol for CO₂. The dissimilarity between these values suggests independent reaction paths are responsible for the formation of each of the gas species, and this dissimilarity is consistent with the results of previous SCWG studies using

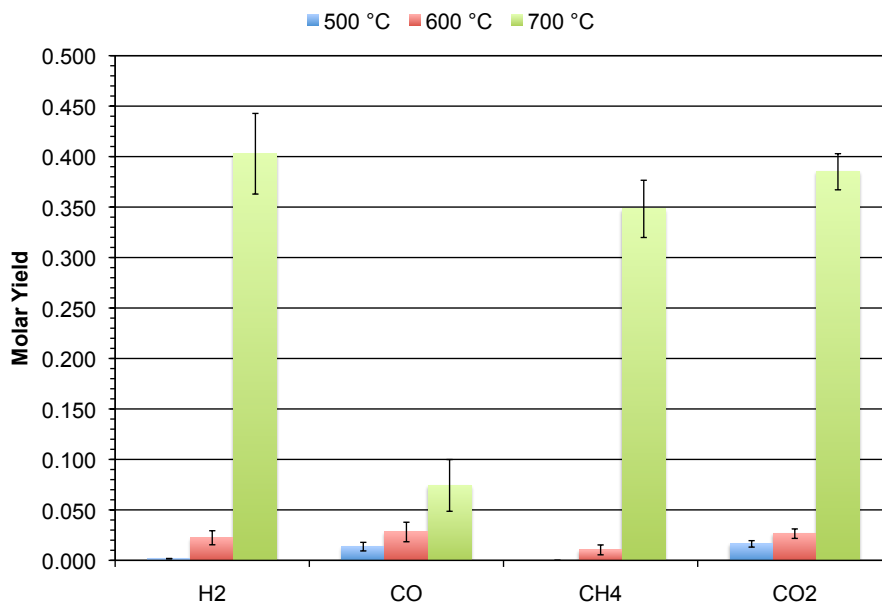


Figure 4.3: Effect of temperature on gas yields from phenol SCWG (30 min, 0.079 g/cm³ water density, 0.095 mol/L phenol concentration).

lignin, cellulose, or algae as a feedstock [70, 21]. The present activation energies are higher, however, than those estimated for the gas products in each of these studies, highlighting the difficulty with which phenol is gasified.

Figure 4.4 illustrates how the yields of several major products—benzene, naphthalene, and biphenyl—in the liquid phase increase considerably with temperature due to higher conversion. The yield of dibenzofuran, however, decreases from 600 to 700 °C, suggesting its instability at high temperatures. Dibenzofuran may readily participate in polymerization reactions to form polycyclic aromatic hydrocarbons (*i.e.*, char precursors). This hypothesis is supported by the observation of significant char on reactor walls (*c.f.* Figure 4.1) and the detection of anthracene and phenanthrene (three-ring PAHs) at 700 °C but not at 500 or 600 °C. An increase in char formation with increasing temperature is also consistent with the

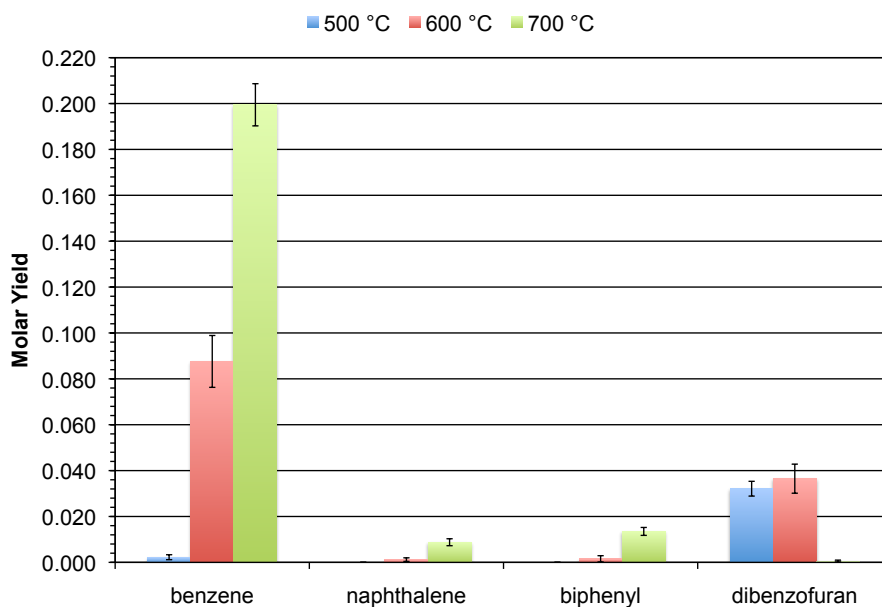


Figure 4.4: Effect of temperature on yields of representative liquid phase intermediates from phenol SCWG (30 min, 0.079 g/cm³ water density, 0.095 mol/L phenol concentration).

Table 4.3: Fraction of initial carbon in quantified products from phenol SCWG (30 min, 0.079 g/cm³ water density, 0.095 mol/L phenol concentration).

T (°C)	Carbon Recovery (fractional)
500	1.02 ± 0.06
600	0.70 ± 0.10
700	0.26 ± 0.02

stark drop in carbon recovered in gas and liquid phases at 700 °C, as shown in Table 4.3. Dibenzofuran may therefore represent a key gateway molecule to char formation pathways. In summary, higher temperatures lead to greater production of H₂-rich gas, which is desired, but also greater byproduction of char and char precursor molecules, which is undesired.

If all carbon not reported in Table 4.3 is assumed to be char, the apparent activation energy for char formation can be estimated for the reaction conditions in Table 4.3, Figure 4.3, and Figure 4.4. The result is 64 kJ/mol, suggesting the char

formation pathway is relatively favorable kinetically. Of the converted phenol, the fraction that ends up as unrecovered carbon is about 50% at 600 °C and 60–80% at 700 °C.

Comparison of the results at 600 °C to those of DiLeo et al. reveals that the present gas yields are an order of magnitude lower, despite conversions and yields of liquid phase intermediates of similar magnitude [49, 51]. In calculating gas yields, however, DiLeo et al. assumed that all of the initial carbon not accounted for by the liquid phase products resided in the gas phase. This assumption would result in gas yields higher than actual if solids or liquid phase byproducts other than benzene, biphenyl, and dibenzofuran formed. Char and additional liquid phase byproducts were observed at 600 °C in the present experiments, which indicates that the assumption of DiLeo et al. is incorrect. In the present work, the use of an internal standard in the gas phase analysis allows for more reliable calculation of gas yields.

Prior to reaction, the reactor headspace contained air and hence atmospheric O₂. In the worst case scenario, in which complete combustion of phenol consumes all available O₂, only 3 mol % of the initial phenol will have reacted to produce a molar yield for CO₂ of about 0.18. Yet, as shown in Figure 4.3, the observed molar yields for CO₂ are well below this value at 500 and 600 °C, and the yield is well above this value at 700 °C. Consequently, combustion due to residual atmospheric O₂ does not seem to play a major role in the gasification. Nevertheless, a small amount of oxygen may contribute to the formation of byproducts *via* partial oxidation. Two recent studies added O₂ to facilitate Na₂CO₃-catalyzed SCWG of phe-

nol and likewise observed benzene and dibenzofuran as intermediates [109, 110]; however, the ratio of oxygen to phenol in these studies was at least an order of magnitude higher than in the present work.

4.3 Effect of water density

To understand more fully the effect of water density on phenol SCWG, we conducted a set of experiments at five different water densities. Figure 4.5 shows that the gas yields tend to increase with increasing water density, which is consistent with hydrothermal reactions aiding the decomposition of phenolic molecules into gases. This trend agrees with results of the previous investigation of phenol SCWG by DiLeo et al. [51]. An increase in H₂ and CH₄ yields with increasing water density is also seen in SCWG of lignin [116], cellulose [117], and algae [21]. No CO was detected at the highest water density investigated, possibly due to an increase in the rate of the water-gas shift reaction at higher water concentrations. The water-gas shift reaction is known to have a high-order rate dependence on water density under supercritical conditions [118].

Competing effects are observed for the yields of intermediates, as depicted in Figures 4.6 and 4.7. For all intermediates, the molar yield initially decreases from a relatively high value at 0.080 g/cm³, reaches a minimum at 0.120 g/cm³, and increases back to nearly the initial value at 0.160 g/cm³. This trend in intermediate yields closely tracks the conversion shown in Figure 4.8, which initially decreases from 60% to an apparent minimum of 24% at 0.120 g/cm³, then increases again

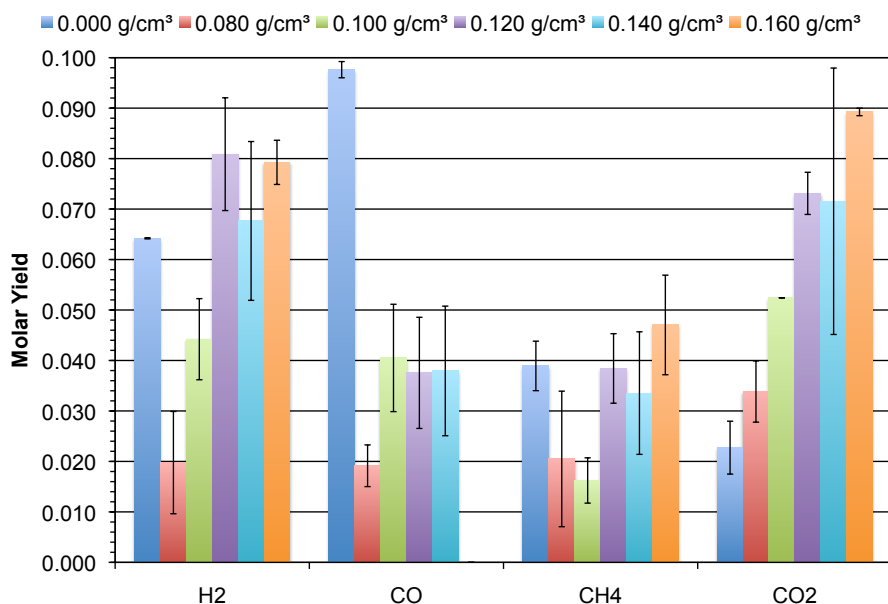


Figure 4.5: Effect of water density on gas yields from phenol SCWG (60 min, 600 °C, 0.100 mol/L phenol concentration).

to 53%. In experiments with guaiacol and supercritical water, [Lawson and Klein](#) explained trends identical to these as a competition between pyrolysis and hydrolysis tied to the water density [119]. High conversion at lower water densities may be due to a reduction in the availability of water molecules, allowing phenol and its derivatives to pyrolyze more easily and participate in second-order reactions. In addition to promoting competing reactions, water could also have an inhibitive effect on these pyrolytic reactions indicative of the solvent cage effect [9, 119]. These water effects would explain the predominance of benzene and dibenzofuran—known pyrolysis products [95, 98, 108, 115]—as well as other dimers at lower water densities. High conversion at higher water densities may be attributed to the greater abundance of water molecules that readily participate in hydrothermal reactions such as steam reforming and hydrothermolysis and thereby facilitate

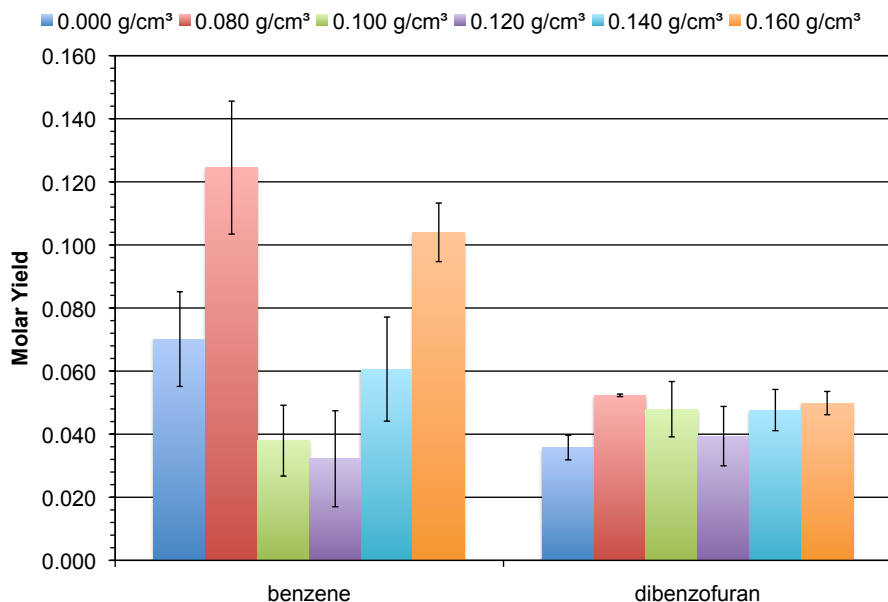


Figure 4.6: Effect of water density on yields of major liquid phase intermediates from phenol SCWG (60 min, 600 °C, 0.100 mol/L phenol concentration).

decomposition as well as the production of the same free radicals active during pyrolysis (*e.g.*, phenoxy). As a result, the same dimerization products are more abundant at both higher and lower water densities, but not at intermediate water densities.

For the purpose of comparison, we conducted experiments with no added water (*i.e.*, pyrolysis), and Figures 4.5–4.8 include the results, which correspond to a water density of 0.00 g/cm³. In pyrolysis, H₂ and CH₄ production is nearly identical to that at the highest water densities investigated, but there is much less CO₂ and much more CO. This difference in CO and CO₂ yields can be attributed to the absence of the water-gas shift reaction, highlighting the importance of this reaction for H₂ production in a hydrothermal environment. Interestingly, the byproduct yields at these conditions tend to be comparable to or slightly higher than the low-

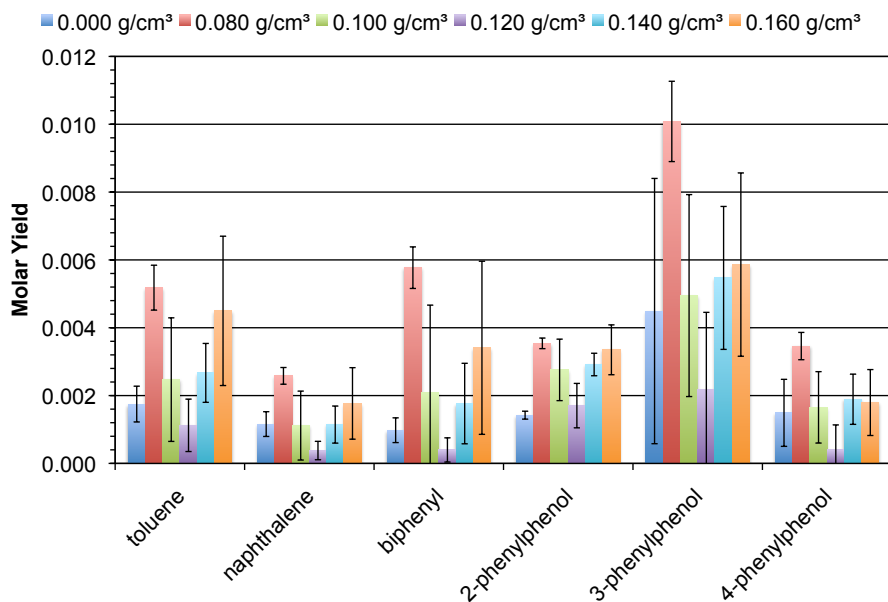


Figure 4.7: Effect of water density on yields of minor liquid phase intermediates from phenol SCWG (60 min, 600 °C, 0.100 mol/L phenol concentration).

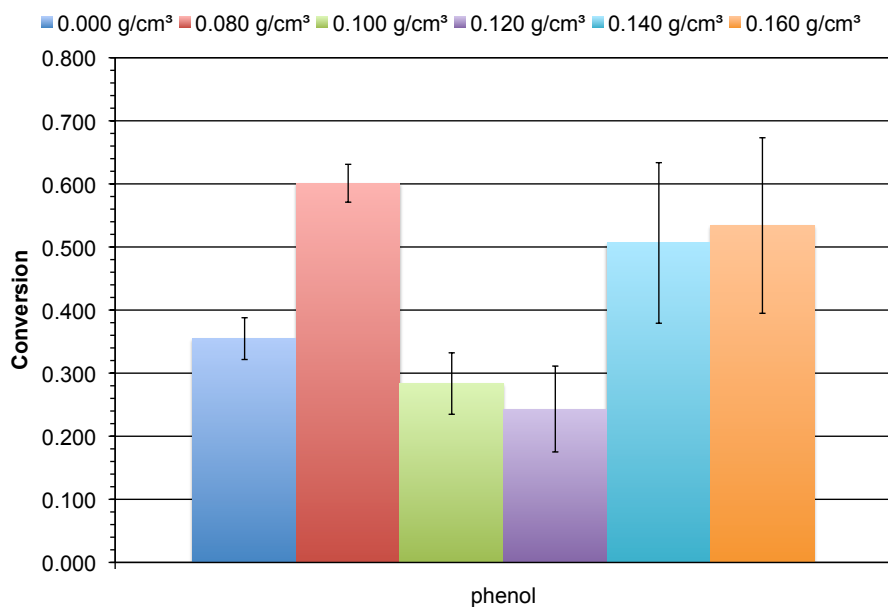


Figure 4.8: Effect of water density on conversion from phenol SCWG (60 min, 600 °C, 0.100 mol/L phenol concentration).

est yields obtained at an intermediate water density, but they are still much lower than the highest yields obtained at lower and higher water densities. The conversion of 35% for pyrolysis also follows this trend (*c.f.* Figure 4.8). These results indicate that the presence of water, and supercritical water more specifically, has a profound effect on the outcome of the reactions. The pyrolysis experiments also suggest that, on the water density continuum, there is not only a local minimum for conversion, but a local maximum as well.

4.4 Effect of initial concentration

DiLeo *et al.* investigated the effect of phenol loading as represented by its weight percent of the total material loaded into the reactor [51]. This variable depends on the water density, however, so we instead sought to decouple the influence of phenol and water by studying the effect of initial phenol concentration. To our knowledge, no other studies have isolated and examined this variable for uncatalyzed SCWG.

The initial concentration of phenol can influence SCWG outcomes if there are non-first-order reactions (*e.g.*, parallel reactions with different phenol reaction orders). From a technological standpoint, higher feedstock concentrations are desirable because they typically reduce capital and operating costs. If the feedstock concentration is low, more processing time is required to obtain the same absolute amount of product. On the other hand, high feedstock concentrations can lead to deposition and fouling problems, and this is especially true if there is an increase

in second-order polymerization reactions that produce char and tar byproducts.

Phenol SCWG experiments were carried out using five different initial phenol concentrations to determine the effect of this parameter on conversion and product yields. Figure 4.9 shows how the gas yields are affected by initial phenol concentration. As the initial concentration increases, the yields of CO and CO₂ decrease significantly while the respective yields of H₂ and CH₄ remain relatively constant or increase, resulting in a gas that is richer in H₂ and CH₄. This is a favorable outcome for commercialization of the SCWG process. One explanation for this trend is a reduction in decarbonylation and decarboxylation of phenol and phenolic derivatives, which give way to polymerization reactions at higher phenol concentrations. Another potential explanation is decreased combustion reactions, which produce CO and CO₂, at higher phenol/O₂ ratios. The molar yield of H₂ does not appear to be strongly affected by changes in initial phenol concentration, whereas the molar yield of CH₄ seems to increase slightly.

Figures 4.10 and 4.11 present the effect of initial phenol concentration on the molar yields of the most abundant intermediates. The trend here is similar to that in Figure 4.4 in that the yields of all compounds except for dibenzofuran increase, which is consistent with second-order reactions being favored and dibenzofuran acting as a gateway molecule to char formation. Unlike in Figure 4.4, however, the phenol conversion does not increase monotonically, but rather goes through a minimum value, as shown in Figure 4.12. This behavior implies there are at least two competing pathways by which phenol is consumed.

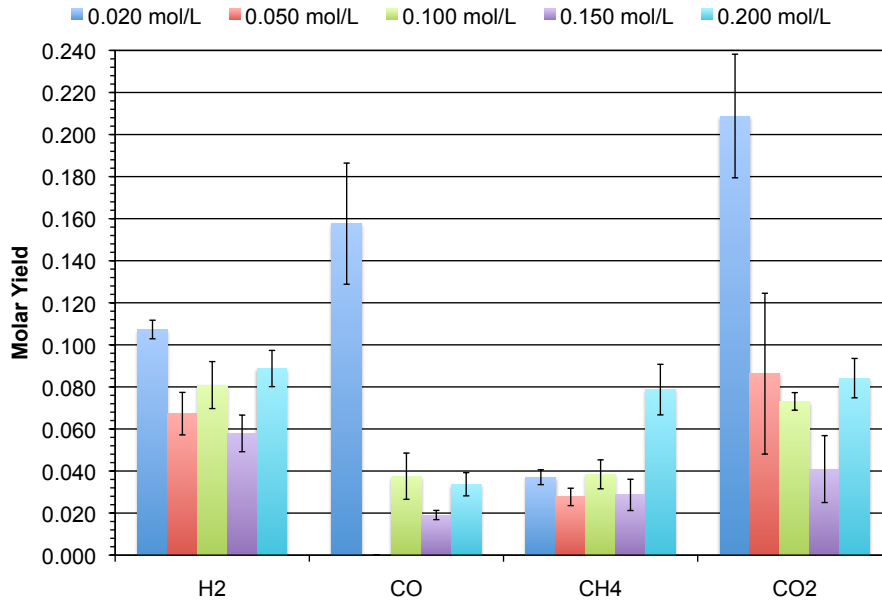


Figure 4.9: Effect of phenol concentration on gas yields from phenol SCWG (60 min, 600 °C, 0.120 g/cm³ water density).

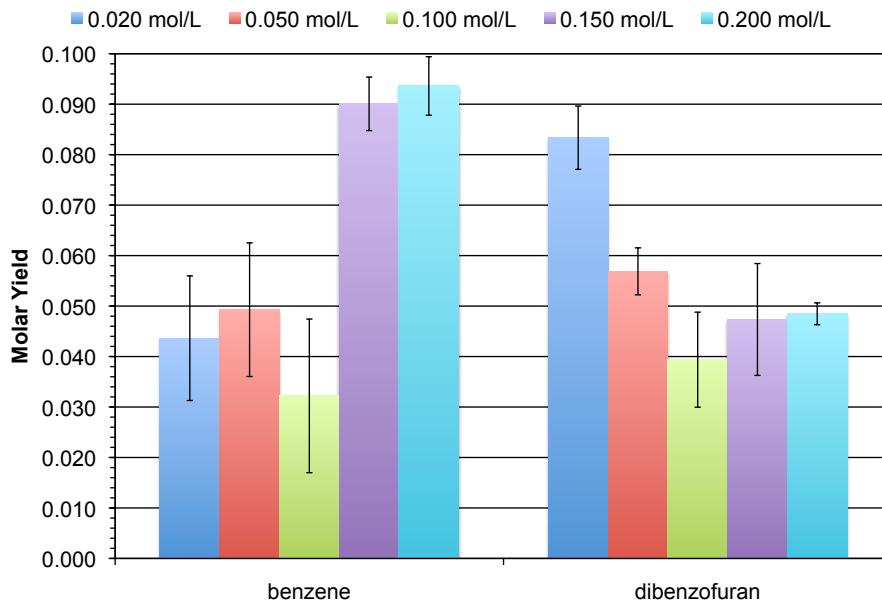


Figure 4.10: Effect of phenol concentration on yields of major liquid phase intermediates from phenol SCWG (60 min, 600 °C, 0.120 g/cm³ water density).

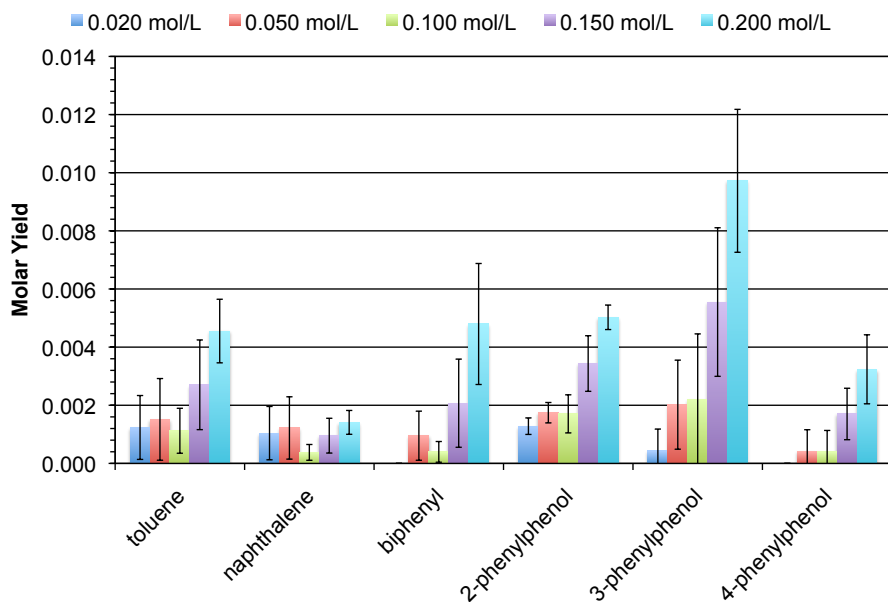


Figure 4.11: Effect of phenol concentration on yields of minor liquid phase intermediates from phenol SCWG (60 min, 600 °C, 0.120 g/cm³ water density).

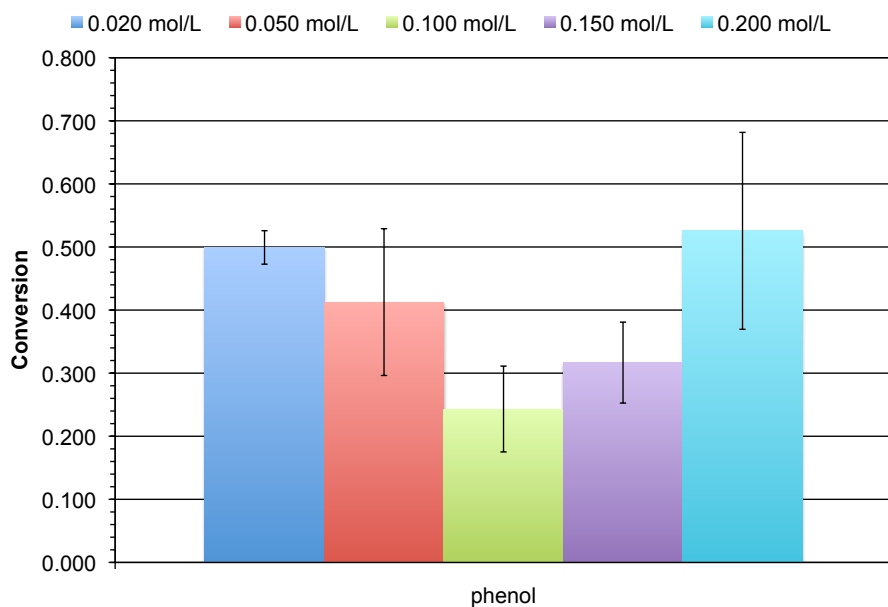


Figure 4.12: Effect of phenol concentration on conversion from phenol SCWG (60 min, 600 °C, 0.120 g/cm³ water density).

CHAPTER 5

Kinetics of Phenol Conversion

Chapter 4 discussed the effects of temperature, water density, and initial concentration on conversion and product yields from phenol SCWG. In this chapter, experimental conversion data (*c.f.* Table 4.1) informs the development of a phenol SCWG kinetics model that can account for these effects.

5.1 Modeling of water density effects

The competing water density effects observed in Section 4.3 (*i.e.*, high conversion at low water density, low conversion at intermediate water density, and high conversion at high water density) have appeared for other reactions in supercritical water. [Henrikson et al.](#) documented these same dual effects in their study of water density on phenol oxidation in supercritical water. Increasing water density inhibited the reaction at low water densities but accelerated it at high water densities [120, 121]. [DiLeo et al.](#) encountered the competing effects of water in their investigation of phenol SCWG, but the trend manifested as an optimum conversion at some intermediate water density rather than a minimum [51]. It is possible this

maximum is the same one implied by the 0.000–0.100 g/cm³ water density range in Figure 4.8. Oshima *et al.* encountered inhibition due to increasing water density in the density range they investigated, which manifested as a negative reaction order for water in their phenol oxidation model [122]. There are examples in the literature of water density-dependent reaction rates for other feedstocks. Henrikson *et al.* developed a detailed chemical kinetics model that accounts for higher water concentrations promoting supercritical water oxidation of methanol [123]. Rate analysis showed the generation of highly reactive hydroxyl radicals was largely responsible for this dependence. Fujii *et al.* also observed increased conversion of methanol with increasing water density in SCWO experiments, and they likewise explained this increase as a result of increased reaction with water and hydroxyl radical production [124].

The question arises of how to model the observed effect of water density on the overall kinetics of phenol consumption in SCW. One obvious approach is the inclusion of water concentration in the reaction rate equation. This was the approach taken by Thornton and Savage and Gopalan and Savage in their kinetic modeling of phenol SCWO [104, 105]. A non-zero reaction order in water implies that water is an active participant in the conversion of phenol either as a collision partner or as a reactant, and this notion is certainly substantiated by the broader SCW literature. Incorporating water concentration into the rate equation is not the only approach one could take to modeling the water density dependence of reaction rates, however. Water density effects might also be captured by a model using activation volume or rate coefficients that are functions of the density or dielectric

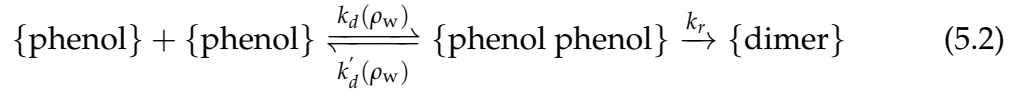
constant [125, 126, 127, 128, 129]. As mentioned previously, the dielectric constant of water is much lower under supercritical conditions than the value of about 78 at ambient conditions, but it still varies with water density. At 600 °C, for example, the dielectric constant ranges from about 1.34 at a density of 0.080 g/cm³ to 2.03 at a density of 0.160 g/cm³ [130]. Consequently, all these variables—water concentration, density, activation volume, and dielectric constant—can be said to play a role in the rate because they are interrelated. Since water concentration must be included in the reaction rate equation to model hydrothermal reactions anyway, it is expected this will be sufficient to account for other complicating water density effects as well. Using water concentration to model all these water-dependent effects is therefore primarily a matter of convenience.

It is necessary to construct a kinetic model capable of capturing the inhibitive and accelerative effects observed in Section 4.3. Inclusion of water concentration raised to some positive power in the reaction rate equation models the accelerative behavior, since the reaction rate will increase as water concentration increases. This approach adequately describes the kinetics of hydrothermal (*i.e.*, water-participatory) reactions. For an inhibitive effect in which the reaction rate decreases with increasing water density, however, the exponent of the water concentration term in the reaction rate equation must be negative. One manner in which such an equation might arise is due to a diffusion-controlled reaction rate. Invocation of diffusion limitations to explain water-inhibited behavior is predated, but not previously modeled, in SCW literature [9, 119]. The conventional way to model such an effect for a bimolecular reaction is with a reversible diffusion

step, as shown in Equation 5.1,



where k_d is the bimolecular rate coefficient for diffusion of reactive solutes toward each other, k'_d is the dissociative rate coefficient for diffusion of reactive solutes away from each other, and k_r is the reaction rate coefficient. In the case of phenol as a reactant in SCW, species A and B would both be phenol molecules and/or phenoxy radicals that must diffuse into the same water cage prior to reaction into some kind of phenolic dimer, C, as in



Phenol concentration would thus appear in the reaction rate equation, and the diffusion rate coefficients, k_d and k'_d , would be functions of the water density, ρ_w . Assuming the cage complex $\{\text{phenol phenol}\}$ exists in very small concentrations in order to apply a steady state approximation, the rate of phenol conversion would then take the form of Equation 5.3,

$$\text{rate} = \frac{k_d(\rho_w) k_r}{k_r + k'_d(\rho_w)} [\text{phenol}]^2 = k_{\text{eff}}(\rho_w) [\text{phenol}]^2 \quad (5.3)$$

where k_{eff} is the effective or observed reaction rate coefficient.

It is convenient here to compare rate coefficients and thereby reveal limiting cases that lead to simplified forms of k_{eff} . In one case, $k_r \gg k_d, k'_d$, and k_{eff} reduces

to k_d . Equation 5.3 thus simplifies to

$$\text{rate} = k_d(\rho_w) [\text{phenol}]^2 \quad (5.4)$$

This case represents a reaction that is diffusion controlled. [Henrikson and Savage](#) found diffusion influence on reaction rates to be a plausible explanation for the inhibitive effect of water density in phenol SCWO, noting that the variation of diffusion coefficients with water density closely resembles the variation of phenol conversion with water density [121]. Experiments have shown that doubling water densities in this region leads to a halving of the self-diffusion coefficient in water [131]. Since phenol diffusivity in supercritical water is likewise inversely correlated to water density [132], so, too, are the diffusion rate coefficients, k_d and k'_d . Consequently, the dimerization reaction could become more and more diffusion controlled as water concentration increases. For convenience, this inverse correlation can be modeled adequately by retaining a water-independent k_{eff} and absorbing the water density inverse-dependence into a negative reaction order in water, b :

$$\text{rate} = k_{\text{eff}} [\text{phenol}]^2 [\text{H}_2\text{O}]^b, b < 0 \quad (5.5)$$

Writing a more generalized reaction rate equation that could account for many different kinds of reactions, including hydrothermal ones, leads to

$$\text{rate} = k_{\text{eff}} [\text{phenol}]^a [\text{H}_2\text{O}]^b \quad (5.6)$$

In the other case, $k_r \ll k_d, k'_d$, and k_{eff} reduces to $k_r K_d$. This case represents a reaction that is activation controlled. Although such a situation would not be able to account for the inhibitive effect of water density, it would still be modeled well by a water-independent k_{eff} and explicit terms for phenol concentration and water concentration. If the theory that H₂O molecules readily solvate their reaction partner in SCW is correct, reactions with water (*i.e.*, hydrothermal reactions) are expected to be activation controlled.

It must be reiterated that the preceding equation development for diffusion-controlled reactions of phenol in SCW merely shows one manner in which a water concentration term might arise in the denominator of the reaction rate equation. No claim is being made here that diffusion limitations are solely responsible for the water density inhibitive effect described in Section 4.3, nor is a water concentration term in the denominator the only way of modeling such an effect. For example, yet another way one might choose to model the inhibitive effect of water density is with an activation barrier term to describe a reorganization energy associated with shedding of waters in a solvent cage when two reactive solutes come together. Again, the inclusion of a water concentration power law term in the reaction rate equation is merely a convenient way to model the water density effects of Section 4.3 in the absence of any conclusive explanation for those effects.

5.2 Modeling of initial concentration effects

Examination of the effect of initial phenol concentration on conversion in Section 4.4 led to a hypothesis that there are at least two competing pathways by which phenol is consumed. A scenario that would be consistent with these results involves one path having an apparent reaction order for phenol that is less than one, such that the initial rate of phenol consumption increases more slowly than the initial phenol concentration. If this path is dominant at low initial phenol concentrations, it would explain the decreasing conversion in this region. If the amount of phenol consumed increases more slowly than the initial amount of phenol increases, the conversion will decrease with increasing initial phenol concentration. The second pathway would be less important at low phenol concentrations, and it could account for the increasing conversion as initial phenol concentration increases if it is greater than first-order in phenol.

Taking Equation 5.6 as a starting point, a rate law expression for the consumption of phenol by two competing pathways would take the form

$$-\frac{d[\text{phenol}]}{dt} = \text{rate} = k_1(T)[\text{phenol}]^a[\text{H}_2\text{O}]^b + k_2(T)[\text{phenol}]^c[\text{H}_2\text{O}]^d, \quad a \geq 1 \geq c \quad (5.7)$$

The presence of these two competing paths could also explain the trends in Section 4.3, which were suggested to be a result of competing thermal and hydrothermal reactions. Thermal reactions, represented by the k_1 term in Equation 5.7, are expected to take a reaction order in phenol greater than or equal to unity (*i.e.*,

$a \geq 1$), since bimolecular thermal reactions require multiple phenol molecules. For such reactions to occur, the reactants would have to navigate a superabundance of H₂O molecules, and the speculated diffusion limitation that results would correspond to an inverse correlation with water density that manifests as a negative reaction order in water, b , as discussed in Section 5.1. Hydrothermal reactions, represented by the k_2 term in Equation 5.7, are expected to take a reaction order in phenol less than or equal to unity (*i.e.*, $c \leq 1$), since bimolecular hydrothermal reactions would require at most one phenol molecule. These reactions would, by definition, depend upon water concentration such that the reaction order in water, d , is a positive value, and diffusion would likely not exert an influence on the reaction rate because phenol molecules would already be solvated with a cage of readily available H₂O molecules.

A rough pictorial explanation may be instructive. Figure 5.1 is a proposed schematic of *in situ* structure for phenol in SCW. It must first be noted that this proposed arrangement of structures was not drawn to give a realistic sense of space-averaged concentration and scale or of molecular orientation. For example, water molecules outnumber phenol molecules by approximately two orders of magnitude in the experiments of Table 4.1 (the ratio in Figure 5.1 is lower, about 35). Speculative though it may be, Figure 5.1 could nevertheless help explain the proposed kinetic considerations that weigh on thermal *vs.* hydrothermal reactions. Despite H₂O not directly participating in thermal reactions as a reactant, the proposed schematic suggests that reactive solutes would need to traverse a minefield of H₂O molecules before reaction could occur. Most difficult, however, would be

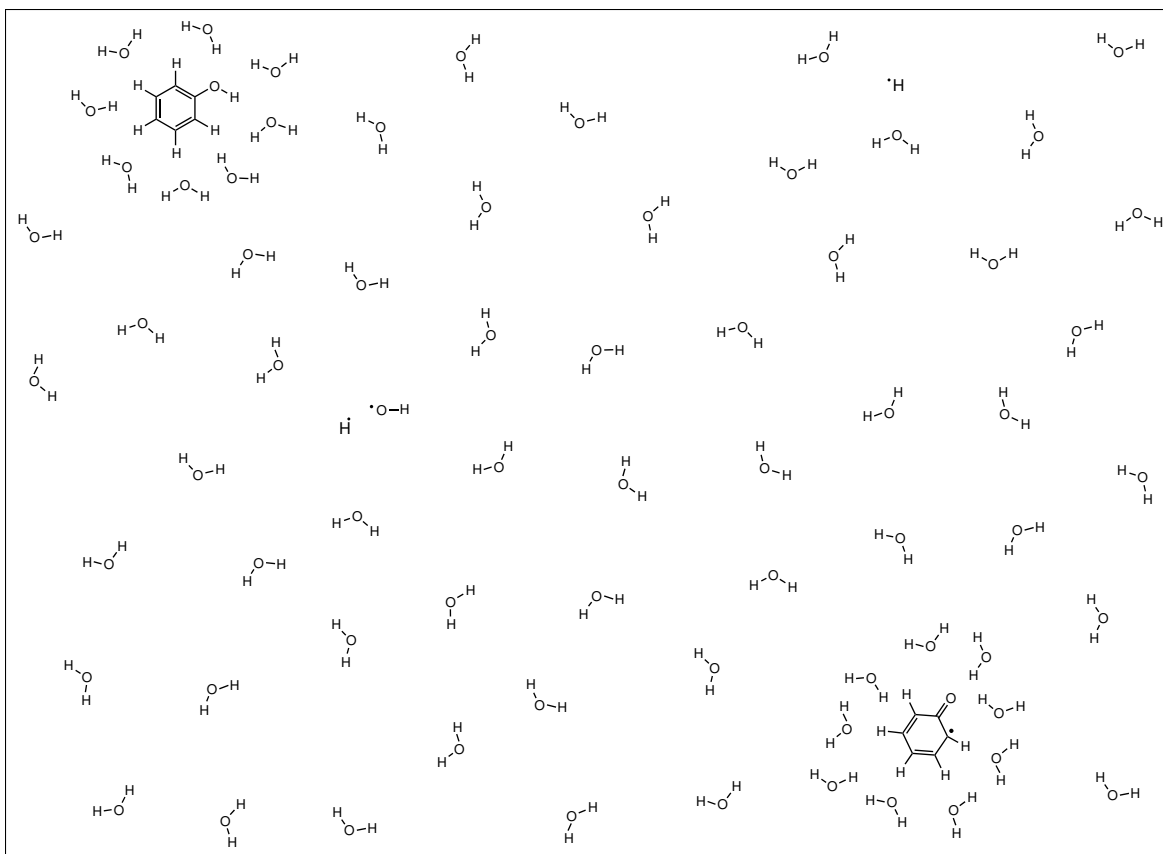


Figure 5.1: Proposed schematic of *in situ* structures for phenol in SCW. Note that ratios, orientations, and distances between species are not drawn with stringent accuracy.

solute penetration through a cage of water molecules, if it exists as conjectured in Figure 5.1. This could lead to strong dependence of the reaction rate upon diffusive mass transfer, which is in turn dependent upon water density. On the other hand, the superavailability of H₂O molecules highlights the ease with which hydrothermal reactions might initiate and the theoretical lack of any diffusion considerations for solute-water reactions. Figure 5.1 also depicts the hypothesized brief existence of some reactive free radicals (*e.g.*, hydroxyl, phenoxy, and H), which are thought to play an important role in high temperature supercritical water chemistry.

5.3 Data-fitting procedure and results

Having obtained a body of data revealing the influence of reaction time, temperature, water density, and initial concentration on phenol SCWG, the next step was to fit a kinetic model to the data in order to glean useful information about the reaction kinetics of phenol consumption. Analysis of the general effects of temperature, water density, and initial phenol concentration in Chapter 4 suggested a rate law of the form given by Equation 5.7.

A two-step data-fitting process was used. A best fit was obtained in each step by simultaneous numerical integration of Equation 5.7 using the Euler method and minimization of the sum of squared residuals for phenol conversion using Solver for Microsoft Excel 2008. This program employs the Generalized Reduced Gradient (GRG2) Algorithm for optimizing nonlinear problems developed by Leon Lasdon and Allan Waren [133]. The reaction orders in phenol were constrained by the bounds in Equation 5.7.

Since virtually all of the kinetic behavior due to changes in phenol and water concentration was observed at 600 °C, the reaction orders in phenol and water were first obtained by fitting the numerically-integrated Equation 5.7 to the 600 °C data. The water concentration was taken to remain invariant during reaction because it is in considerable excess. This data-fitting resulted in best-fit values for the reaction orders a , b , c , and d , as well as the rate coefficients $k_1(600\text{ °C})$ and $k_2(600\text{ °C})$.

In the second step, the temperature dependence of the rate coefficients was

modeled by the Arrhenius equation

$$k_i(T) = A_i \exp\left(-\frac{E_{ai}}{RT}\right) \quad (5.8)$$

where A is the pre-exponential factor and E_a is the activation energy. Inserting Equation 5.8 into Equation 5.7 and fitting this expanded model (with fixed a , b , c , and d) to data at all temperatures resulted in best-fit values for A_1 , A_2 , E_{a1} , and E_{a2} .

Table 5.1 gives the kinetic parameters for phenol disappearance obtained through this two-step data-fitting process. Note that the value of -16.60 for one of the reaction orders simply indicates a strong inhibition by water (possibly, but not certainly, caused by diffusion limitations). It does not provide any specific chemical insight into the number of water molecules involved. The parity plot in Figure 5.2 compares experimental phenol concentration data with the values calculated by the model using these best-fit parameters. A perfect fit of the model to the data would result in all points lying on the diagonal in Figure 5.2. A coefficient of determination of 0.985 indicates the model describes the data very well, with reasonable scatter around the diagonal and no trends in the residuals. Included also in Figure 5.2 are concentration data from the phenol SCWG work by [DiLeo et al. \[51\]](#), and these data are in good agreement with predicted values and serve to validate our kinetic model. There are three data points from [DiLeo et al.](#) that are not well-predicted by the model; however, these points correspond to very low, near-critical densities outside the parameter space investigated here.

Table 5.1: Kinetic parameters for phenol conversion.

a	1.73
b	-16.60
c	0.92
d	1.39
A_1 ($\text{mol}^{15.87}\text{L}^{-15.87}\text{s}^{-1}$)	1.92×10^{15}
A_2 ($\text{mol}^{1.47}\text{L}^{-1.47}\text{s}^{-1}$)	4.42×10^{11}
E_{a1} (kJ/mol)	125
E_{a2} (kJ/mol)	280
R^2	0.985

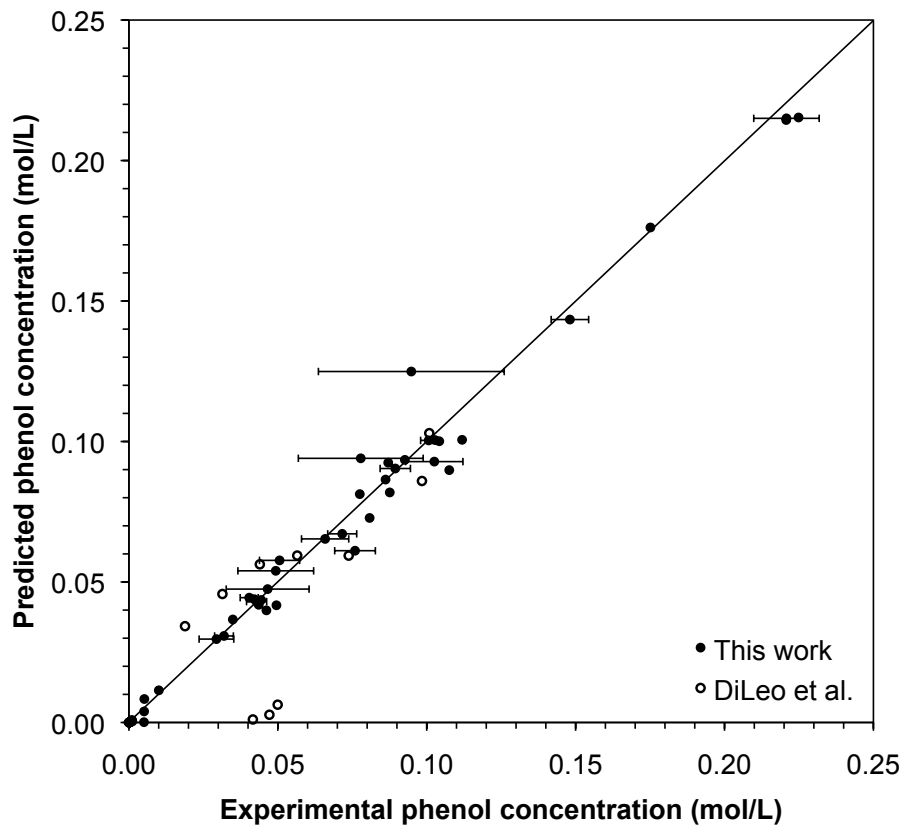


Figure 5.2: Comparison of experimental and predicted concentration values for phenol SCWG. Note that many data points overlap near the origin. Concentration data from previous experiments by [DiLeo et al.](#) are also shown [51].

5.4 Discussion

Kinetic modeling confirms that the experimental results can be explained by at least two competing paths with different rate laws for phenol consumption in SCWG. The thermal pathway reaction rate is 1.73 order in phenol and -16.60 order in water. A reaction order in phenol of 1.73 is consistent with the observation of a mix of mainly second-order phenol dimerization products (*e.g.*, dibenzofuran) and some first-order non-phenolic dimerization or hydroxyl displacement products (*e.g.*, 2-phenylphenol and benzene, respectively). A reaction order in water of -16.60 attests to the difficulty with which these reactions occur amongst H_2O molecules and indicates this pathway is strongly inhibited by water. The hydrothermal pathway reaction rate is 0.92 order in phenol and 1.39 order in water and is thus accelerated by water. A reaction order in phenol of 0.92 is consistent with mainly first-order phenol hydrolysis or steam reforming reactions and other, more complex, fractional-order reactions involving H_2O . A reaction order in water of 1.39 indicates the importance of H_2O molecules for such hydrothermal reactions to occur. Using these parameters, the kinetic model captures the trends observed for water density and initial phenol concentration discussed in Chapter 4.

Additionally, the experimentally observed temperature trends are modeled well by the Arrhenius equation, which gives activation energies of 125 and 280 kJ/mol for the water-inhibited and water-accelerated reactions, respectively. The activation energy for phenol consumption by water-accelerated reactions is higher in magnitude than that for SCWG of glucose (121 kJ/mol) [134], whereas that for

the water-inhibited reactions is about the same. This further highlights the relative difficulty with which phenol reacts in supercritical water. In SCW, there is a fight between accessibility and reactivity. Thermal pathways involving phenol and other non-H₂O molecules possess a lower barrier to reaction as evidenced by the activation energy of 125 kJ/mol; however, these molecules have difficulty finding each other in a sea of H₂O. On the other hand, hydrothermal pathways involving H₂O molecules are greatly favored in terms of reactant access, but the barrier to reaction is much higher at 280 kJ/mol. This activation energy for phenol consumption by hydrothermal reactions is also greater than those given earlier for gas and char formation, indicating that the breaking down of phenol under hydrothermal conditions is the difficult first step, but forming gases from the fragments or char from dimers is easier.

As previously stated, the observation and modeling of both inhibition and acceleration by supercritical water is not surprising in light of previous work by [Lawson and Klein](#) and [Henrikson et al.](#), which documented and modeled the same effect, albeit for different reactions in supercritical water [119, 120, 121]. In contrast to conventional gasification, which relies upon pyrolysis and combustion reactions, the overwhelming presence of H₂O molecules in SCWG assists by isolating reactants from each other, thereby hindering tar- and char-forming second-order reactions. H₂O molecules also assist in first-order reactant decomposition, but, as a tradeoff, the rate is slower than in a purely thermal process. This result clarifies all previous modeling work with phenol SCWG, which assumed first-order kinetics for phenol disappearance.

CHAPTER 6

Reaction Pathways

In this chapter the reaction pathways for phenol SCWG are investigated. This investigation is informed by experimental data already obtained, additional experiments in which dibenzofuran and benzene served as the reactant, and results from the literature. Elucidation of reaction pathways will then serve as a foundation for the development of a kinetic model in Chapter 7.

6.1 Primary products

A first step in analysis of reaction pathways is the identification of primary products (*i.e.*, products that form directly from the reactant), and this is most simply done by considering product selectivities at low conversions. The y-intercept of a plot of selectivity (moles of product formed per mole of reactant consumed) versus conversion, known as a first-rank Delplot [135], visually expresses the initial selectivity. If data plotted on a first-rank Delplot extrapolate to a non-zero y-intercept, then the product is primary because it forms when only the reactant is present. If the y-intercept is zero, then the product is non-primary.

Figure 6.1 shows Delplots for dibenzofuran and benzene. These data are from phenol SCWG experiments carried out previously at three temperatures (500, 600, and 700 °C), two water densities (0.079 and 0.180 g/cm³), and various phenol loadings (0.044–0.216 mol/L). The Delplot for dibenzofuran has a non-zero y-intercept (of approximately 0.40), indicating that dibenzofuran is a primary product. Furthermore, for every mole of phenol initially reacting, 0.80 moles of phenol dimerize to directly form 0.40 moles of dibenzofuran (*i.e.*, the initial selectivity to dibenzofuran is ~40%). Benzene is likewise a primary product, since its y-intercept is non-zero. This non-zero intercept is more apparent from the 600 °C data, since benzene yields (and hence selectivities) were so low at 500 °C. Regardless, the data suggest that initially 0.01–0.20 moles of benzene form directly for every mole of phenol that reacts (*i.e.*, the initial selectivity to benzene is anywhere from 1 to 20% depending on the temperature). These two products account for nearly all phenol consumption at the outset of the reaction. For the conditions investigated in this study at least, it seems SCWG of phenol is tantamount to SCWG of dibenzofuran and benzene.

Mechanistically, high temperature SCWG is dominated by the chemistry of free radicals [50]. Pyrolytic studies with phenol have shown that resonance-stabilized phenoxy radicals rapidly form—releasing hydrogen atoms—and are largely responsible for phenol decomposition [114, 95, 98]. These phenoxy radicals combine with each other at the *ortho* position and, after intramolecular dehydration, produce dibenzofuran [108, 136]. Hydrogen atoms quickly pair with each other to evolve H₂ gas or displace the hydroxyl groups of intact phenol molecules to form

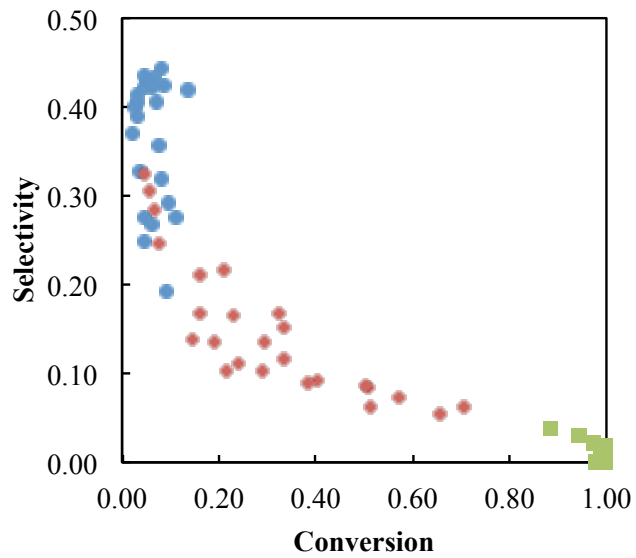
benzene [95, 98, 115].

Additional Delplots for other species in the reaction, including gases, did not reveal any other products with obviously non-zero initial selectivities; therefore, the only significant primary pathways available to phenol in SCWG appear to be dehydroxylation to benzene or dimerization to dibenzofuran. Figure 6.1a shows the selectivity of dibenzofuran decreases with increasing conversion. This result, which is not unexpected, indicates dibenzofuran participates in secondary reactions. We previously observed a decrease in dibenzofuran yield and an increase in char yield between 600 and 700 °C and postulated dibenzofuran may be a key gateway molecule for char formation pathways (*c.f.* Chapter 4). The findings discussed above prompted SCWG studies in which dibenzofuran or benzene is the reactant.

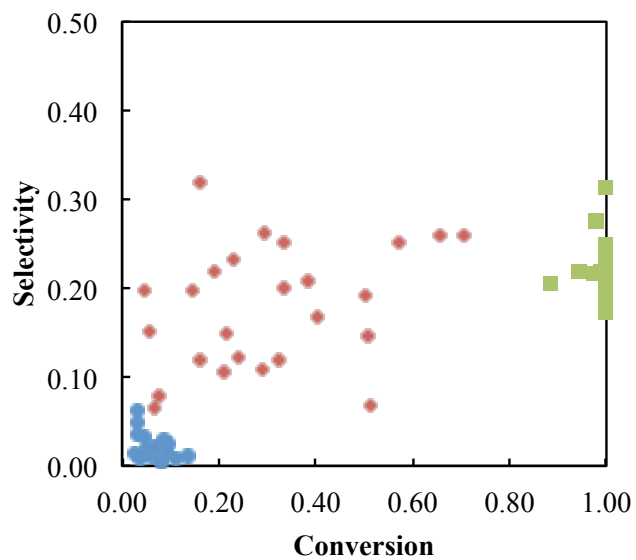
6.2 Dibenzofuran SCWG

SCWG experiments were carried out with dibenzofuran as the reactant to elucidate its reaction pathways in SCW. The water density was set at 0.18 g/cm³ (or 10. mol/L). Five different temperatures were explored (500, 550, 600, 650, and 700 °C) at a 0.10 mol/L dibenzofuran initial concentration and 30 minute reaction time, with at least three replicate reactions per temperature. Select results of these experiments are presented in Figures 6.2–6.5. Complete data obtained from these experiments are tabulated in Table A.1 in Appendix A.

Yields of dibenzofuran, benzene, and carbon are plotted as a function of tem-



(a)



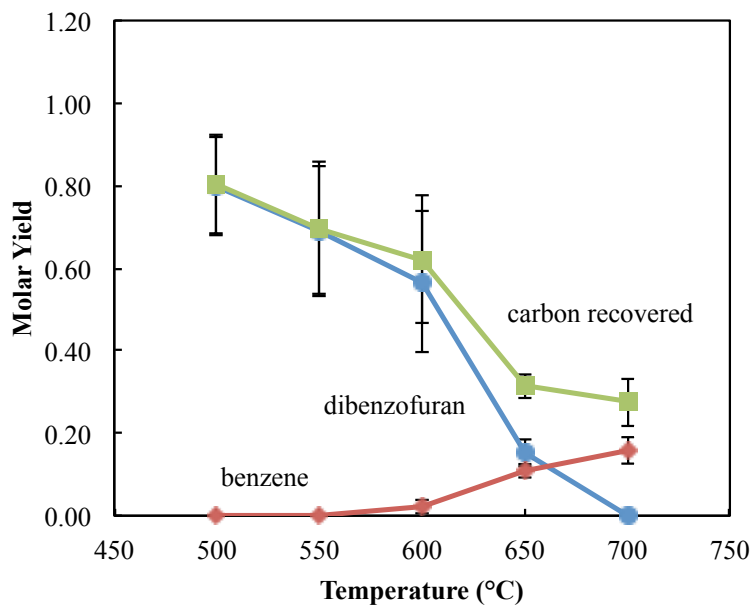
(b)

Figure 6.1: Delplots for (a) dibenzofuran and (b) benzene from phenol SCWG at 500 (●), 600 (◆), and 700 °C (■).

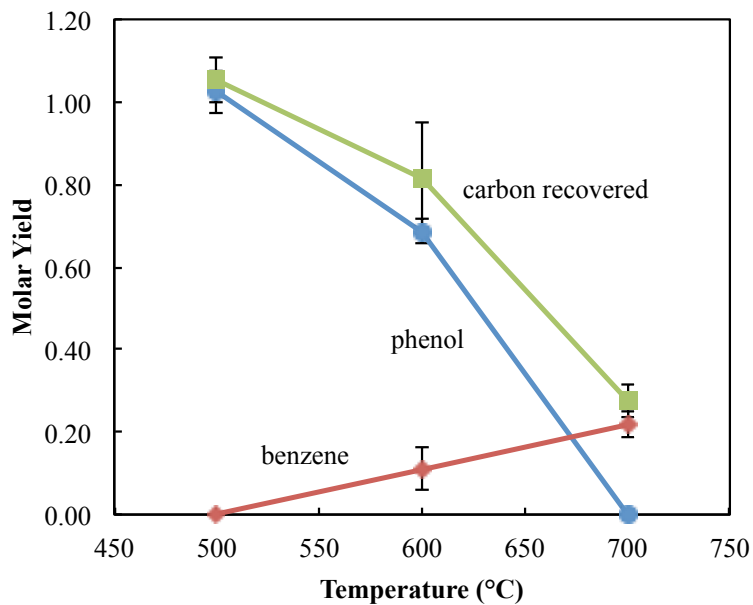
perature in Figure 6.2a. Dibenzofuran yield decreases (and conversion increases) steadily with increasing temperature through 600 °C, but there is a larger decrease in the yield (increase in conversion) from 600 to 650 °C that coincides with a significant drop in carbon recovery. Since this is the temperature range in which visible solid deposition (“char”) is observed on the quartz reactor walls, we attribute the drop in carbon recovery to thermal reactions that produce unrecoverable char from dibenzofuran. These thermal reactions also result in greater yields of liquid-phase products, such as benzene, above 600 °C.

To make a comparison between dibenzofuran and phenol SCWG, results for the latter at identical conditions are shown in Figure 6.2b. The comparison is made on the basis of identical initial atomic carbon concentration to account for the fact that two molecules of phenol must react to form one molecule of dibenzofuran. Figures 6.2a and 6.2b contain very similar trends, and this similarity reaffirms the notion that phenol SCWG is well-approximated by SCWG of dibenzofuran and benzene and that the primary pathways by which phenol reacts are responsible for these two species. The only apparent difference between the results from these two sets of experiments is slightly lower conversion and higher benzene yields at moderate temperatures when the reactant is phenol rather than dibenzofuran. While generally more stable than dibenzofuran at temperatures in the 500–600 °C range, phenol may still decompose to produce benzene more directly *via* its primary pathway.

The effect of temperature on gas yields from both dibenzofuran and phenol gasification is shown in Figure 6.3. We use a carbon atom basis and present the



(a)

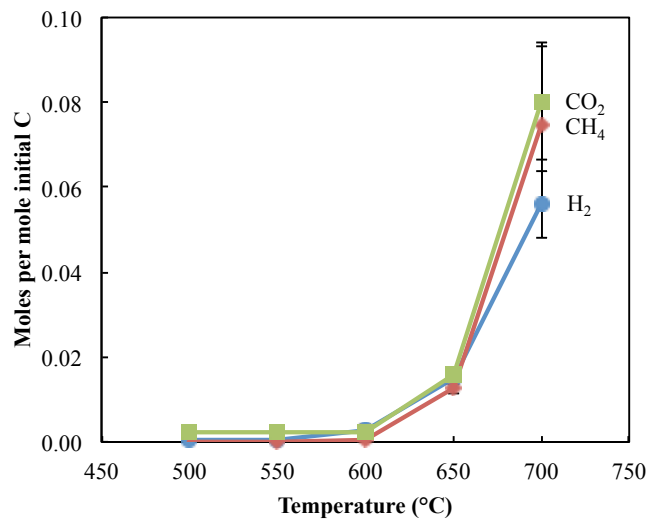


(b)

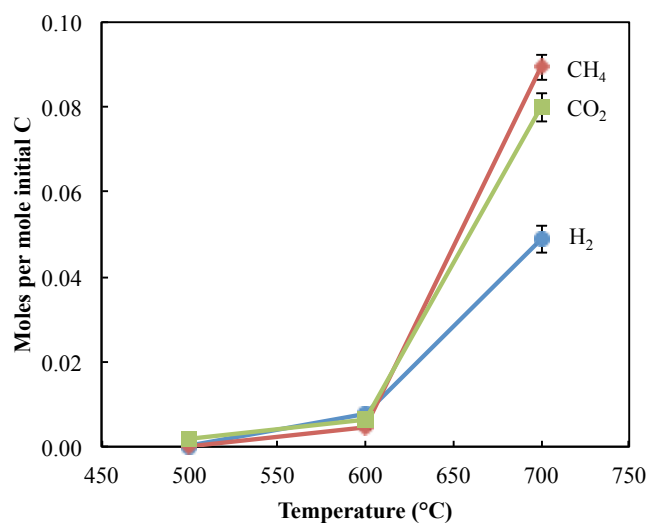
Figure 6.2: Effect of temperature on yields of the reactant (●), benzene (◆), and carbon (■) from (a) dibenzofuran SCWG and (b) phenol SCWG (30 min, 0.18 g/cm³ water density, 1.2 mol/L atomic carbon concentration).

moles of gas per mole of initial carbon atoms since a phenol molecule has half the atomic carbon of dibenzofuran. Note the yields of H₂, CH₄, and CO₂ from dibenzofuran (Figure 6.3a) are nearly identical to those from phenol (Figure 6.3b) at identical reaction conditions. These results confirm dibenzofuran serves as a key gateway molecule not just for char formation pathways, but also for gas formation pathways.

By far, the most abundant liquid phase product from dibenzofuran SCWG was benzene (*c.f.* Figure 6.2a), but many other liquid phase products were observed in lower concentrations. Figure 6.4 shows the temperature dependence of molar yields for the next three most abundant of these products: phenol, biphenyl, and 2-phenylphenol. Notably, the presence of phenol suggests reversibility of phenol dimerization; however, since benzene is so prevalent, it is more likely that dibenzofuran preferentially decomposes to yield a molecule each of phenol and benzene. 2-phenylphenol, abundant at moderate temperatures, probably also forms directly from dibenzofuran. The yields of all three products increase with increasing temperature up to some maximum value, after which the yields decrease. The maximum yield is observed around 600 °C for 2-phenylphenol and around 650 °C for phenol and biphenyl. These compounds thus become increasingly unstable at higher temperatures and react further to produce secondary products. In fact, the structures of these compounds and the thermal progression of their yield maxima suggest that phenol and 2-phenylphenol contribute to biphenyl production. It is likely 2-phenylphenol leads directly to the formation of biphenyl, which only accumulates at extreme temperatures. There is precedence for this reaction pathway in



(a)



(b)

Figure 6.3: Effect of temperature on moles of H₂ (●), CH₄ (◆), and CO₂ (■) formed per mole of initial carbon from (a) dibenzofuran SCWG and (b) phenol SCWG (30 min, 0.18 g/cm³ water density, 1.2 mol/L atomic carbon concentration).

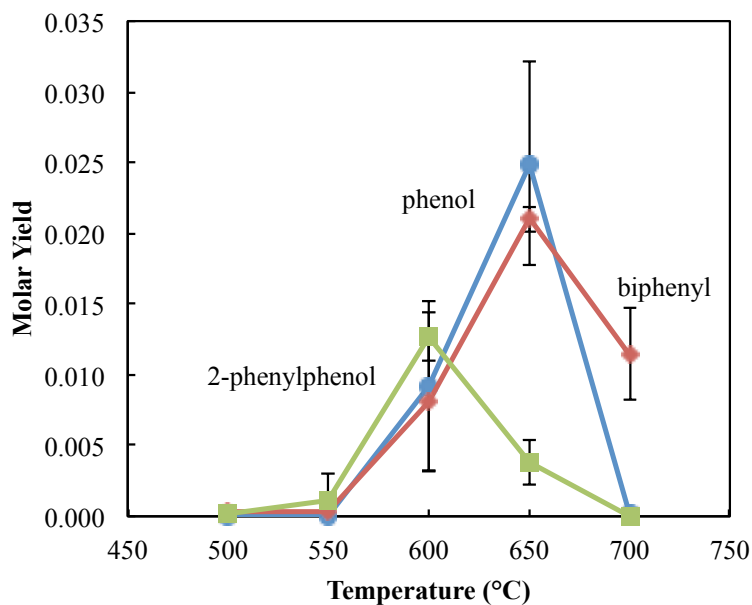


Figure 6.4: Effect of temperature on yields of phenol (●), biphenyl (◆), and 2-phenylphenol (■) from dibenzofuran SCWG (30 min, 0.18 g/cm³ water density, 0.10 mol/L dibenzofuran concentration).

that it is chemically analogous to the direct transformation of phenol into benzene as summarized in Section 6.1: a hydroxyl group on the aromatic ring is replaced by a hydrogen atom.

Many polycyclic aromatic hydrocarbons (PAHs) were detected in low concentrations when dibenzofuran underwent SCWG, and the yields of some of these compounds are shown in Figure 6.5. The trends for these PAHs generally adhere to a pattern of increasing molar yield with increasing temperature, particularly once the temperature surpasses 600 °C. Pyrene, however, while detected at 650 °C, disappears entirely at 700 °C. Pyrene may become unstable at this harsh temperature and form larger polycyclic molecules that remain undetected as a result of either limited solubility in acetone, which was used to recover these products, or the limitations of our chromatographic method. Regardless, Figures 6.2–6.5 show

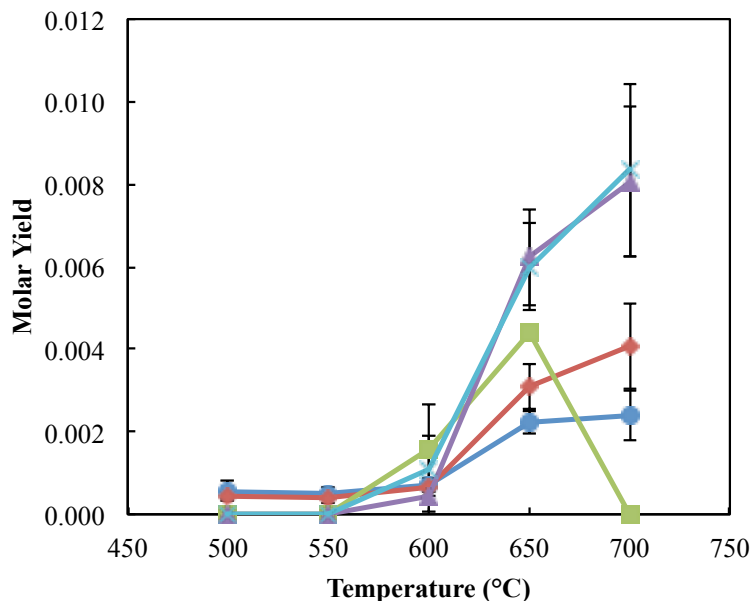


Figure 6.5: Effect of temperature on yields of fluorene (●), anthracene/phenanthrene (◆), pyrene (■), triphenylene (▲), and naphthalene (×) from dibenzofuran SCWG (30 min, 0.18 g/cm³ water density, 0.10 mol/L dibenzofuran concentration).

a clear acceleration in reaction kinetics between 600 and 650 °C that results in more gas, liquid, and solid phase products.

6.3 Benzene SCWG

Although the results of phenol and dibenzofuran SCWG suggest benzene molecules are recalcitrant in SCW, we conducted several experiments at 600 °C with benzene as the reactant. The results of these experiments are shown in Table 6.1. The conversion and carbon recovery are actually comparable to those for dibenzofuran and phenol, and this indicates all three of these molecules have similar reactivities in SCWG at 600 °C. The only observed liquid phase products from benzene are phenyl oligomers: biphenyl and terphenyl. We thus have a second explanation

Table 6.1: Conversion and major product yields from benzene SCWG (30 min, 600 °C, 0.18 g/cm³ water density, 0.10 mol/L benzene concentration).

	Results
Fractional Conversion	0.329 ± 0.038
Fractional Carbon Recovery	0.842 ± 0.023
Product Molar Yield	
Benzene	0.671 ± 0.038
Biphenyl	0.071 ± 0.005
Terphenyl	0.009 ± 0.002
H ₂	0.085 ± 0.042
CH ₄	0.005 ± 0.003
CO ₂	0.041 ± 0.023

“-” indicates no peak was observed at all.

for biphenyl synthesis in phenol SCWG besides 2-phenylphenol dehydroxylation: benzene-benzene combination. Mechanistically, this reaction is initiated by H removal at high temperatures to form a phenyl radical. The phenyl radical then readily adds to benzene (or biphenyl, in the case of terphenyl formation), releasing a second H atom [137]. Ultimately these H atoms recombine to produce H₂ gas, making the overall reaction a kind of dehydrogenation. It is possible that analogous benzene-phenol dimerization reactions can also occur by this mechanism. As is the case with phenol and dibenzofuran, benzene SCWG produces very little gas initially, and the composition of this gas is consistent with dehydrogenation reactions in that it is mainly H₂ at 600 °C.

6.4 Reaction network for gas and primary products

Figure 6.6 depicts a reaction network model for phenol SCWG. The structure of this network was informed by the reaction pathways analyses detailed in Sections 6.1–

6.3. Pathway 1 (corresponding to k_1) and Pathway 4 (corresponding to k_4) represent phenol dimerization and dehydroxylation reactions to produce primary products dibenzofuran and benzene, respectively, as was discussed in Section 6.1. Pathways 3 and 5 account for benzene-phenol and benzene-benzene dimerization to phenylphenols and biphenyl, respectively, as suggested in Section 6.3. Pathway 2 represents conversion of dibenzofuran to gasifiable secondary products like 2-phenylphenol as discussed in Section 6.2. Pathway 6 reflects dibenzofuran decomposition to regenerate phenol and benzene (cf. Section 6.2). All non-primary liquid phase products, such as phenylphenols and biphenyl, were lumped together into a pseudo-component called “gasifiable products.” This lumped species directly produces gaseous molecules (*via* Pathways 7–10) to account for gasification reactions such as dehydrogenation, decarbonylation, and pyrolytic bond cleavage. Non-primary gasification pathways are consistent with Delplot results in Section 6.1. Pathway 11 describes the depletion of lumped gasifiable products by the formation of “stable products” that represent any refractory char precursor molecules that are more resistant to gasification. The reversible water-gas shift reaction is active under these conditions and was included in the network as Pathway 12. Another important hydrothermal reaction is steam reforming to produce H_2 and CO , which is represented by Pathway 13. Initially, the network also included the reversible methanation reaction; however, preliminary results revealed methanation exhibits virtually no product formation under these conditions, which is consistent with previous work [46].

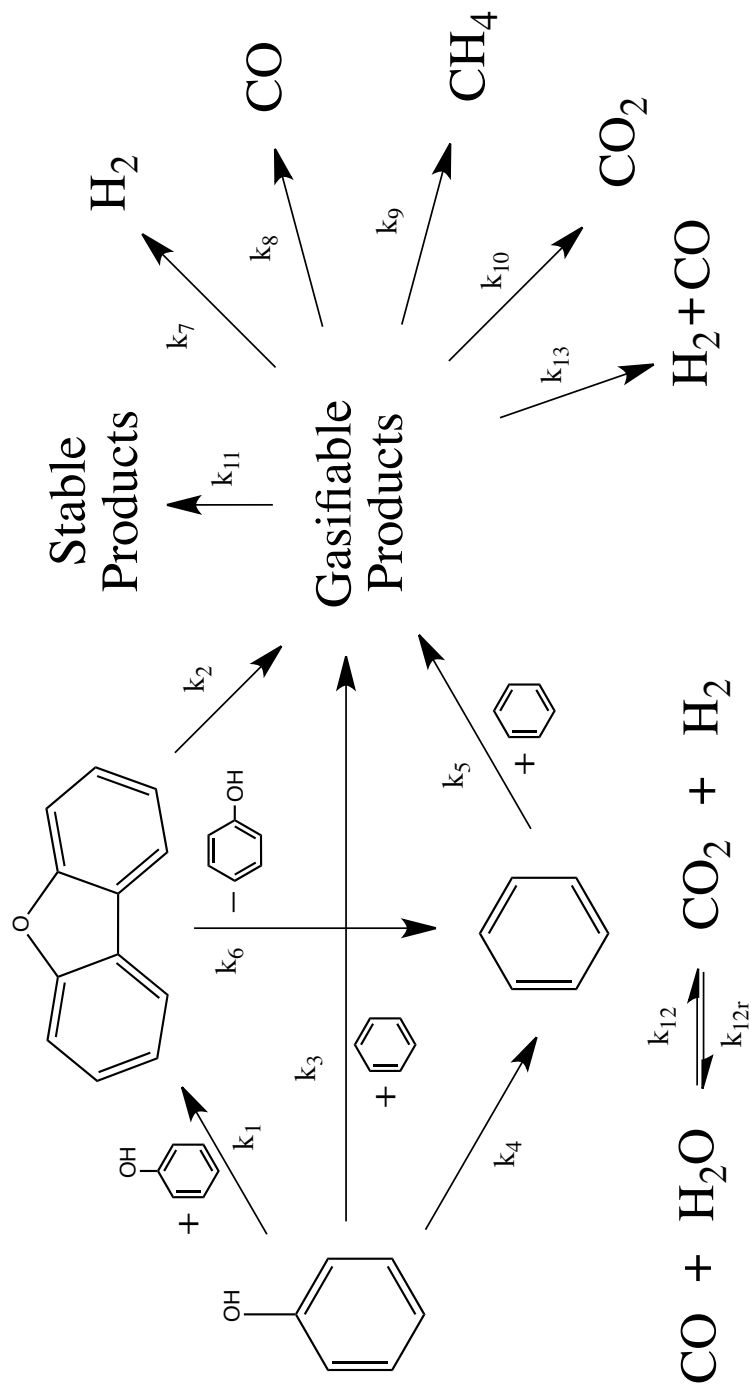


Figure 6.6: Phenol SCWG reaction network.

CHAPTER 7

Kinetic Model for Phenol SCWG Pathways

Chapter 6 concluded with the construction of a reaction network describing the formation and consumption of primary products and gases. This chapter showcases the development of a phenomenological kinetic model based on the reaction network that can accurately correlate and predict product yields from phenol SCWG

7.1 Reaction engineering

Reaction engineering principles guided the formulation of differential mole balances for modeled species. The kinetics for each pathway in Figure 6.6 were taken to follow the law of mass action. Water concentration was excluded from the rate law for steam reforming and other irreversible pathways, because water is in considerable excess and the initial concentration of water was invariant in the experiments. The exclusion of water concentration does not, however, mean that it is not reactive, only that its reactivity manifests as a constant factor that can be absorbed into the rate coefficient for each irreversible pathway. The “gasifiable products”

lumped species does not deplete *via* the gasification pathways, but only *via* Pathway 11 in Figure 6.6. Temperature dependence of the reaction rate coefficients was modeled with the Arrhenius relationship (*c.f.* Equation 5.8). The general form of the reaction rate equation for a given bimolecular pathway is thus denoted by Equation 7.1,

$$\text{rate} = r = A \exp\left(-\frac{E}{RT}\right) [\text{reactant 1}][\text{reactant 2}] \quad (7.1)$$

where A is the pre-exponential factor and E is the activation energy (collectively, “Arrhenius parameters”).

In a constant-volume batch reactor, a mole balance on species i will take the form of Equation 7.2,

$$\frac{dC_i}{dt} = \sum_j r_{ij} \quad (7.2)$$

where r_{ij} is the rate of reaction for component i in pathway j . Writing the mole balance for each species results in a system of i ordinary differential equations, which may be solved if initial concentrations and values for the Arrhenius parameters are given. In the model, there are $i = 10$ species and $j = 13$ independent reaction pathways, for a total of 26 parameters (*i.e.*, one pre-exponential factor and one activation energy per pathway).

The following lists the differential mole balance equations for each of the 10 species involved in the phenol SCWG kinetic model.

Mole balance on benzene:

$$\frac{d[\text{benzene}]}{dt} = -k_3[\text{benzene}][\text{phenol}] + k_4[\text{phenol}] - 2k_5[\text{benzene}]^2 + k_6[\text{DBF}] \quad (7.3)$$

Mole balance on phenol:

$$\frac{d[\text{phenol}]}{dt} = -2k_1[\text{phenol}]^2 - k_3[\text{benzene}][\text{phenol}] - k_4[\text{phenol}] + k_6[\text{DBF}] \quad (7.4)$$

Mole balance on dibenzofuran (denoted here by "DBF"):

$$\frac{d[\text{DBF}]}{dt} = k_1[\text{phenol}]^2 - k_2[\text{DBF}] - k_6[\text{DBF}] \quad (7.5)$$

Mole balance on lumped gasifiable products (denoted here by "GP"):

$$\frac{d[\text{GP}]}{dt} = k_2[\text{DBF}] + k_3[\text{benzene}][\text{phenol}] + k_5[\text{benzene}]^2 - k_{11}[\text{GP}] \quad (7.6)$$

Mole balance on lumped stable products (denoted here by "SP"):

$$\frac{d[\text{SP}]}{dt} = k_{11}[\text{GP}] \quad (7.7)$$

Mole balance on H₂:

$$\frac{d[\text{H}_2]}{dt} = k_7[\text{GP}] + k_{12}[\text{CO}][\text{water}] - k_{12r}[\text{H}_2][\text{CO}_2] + k_{13}[\text{GP}] \quad (7.8)$$

Mole balance on CO:

$$\frac{d[\text{CO}]}{dt} = k_8[\text{GP}] - k_{12}[\text{CO}][\text{water}] + k_{12r}[\text{H}_2][\text{CO}_2] + k_{13}[\text{GP}] \quad (7.9)$$

Mole balance on CH₄:

$$\frac{d[\text{CH}_4]}{dt} = k_9[\text{GP}] \quad (7.10)$$

Mole balance on CO₂:

$$\frac{d[\text{CO}_2]}{dt} = k_{10}[\text{GP}] + k_{12}[\text{CO}][\text{water}] - k_{12r}[\text{H}_2][\text{CO}_2] \quad (7.11)$$

Mole balance on water:

$$\frac{d[\text{water}]}{dt} = -k_{12}[\text{CO}][\text{water}] + k_{12r}[\text{H}_2][\text{CO}_2] \quad (7.12)$$

7.2 Equilibria calculations with ASPEN

Equilibrium concentrations and constants for the water-gas shift reaction were estimated using the RGibbs reactor module in Aspen Plus V7.3 with the Peng-Robinson equation of state property model. Peng-Robinson was chosen for its demonstrated applicability in supercritical water [138, 139, 140, 141]. Given initial concentrations of each species and the reaction conditions, the RGibbs block calculates equilibrium concentrations by minimizing the Gibbs free energy. The equilibrium constants, which relate forward and reverse rate coefficients, were then

determined from these output concentrations using Equation 7.13.

$$K_{12} = \frac{k_{12}}{k_{12r}} = \frac{[\text{H}_2][\text{CO}_2]}{[\text{CO}][\text{H}_2\text{O}]} \quad (7.13)$$

In all Aspen calculations, the input concentrations were 10. mol/L for water and averaged experimental concentrations for permanent gases. Since equilibrium constants are temperature-dependent, separate calculations were performed at each investigated temperature, and the temperature dependence was correlated using the van 't Hoff relationship,

$$K = \exp\left(-\frac{\Delta H}{RT} + \frac{\Delta S}{R}\right) \quad (7.14)$$

where ΔH is the enthalpy of reaction and ΔS is the entropy of reaction. These van 't Hoff parameters were determined through regression of the Aspen results, which resulted in an excellent fit. For the water-gas shift reaction in supercritical water, $\Delta H/R$ is -2975.5 K and $\Delta S/R$ is -3.1376 . Consequently, only the forward rate coefficient of the reversible water-gas shift reaction was treated as a variable in the kinetic model, because the reverse rate was set by the known equilibrium constant obtained from Equation 7.14.

7.3 Data-fitting with MATLAB

Code was written in MATLAB 7.12 to fit the kinetic model resulting from Section 7.1 to experimental data. Complete code for the MATLAB optimization pro-

gram can be found in Appendix B. The program repeatedly solves the set of ordinary differential equations describing mole balances for all species and adjusts the kinetic parameters to minimize an objective function. The MATLAB function `ode15s` was used to solve the system of ODEs, and the function `fminsearch` was used to accomplish the unconstrained nonlinear optimization for 26 kinetic parameters. The `fminsearch` function employs the Nelder-Mead simplex search algorithm of Lagarias et al. [142]. For each minimization, the algorithm was reset several times to overcome iterative stagnation that sometimes afflicts Nelder-Mead. The objective function for minimization was the summation of squared relative errors (SSRE) between the experimental concentration data and the values calculated by the phenol SCWG model, as given by Equation 7.15,

$$f(\mathbf{A}, \mathbf{E}) = \sum_n \sum_i \left(\frac{[\text{species } i]_n^{\text{experimental}} - [\text{species } i]_n^{\text{calculated}}(\mathbf{A}, \mathbf{E})}{([\text{species } i]_n^{\text{experimental}} + [\text{species } i]_n^{\text{calculated}}(\mathbf{A}, \mathbf{E})) / 2} \right)^2 \quad (7.15)$$

where n corresponds to a single experiment among all experiments we have conducted at a water density of 0.18 g/cm³ (116 total), and \mathbf{A} and \mathbf{E} are vectors of length j containing the pre-exponential factors and activation energies for every distinct pathway. Relative errors were used instead of absolute errors in order to give proportionate weight to the many experimental data points at low concentrations. All experimental data at a water density of 0.18 g/cm³, in Table 6.1, in Figures 6.2–6.4, and in Table 4.1, were modeled. To generate reasonable initial values for the Arrhenius parameters when fitting all of the data simultaneously, we first modeled the network as two separate subnetworks. First, only Pathways 1–6 were

Table 7.1: Kinetic parameters for the phenol SCWG network. The units for A_j and k_j are $\text{s}^{-1}(\text{L}/\text{mol})^{n-1}$, where n is the overall reaction order (excluding water) for pathway j .

	n	A	E (kJ/mol)
k_1	2	6.93×10^1	88
k_2	1	3.48×10^6	171
k_3	2	2.31×10^{-1}	13
k_4	1	2.17×10^8	201
k_5	2	4.01×10^{-2}	15
k_6	1	5.00×10^8	225
k_7	1	2.15×10^5	105
k_8	1	4.05×10^0	29
k_9	1	1.32×10^{16}	289
k_{10}	1	4.00×10^1	38
k_{11}	1	8.94×10^6	118
k_{12}	2	1.34×10^7	196
k_{12r}	2	3.10×10^8	221
k_{13}	1	3.35×10^{24}	449

modeled, and Arrhenius parameters were obtained for k_1 – k_6 . Next, the model was expanded to include Pathways 7–13, the Arrhenius parameters for k_1 – k_6 were held constant, and Arrhenius parameters were then obtained for k_7 – k_{13} . These Arrhenius parameters served as initial values for the final data-fitting, which optimized for all pathways simultaneously. This final data-fitting resulted in the Arrhenius values in Table 7.1.

7.4 Results and discussion

Figure 7.1 compares experimental and calculated concentrations for H_2 , phenol, dibenzofuran, and benzene at one set of conditions organized by temperature. Although the experimental data presented in each of these figures spans several orders of magnitude, the kinetic model generally does a good job of correlating

values and capturing the trends in concentration for phenol SCWG under these conditions. The model is generally most accurate at 30 min, the reaction time at which the majority of data was collected.

The parity plot in Figure 7.2 visually represents the goodness of fit by comparing all experimental concentration data with the values calculated by the model using the best-fit parameters in Table 7.1. A perfect fit of the model to the data would result in all points lying on the diagonal. Although there are no systematic trends in the residuals, there is considerable scatter around the diagonal, particularly at low concentrations. The largest outliers are for the low concentrations of dibenzofuran and phenol obtained at 700 °C. Dibenzofuran and phenol concentrations span many orders of magnitude at this temperature, and, consequently, the model commonly deviates from experimental results by an order of magnitude or more at low concentrations while still reliably capturing the results at high concentrations. Larger deviations at the very low concentrations are not problematic. Whether the final phenol concentration is on the order of 10^{-3} or 10^{-5} mol/L is of little consequence when the initial phenol concentration is $\sim 10^{-1}$ mol/L, since nearly all phenol is consumed in either case.

The Delplots created from experimental data in Figure 6.1 are reproduced in Figure 7.3 using the kinetic model at a 0.18 g/cm^3 water density. The initial selectivities toward dibenzofuran and benzene at 500 °C are comparable between experimental and calculated results, as are the trends in selectivity with respect to conversion and temperature. The selectivity depends weakly on the initial phenol concentration for a given conversion and temperature, and this dependence can be

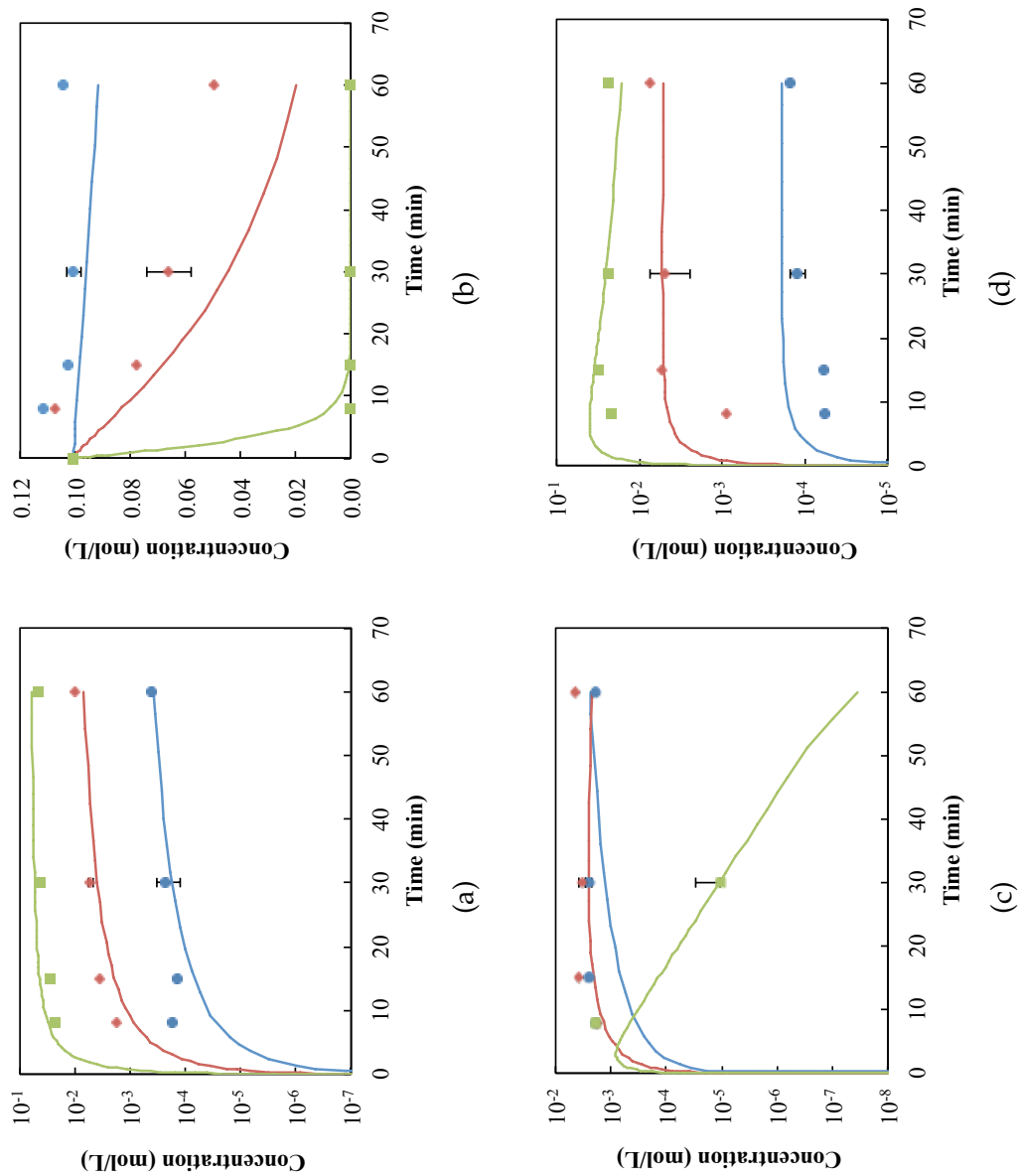


Figure 7.1: Comparison of experimental data and kinetic model at 500 (●), 600 (◆), and 700 °C (■) for (a) H₂, (b) phenol, (c) dibenzofuran, and (d) benzene (0.18 g/cm³ water density, 0.10 mol/L phenol concentration).

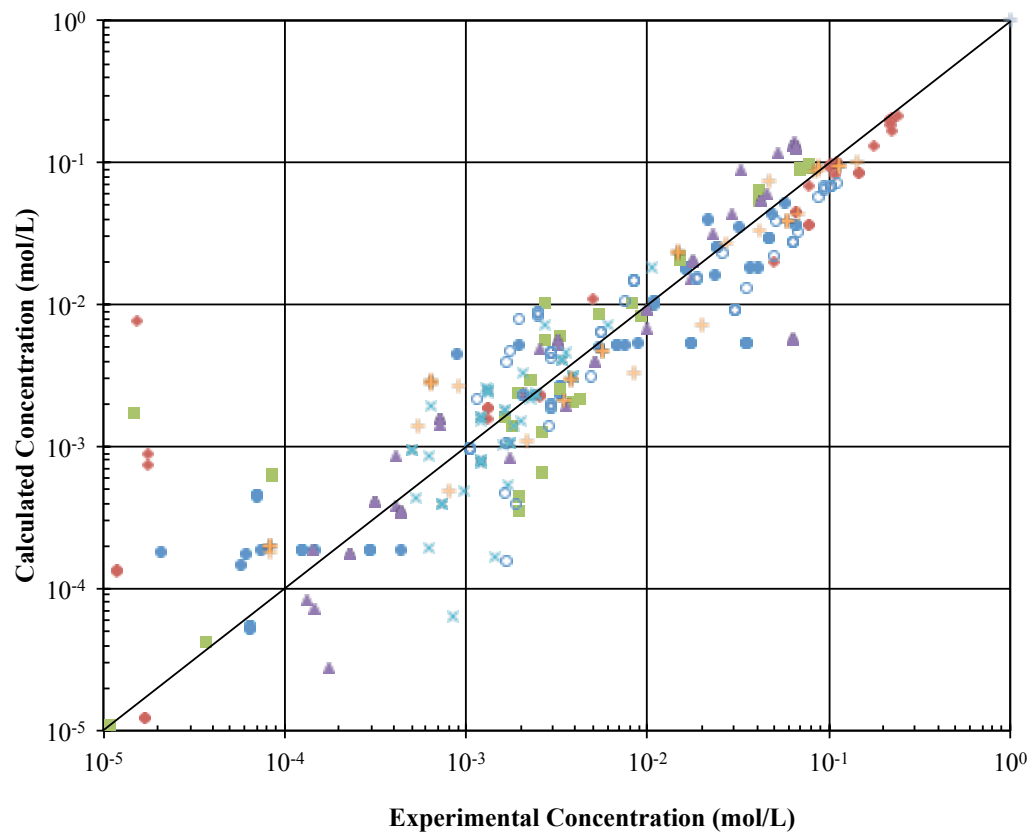


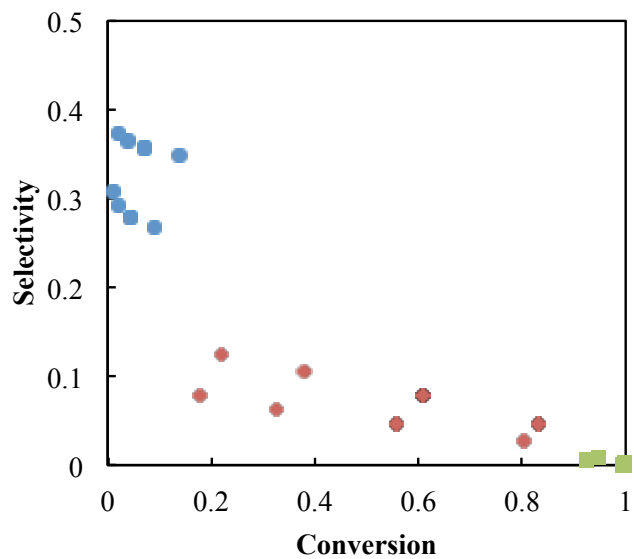
Figure 7.2: Comparison of experimental and calculated concentration values for benzene (●), phenol (◆), dibenzofuran (■), H_2 (▲), CO (×), CH_4 (+), and CO_2 (○) from phenol SCWG (0.18 g/cm^3 water density).

observed in some of the data points (note the two slightly different y-intercepts in Figure 7.3a for the data at 500 °C, which are at two different initial phenol concentrations). It should be noted that Figure 6.1 includes data for water densities other than 0.18 g/cm³, but this is the only water density featured in Figure 7.3 because the model does not account for differences in water density.

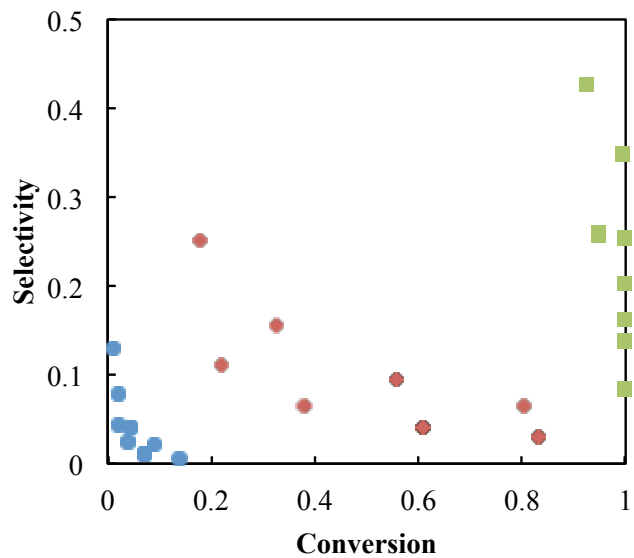
7.5 Rate analysis

Kinetic modeling results in Table 7.1 provide insight into the relative importance of different pathways when used to calculate reaction rates. The activation energies for phenol dimerization and dehydroxylation are 88 and 201 kJ/mol, respectively. These values are comparable in magnitude to those obtained for phenol consumption kinetics in Chapter 5. To our knowledge, no other kinetic parameters have been reported in the literature for any of these pathways under comparable SCWG conditions.

Rates of relevant pathways at demonstrative temperatures are presented for reaction species of interest in Figures 7.4–7.7. The rates of pathways that produce or consume H₂ in phenol SCWG are presented in Figure 7.4. At 500 and 600 °C, direct gasification of lumped intermediates is the major source of H₂ production throughout the reaction. The forward water-gas shift reaction becomes significant at longer times and consumes available CO to generate H₂, whereas the reverse water-gas shift and steam reforming reactions have only minimal influence. At 700 °C, steam reforming becomes the dominant pathway for generating H₂, with the forward



(a)



(b)

Figure 7.3: Delplots for (a) dibenzofuran and (b) benzene obtained from the kinetic model for phenol SCWG at temperatures of 500 (●), 600 (◆), and 700 °C (■), a water density of 0.18 g/cm³, and the same phenol concentrations as in Figure 6.1.

water-gas shift also contributing, and direct gasification playing a lesser role. The reverse water-gas shift reaction also plays a small role at 700 °C.

The trends in CO, CH₄, and CO₂ formation are governed by the rates of gasification reactions (Pathways 8–10), steam reforming (Pathway 13), and the water-gas shift reaction (Pathways 12). The rates of the latter two pathways are already plotted for H₂ in Figure 7.4. H₂ and CO₂ formation rates are identical in the case of the water-gas shift reaction, and H₂ and CO formation rates are likewise identical in the case of steam reforming. Although the rates of gasification to H₂, CO, CH₄, and CO₂ are not all identical, the trends are essentially the same: high initial gasification rates while the lumped species accumulates followed by decreasing rates as the lumped species depletes.

Figure 7.5 shows generation and depletion rates for phenol SCWG. At 500 °C, phenol dimerization to produce dibenzofuran is the dominant reaction by which phenol is consumed. At higher temperatures, phenol dehydroxylation to produce benzene becomes dominant; however, any benzene that forms is quick to react with phenol (producing other dimers such as phenylphenols). At 700 °C, nearly all phenol is depleted within the first 10 min. Dibenzofuran decomposition is responsible for the remaking of only a small amount of phenol, although this pathway becomes much more significant when dibenzofuran is initially present.

Reaction rates for the two primary products of phenol SCWG (dibenzofuran and benzene) are presented in Figures 7.6 and 7.7. Formation rates for both species start out high and decrease as phenol depletes. Again, phenol dimerization is responsible for dibenzofuran formation, and phenol dehydroxylation is primarily

responsible for benzene formation. The dibenzofuran decomposition rate is shown in both sets of figures, consuming a very small amount of dibenzofuran to form an equal amount of benzene (and phenol). Most dibenzofuran depletes, however, due to the gasification pathway (Pathway 2). Benzene preferentially combines with the more abundant phenol to form dimers, although benzene-benzene combinations start to play a small role at 700 °C once all phenol has been consumed. In general, however, the dominant formation and consumption pathways for dibenzofuran and benzene do not change with temperature (and thus rates are only shown for 600 °C).

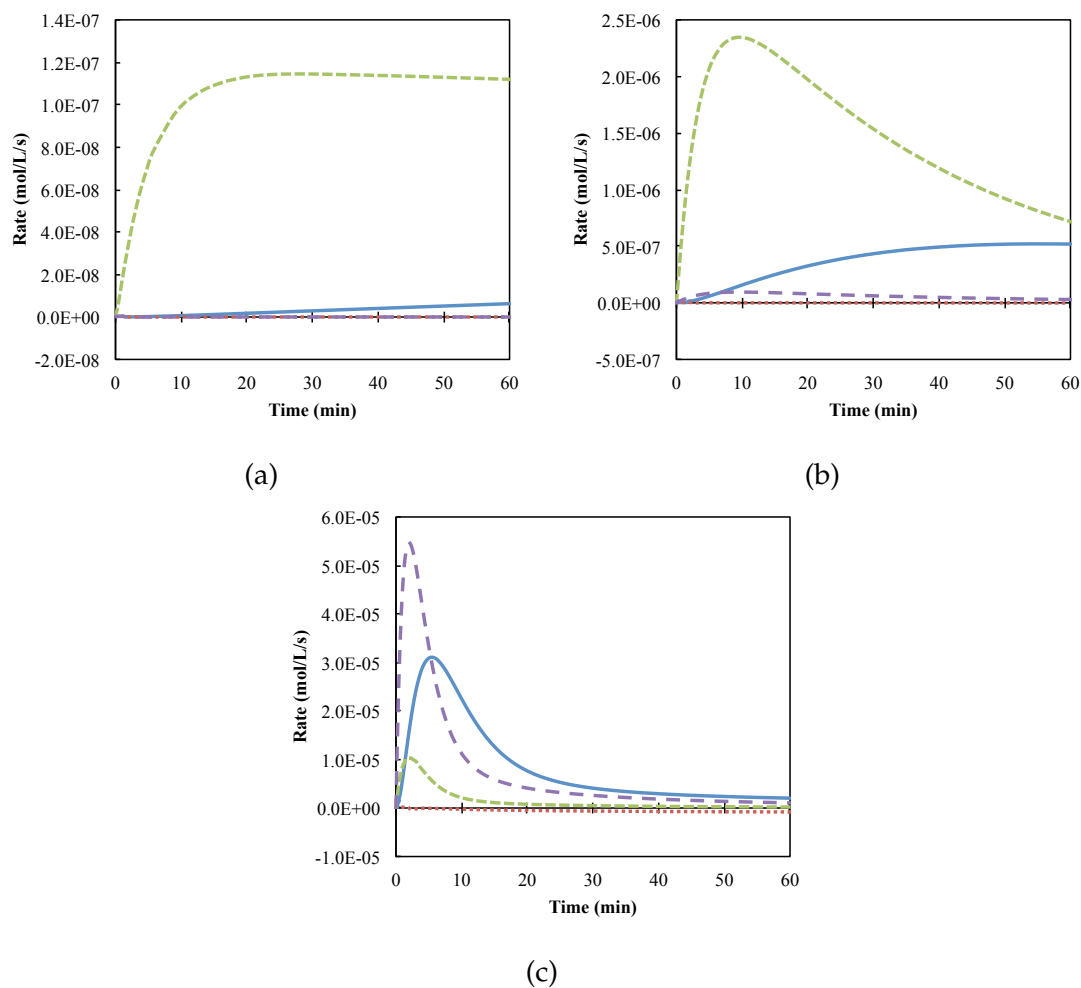


Figure 7.4: Rates of H₂ formation and consumption due to water-gas shift (pathway 12, —), reverse water-gas shift (pathway 12r, -.-), gasification (pathway 7, ---), and steam reforming (pathway 13, - -) at (a) 500, (b) 600, and (c) 700 °C (0.18 g/cm³ water density, 0.10 mol/L phenol concentration).

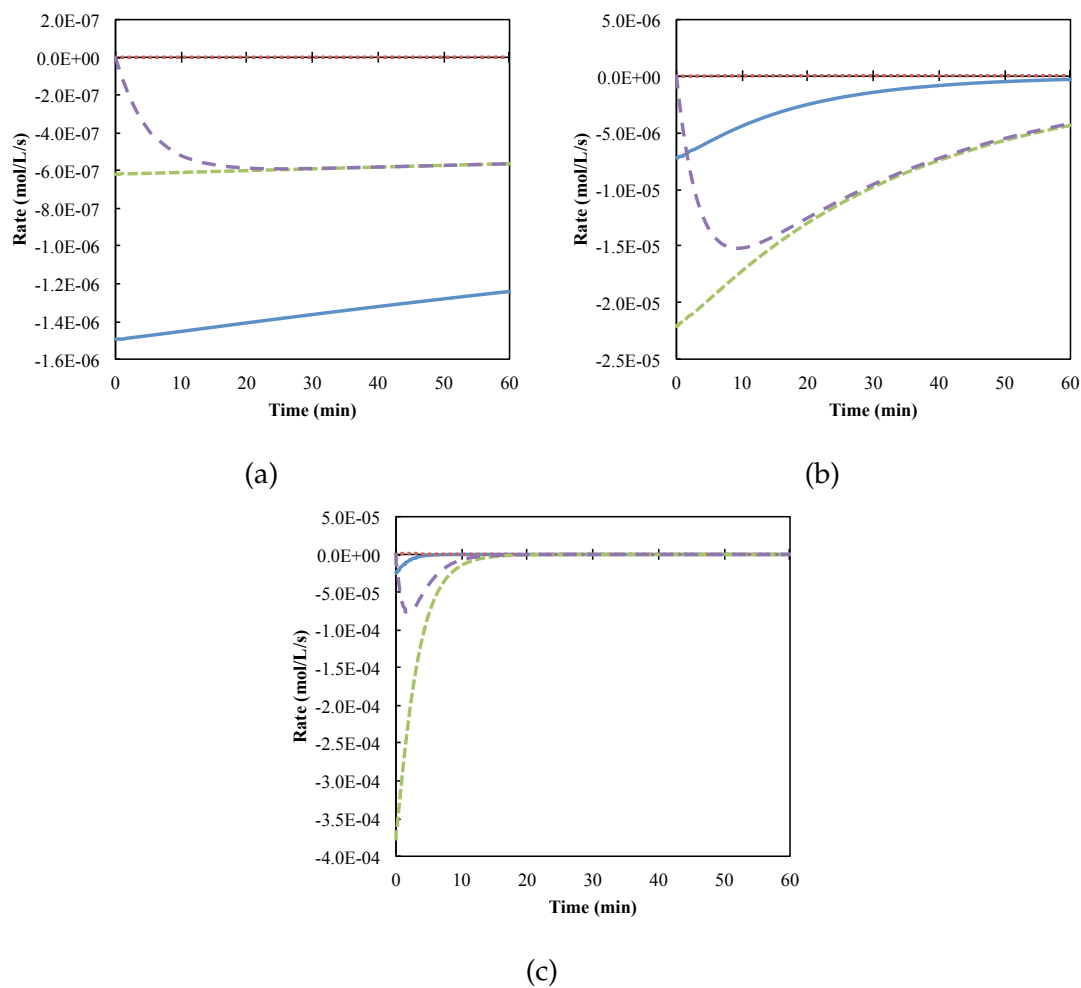


Figure 7.5: Rates of phenol formation and consumption due to phenol+phenol combination (pathway 1, —), dibenzofuran decomposition (pathway 6, - - -), dehydroxylation (pathway 4, - - -), and phenol+benzene combination (pathway 3, - - -) at (a) 500, (b) 600, and (c) 700 °C (0.18 g/cm^3 water density, 0.10 mol/L phenol concentration).

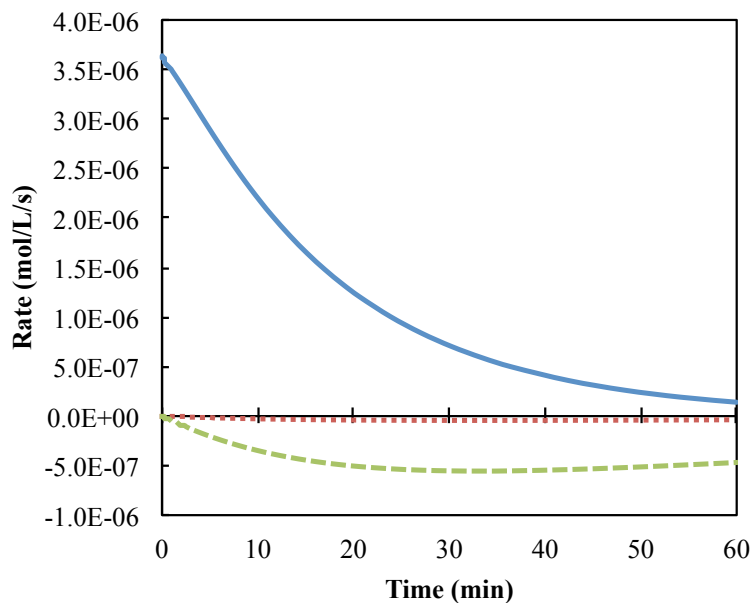


Figure 7.6: Rates of dibenzofuran formation and consumption due to phenol+phenol combination (pathway 1, —), decomposition (pathway 6, -.-), and gasification (pathway 2, - - -) at 600 °C (0.18 g/cm³ water density, 0.10 mol/L phenol concentration).

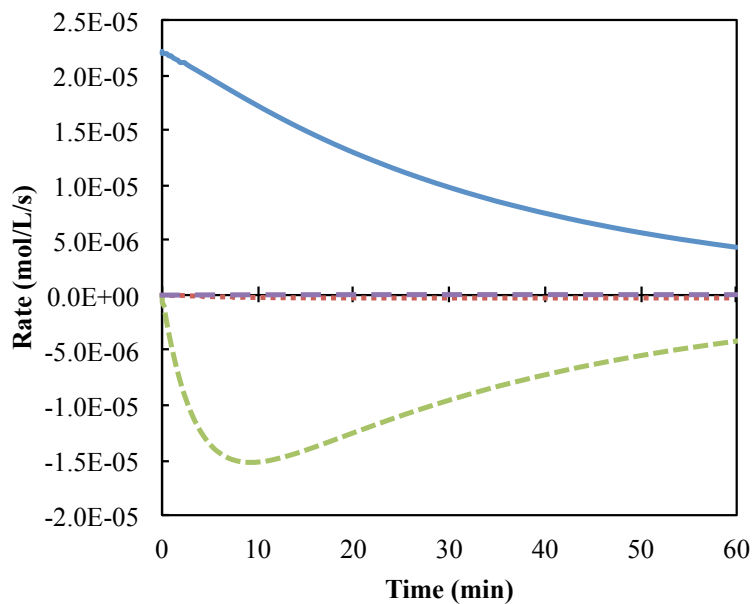


Figure 7.7: Rates of benzene formation and consumption due to phenol dehydroxylation (pathway 4, —), benzene+benzene combination (pathway 5, -.-), phenol+benzene combination (pathway 3, - - -), and dibenzofuran decomposition (pathway 6, - - -) at 600 °C (0.18 g/cm³ water density, 0.10 mol/L phenol concentration).

CHAPTER 8

Toxic Byproducts Characterization

Using supercritical water as a benign reaction medium instead of environmentally harmful organic solvents offers environmental benefits, as does using biomass as a green energy feedstock instead of non-renewable fossil fuels with net-positive carbon emissions. For these reasons, there has been growing interest in commercializing biomass SCWG, which has already led to pilot scale investigations [92, 93]. Several life cycle assessments have been performed attesting to the feasibility of this technology with respect to energy usage and cost [143, 35, 144].

Biomass utilization is not without potential negative environmental impacts, however. One environmental consideration that largely remains to be addressed for biomass gasification and other forms of biomass chemical conversion is the toxicity of byproducts. For example, polycyclic aromatic hydrocarbons (PAHs) commonly form in these reaction systems [145, 146, 147, 23], and the negative human health effects and environmental persistence of such compounds is well known [148]. The present reactions with phenol (*c.f.* Section 4.1) and dibenzofuran (*c.f.* Section 6.2) led to the observation of many PAHs. In this chapter, we experimentally quantify as many of these compounds as possible under various reaction

times and temperatures. We then use this experimental data in conjunction with toxicity modeling to characterize the human- and eco-toxic impacts corresponding to hypothetical emissions of byproduct streams into freshwater. Toxic impacts are normalized and reported “per unit phenol processed” for comparative convenience.

8.1 Importance of toxicity characterization

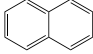
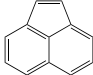
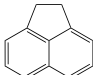
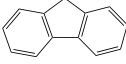
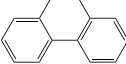
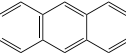
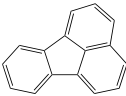
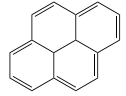
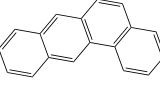
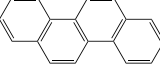
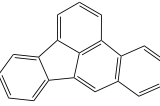
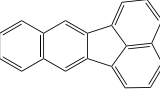
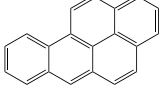
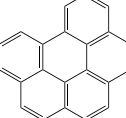
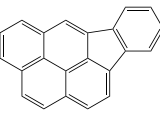
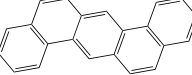
Characterizing the toxicity of byproducts is an important component of addressing human health impacts, which are strikingly under-discussed in biofuel research literature [149]. One study by [Xu et al.](#) investigated PAH formation from supercritical water gasification of sewage sludge (400–455 °C, 0–60 min reaction time, 5.6–23.8 wt%) [145]. Xu and coworkers analyzed for 16 EPA priority PAHs in recovered solid residues, and they found benzo[a]anthracene, benzo[a]pyrene, and dibenzo[a,h]anthracene concentrations that exceeded land quality standards set by the U.S. EPA. Another study by [Bircan et al.](#) investigated dioxin formation from hydrothermal gasification of chicken and cattle manure (200–400 °C, 40 min reaction time) [150]. Dioxin concentration was higher in residues recovered from hydrothermal gasification of cattle manure than that in chicken manure, but solid and liquid residue concentrations from both feedstocks were within allowable limits set forth by the Japanese Ministry of the Environment. To our knowledge, these studies are the only instances in which byproduct toxicity was evaluated for a gasification process in supercritical water. There is clearly a need for greater consider-

ation of byproducts toxicity in biofuels literature.

Table 8.1 shows 16 PAHs that are actively regulated by the U.S. EPA as priority pollutants [151, 152]. PAHs as a class are notorious for being both persistent in the environment due to their stability and toxic to ecosystems or human health. For example, benzo[a]pyrene (#13 in Table 8.1) metabolizes in the body to the mutagen benzo[a]pyrene diol epoxide, which intercalates DNA to form DNA adducts. These adducts disrupt DNA replication and induce mutations in genes that specifically regulate cell growth. The exact mechanism by which benzo[a]pyrene leads to cancer is known, and the International Agency for Research on Cancer (IARC) thus classifies benzo[a]pyrene as a Group 1 carcinogen. Of compounds we previously identified as phenol SCWG byproducts, benzo[a]pyrene represents the most toxic to human health, but a handful of other compounds are similarly classified by the IARC as carcinogenic (*e.g.*, benzene), probably carcinogenic (*e.g.*, benz[a]anthracene), or possibly carcinogenic (*e.g.*, chrysene).

Rather than waiting to learn the unintended consequences of an emerging energy conversion technology until after it goes commercial, this work adopts a forward-looking approach and calls upon other investigators to do the same. Quantification and toxic characterization of the byproducts from a new technology provides vital information for an eventual environmental impact assessment. Obtaining this toxicity information at many different reaction conditions offers the opportunity to engineer ways to minimize the production of potentially harmful compounds and thereby optimize the process according to environmental impacts.

Table 8.1: Polycyclic aromatic hydrocarbons regulated by the U.S. EPA as priority pollutants.

	Compound	Structure	M.W.	CAS
1	naphthalene		128.2	[91-20-3]
2	acenaphthylene		152.2	[208-96-8]
3	acenaphthene		154.2	[83-32-9]
4	fluorene		166.2	[86-73-7]
5	phenanthrene		178.2	[85-01-8]
6	anthracene		178.2	[120-12-7]
7	fluoranthene		202.2	[206-44-0]
8	pyrene		202.2	[129-00-0]
9	benz[a]anthracene		228.3	[56-55-3]
10	chrysene		228.3	[218-01-9]
11	benzo[b]fluoranthene		252.3	[205-99-2]
12	benzo[k]fluoranthene		252.3	[207-08-9]
13	benzo[a]pyrene		252.3	[50-32-8]
14	benzo[ghi]perylene		276.3	[191-24-2]
15	indeno[1,2,3-cd]pyrene		276.3	[193-39-5]
16	dibenz[a,h]anthracene		278.4	[215-58-7]

8.2 Additional experiments and results

Characterization of toxic byproducts requires reliable experimental data for compounds with significant toxicity, because highly toxic compounds may introduce a noteworthy toxic impact even in low concentrations. Since previous experiments were not carried out with the goal of quantifying low abundance, high molecular weight compounds (typical for PAHs), additional experiments were conducted to maximize both sample recovery and analyte quantification.

Mini-batch 316 stainless steel reactors were each assembled from a $1/2$ in. port connector (product no. SS-811-PC) and two $1/2$ in. caps (product no. SS-810-C) manufactured by Swagelok. The total internal volume of the reactors was 3.8 mL. A 718. μ L aliquot of a prepared stock solution (1.245 g phenol diluted with deionized water to 25 mL) was loaded into each reactor. Under (supercritical) reaction conditions, this loading of phenol and water corresponds to a phenol concentration of 0.10 mol/L and a water concentration of 10. mol/L. The chosen water loading ensured an excess of water and sufficiently high water density (*i.e.*, 0.18 g/cm³) to maintain a single supercritical phase during reactions at the lowest temperature studied (*i.e.*, 500 °C).

Reactions were carried out for 8, 15, 30, and 60 min at 500, 550, 600, 650, and 700 °C. Reactions at 600 °C or below were conducted in a Techne SBL-2 isothermal fluidized sand bath, and reactions above this temperature were carried out within a Ney Vulcan 3-130 box furnace. Although heat up time was of little concern since the data were not to be used to glean kinetic information, previous work in our

lab manifested heat up times of less than 3 min using identical reactors at milder temperatures [153]. Only the liquid phase was recovered post-reaction.

The recovery and analytical procedures were unchanged from those used for quartz reactors, except for a different GC temperature program: 50 °C for 2 min, 20 °C/min ramp, 180 °C for 2 min, 10 °C/min ramp, 280 °C for 20 min. This temperature program facilitated quantification of the many byproducts of interest, including PAHs. An analytical liquid standard containing the 16 EPA priority PAHs of Table 8.1 was used to prepare three sets of external standards in known concentrations, which were then analyzed and used to construct calibration curves relating peak area and concentration.

Complete data obtained from these additional experiments are tabulated in Table A.2 in Appendix A. Yields are reported on a mass basis instead of molar basis since this unit is more environmentally useful. As a representative example, Figure 8.1 presents the experimental results for benz[a]anthracene and benzo[a]pyrene. Recall from Section 8.1 that the former compound is classified as a probable carcinogen and the latter compound is carcinogenic. The trends in Figure 8.1 are typical of PAHs forming from phenol SCWG; longer reaction times and higher temperatures lead to greater PAH yields up to a point, beyond which additional time and temperature give rise to a decrease in yield. This yield decrease is apparent for benz[a]anthracene after 30 min at 650 °C and after 15 min at 700 °C. Such trends are consistent with the explanations in Sections 4.2 and 6.2 that byproducts of moderate size are consumed in reactions to form larger and larger polycyclic species and ultimately lead to char. In fact, char manifested in observable quanti-

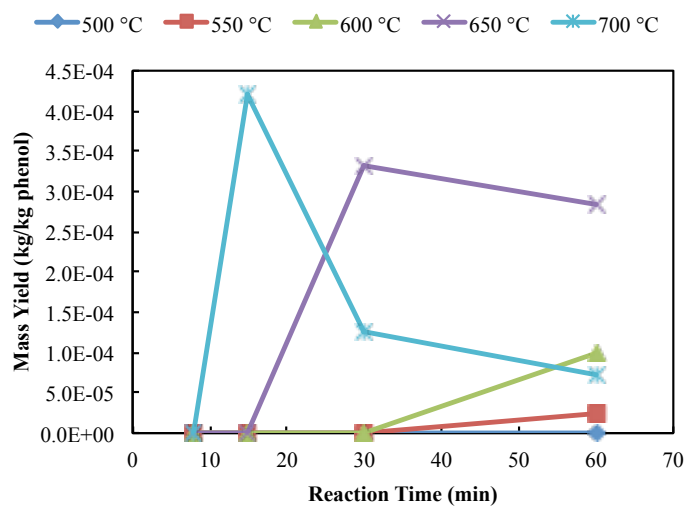
ties on the reactor walls at high temperatures in these experiments.

8.3 USEtox model

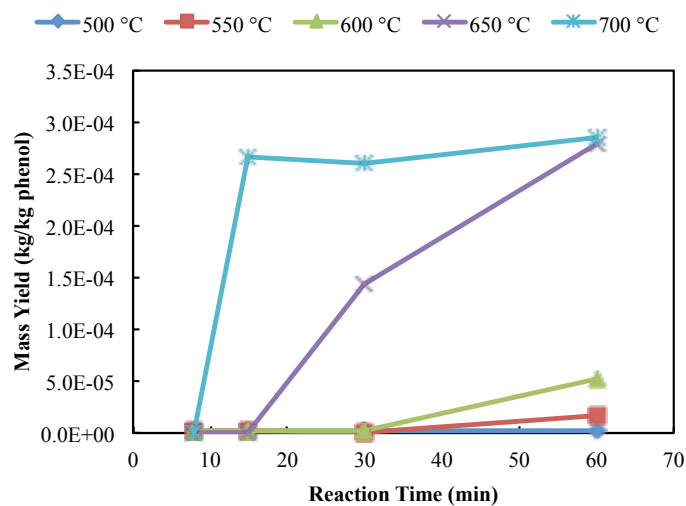
The USEtox™ model¹ (from “UNEP-SETAC toxicity” model) is a multi-media, multi-scale toxicity model for characterization of human and ecotoxicological impacts due to toxic substance emissions in the environment [154, 155, 156, 157]. It was developed by an international team of researchers from the Task Force on Toxic Impacts (TFTI) under the auspices of the UNEP-SETAC Life Cycle Initiative², a joint venture to promote life cycle thinking by the United Nations Environment Programme (UNEP) and the Society of Environmental Toxicology and Chemistry (SETAC). These researchers comprise “model developers responsible for the most commonly used Life Cycle Impact Assessment (LCIA) characterization models worldwide” as well as “disciplinary experts in fate and transport, exposure assessment, health risk assessment, and ecotoxicology.” USEtox is the result of their combined effort to harmonize existing environmental toxicity models (including CalTOX, IMPACT 2002, USES-LCA, and EDIP97) in order to build a global consensus model that is transparent, well-documented, stable, reliable, and parsimonious (*i.e.*, as simple as possible, as complex as needed). The U.S. EPA now recommends and utilizes the USEtox model for comparative chemical toxicity assessment. Consequently, USEtox was selected to assess the toxic impacts of emitted phenol SCWG byproducts in this work.

¹<http://www.usetox.org>

²<http://www.lifecycleinitiative.org/>



(a)



(b)

Figure 8.1: Effect of temperature and time on mass yields of (a) benz[a]anthracene and (b) benzo[a]pyrene from phenol SCWG (0.18 g/cm³ water density, 0.10 mol/L phenol concentration).

8.3.1 Environmental fate

USEtox consists of sub-models for environmental fate, exposure pathways, and toxic effects. In simplest terms, the environmental fate model divides the environment into compartments corresponding to various media (*i.e.*, natural soil, agricultural soil, freshwater, seawater, and air) at multiple scales (*i.e.*, urban, continental, and global) and calculates the steady-state mass of a chemical in each of these compartments (*i.e.*, its “fate”) due to its constant emission into one or more compartments. This calculation results in compartment-specific “fate factors.” These values are equal to the residence time (in days) of the emitted chemical in each compartment and can be multiplied by the emission flow (unit kg/day) to produce the kg of chemical in each compartment. Another way to think of a fate factor is in terms of unit kg in a compartment per unit kg/day emission into a compartment (*i.e.*, units of $\text{kg}/(\text{kg}/\text{day})_{\text{emitted}}$). The environmental fate model accounts for both removal processes, which include bio-/photodegradation and escape to the stratosphere, and intermedia transport, which can be either advective or diffusive. Advective transport refers to one-way transport of a chemical due to the bulk flow of the medium in which it is dissolved or adsorbed. Examples of advective transport are a river transporting a chemical from freshwater to seawater, rain transporting a chemical from the air to the soil, or wind transporting a chemical from one geography to another. Diffusive transport is two-way transport as a result of chemical properties such as lipophilicity/hydrophobicity and volatility, and this kind of transport is modeled using known equilibrium behavior and

partition coefficients (*e.g.*, solubility, Henry's law coefficients, octanol-water and organic carbon-water partition coefficients). Modeling environmental fate thus requires knowledge of key physicochemical properties.

USEtox includes a database of over 3,000 organic and inorganic substances and their requisite properties for fate calculation, but it also accepts user input for properties of other chemicals. This database draws heavily upon EPI Suite™ (from "Estimation Programs Interface" Suite), a collection of freely available³ programs developed by the EPA's Office of Pollution Prevention Toxics and Syracuse Research Corporation (SRC) for physicochemical property estimation. When experimental values were unavailable for the partition coefficients of a chemical, they were estimated with EPI Suite using the KOWWIN model (for octanol-water partitioning), the HENRYWIN model (for air-water partitioning), the KOCWIN model (for organic carbon-water partitioning), and the WSKOWWIN model (for solubility). All these models rely upon quantitative structure-activity relationship (QSAR) correlations between the presence of certain atoms, bonds, groups, and fragments in a chemical structure and consequent physicochemical properties. Degradation pathways in air, water, soil, and sediment are modeled with environmental half-lives or rate coefficients. Degradation in the air compartment is due to atmospheric photolysis, which produces hydroxyl radicals that initiate hydrocarbon oxidation. Experimental values for the hydroxyl radical rate coefficient are available for some chemicals in EPI Suite, but the rest had to be estimated using the AOPWIN model, which employs QSAR methods. Half-lives in water, soil, and sediment due to

³<http://www.epa.gov/opptintr/exposure/pubs/episuite.htm>

biodegradation were estimated with EPI Suite using the BIOWIN3 model, which estimates the time span that is required for ultimate biodegradation (*i.e.*, complete breakdown of the chemical).

Table 8.2 presents the environmental fates of various compounds of interest in this study due to their constant emission into continental freshwater. One column gives the total summation of all compartmental fate factors, and the remaining columns break that fate total down by compartment (the urban air compartment was negligible and therefore excluded). Fluoranthene, pyrene, and phenanthrene are the most persistent in the environment overall (>20 days), while biphenyl, naphthalene, and fluorene are the least persistent (<9 days). A majority of the compounds remain predominantly (>50%) in the continental freshwater compartment once emitted there, but a significant amount (>15%) of benzene, biphenyl, and dibenzofuran goes into the continental air compartment. An immense amount (35%) of the benzene advects into the global atmosphere. Unsurprisingly, much of the emissions into freshwater make their way into seawater (on both continental and global scales). Heavier PAHs (*e.g.*, dibenzofuran, fluorene, phenanthrene, anthracene, fluoranthene, pyrene, and benz[a]anthracene) are more likely to persist in soil compartments, being less water-soluble. Environmental persistence of these compounds plays a major role in their eventual toxic impacts.

Table 8.2: Environmental fate generated by USEtox for select compounds emitted into freshwater.

Substance	Total (days [†])	Cont. Air			Cont. Nat.			Cont. Agri.			Global		
		Freshwater	Seawater	Soil	Freshwater	Seawater	Soil	Freshwater	Seawater	Soil	Freshwater	Seawater	Soil
benzene	17.59	27.37%	6.87%	0.02%	24.34%	6.87%	0.02%	35.24%	6.13%	0.01%	0.01%	6.13%	0.01%
phenol	21.22	0.05%	12.35%	0.20%	86.42%	12.35%	0.20%	0.00%	0.76%	0.00%	0.00%	0.76%	0.00%
naphthalene	7.74	7.42%	19.93%	0.34%	67.83%	19.93%	0.34%	0.57%	3.54%	0.01%	0.01%	3.54%	0.01%
biphenyl	7.68	16.38%	10.27%	0.98%	64.15%	10.27%	0.98%	3.52%	3.56%	0.07%	0.07%	3.56%	0.07%
acenaphthene	8.59	2.51%	21.25%	0.51%	72.01%	21.25%	0.51%	0.07%	3.13%	0.01%	0.01%	3.13%	0.01%
2-phenylphenol	19.44	0.13%	12.31%	0.40%	85.96%	12.31%	0.40%	0.01%	0.78%	0.01%	0.01%	0.78%	0.01%
dibenzofuran	10.26	18.18%	9.43%	3.24%	50.97%	9.43%	3.24%	6.40%	7.73%	0.39%	0.39%	7.73%	0.39%
fluorene	8.40	8.06%	11.90%	1.84%	72.70%	11.90%	1.84%	0.94%	2.57%	0.07%	0.07%	2.57%	0.07%
phenanthrene	22.62	3.26%	24.08%	7.90%	46.36%	24.08%	7.90%	0.36%	9.53%	0.30%	0.30%	9.53%	0.30%
anthracene	16.11	1.74%	26.59%	3.30%	58.36%	26.59%	3.30%	0.07%	6.53%	0.05%	0.05%	6.53%	0.05%
fluoranthene	30.53	0.53%	27.73%	3.53%	57.62%	27.73%	3.53%	0.03%	6.90%	0.06%	0.06%	6.90%	0.06%
pyrene	24.94	0.43%	27.93%	2.77%	59.40%	27.93%	2.77%	0.01%	6.63%	0.03%	0.03%	6.63%	0.03%
benz[a]anthracene	19.97	0.32%	27.86%	2.25%	60.81%	27.86%	2.25%	0.01%	6.45%	0.03%	0.03%	6.45%	0.03%
benzo[a]pyrene	11.92	0.01%	28.01%	0.16%	65.63%	28.01%	0.16%	0.00%	6.03%	0.00%	0.00%	6.03%	0.00%

[†] equivalent to kg/(kg/day)_{emitted}

8.3.2 Exposure pathways

There are many different pathways by which humans are exposed to the environment, and, by extension, chemicals in the environment. The human exposure pathways modeled in USEtox are air inhalation, ingestion of drinking water, ingestion of exposed produce (*i.e.*, above-ground leaf crops), ingestion of unexposed produce (*i.e.*, below-ground root crops), ingestion of meat, ingestion of dairy products, and ingestion of fish. Air inhalation is modeled based on average human respiration, compartment volume, and population. For each ingestion pathway, a bioaccumulation factor (BAF) or biotransfer factor (BTF) is either estimated from chemical properties (*e.g.*, using QSAR methods in EPI Suite) or may be supplied by the user. These factors, which relate the mass of a chemical in an entire environmental compartment to the mass in an organism situated in that compartment, are used in conjunction with consumption per person (of, *e.g.*, crops, meat, milk, or fish) and total compartment mass estimates to calculate human “exposure factors.” These exposure factors have units of day^{-1} and represent the fraction of a chemical in a particular compartment to which humans are exposed on daily basis through a particular modeled exposure pathway. One may multiply a human exposure factor by a compartmental fate factor to obtain a unitless “intake fraction,” which represents the fraction of the total emission rate that is taken in by the human population.

Figure 8.3 presents the human intake of various compounds of interest due to their constant emission into continental freshwater. One column gives the to-

tal summation of all compartmental intake fractions, and the remaining columns break that intake total down by compartment. The major intake pathway for most compounds is fish, as one might expect from an emission to freshwater. Drinking water also plays a significant role and is the major intake pathway (>50%) for benzene, phenol, naphthalene, and 2-phenylphenol. Since 63% of environmental benzene persists in the air compartments, inhalation of air is the second most important pathway (44%) by which benzene is taken in by humans. Intake *via* root crops is negligible ($\leq 0.1\%$). Intake due to consumption of leaf crops is greater, but still small (<5%). Meat and dairy consumption are negligible intake pathways for all compounds except benz[a]anthracene and, to a greater extent, benzo[a]pyrene.

Environmental exposure factors for freshwater ecotoxicity represent the bioavailability of a chemical in the freshwater compartment to aquatic organisms. These exposure factors are unitless and are modeled in USEtox using bioconcentration factors for fish (BCF_{fish}), partition coefficients between suspended solids and water, and partition coefficients between dissolved organic carbon (DOC) and water in order to calculate the truly dissolved fraction of a chemical.

8.3.3 Toxicological effects

Toxicological effects are modeled in USEtox using dose-response relationships (in the case of human toxicology) or concentration-response relationships (in the case of water ecotoxicology), which relate the extent of exposure (intake) to the increased likelihood of an adverse effect (response). These relationships are deduced

Table 8.3: Human intake fraction generated by USEtox for select compounds emitted into freshwater.

Substance	Total (fraction [†])	Drinking Water		Exposed Produce		Unexposed Produce		Meat	Dairy	Fish
		Air	Water	Produce	Produce	Produce	Produce			
benzene	1.65E-05	44.27%	53.61%	0.04%	0.00%	0.00%	0.00%	0.01%	0.01%	2.07%
phenol	4.39E-05	0.03%	86.26%	0.13%	0.01%	0.00%	0.00%	0.01%	0.01%	13.56%
naphthalene	2.00E-05	3.78%	54.20%	0.45%	0.01%	0.00%	0.00%	0.01%	0.01%	41.56%
biphenyl	5.31E-05	3.17%	19.06%	2.44%	0.01%	0.01%	0.01%	0.02%	0.02%	75.30%
acenaphthene	1.00E-04	0.28%	12.66%	0.32%	0.00%	0.00%	0.00%	0.01%	0.01%	86.73%
2-phenylphenol	6.06E-05	0.05%	56.34%	0.55%	0.00%	0.00%	0.00%	0.01%	0.01%	43.05%
dibenzofuran	1.63E-04	1.56%	6.52%	2.27%	0.00%	0.00%	0.00%	0.01%	0.01%	89.64%
fluorene	7.55E-05	1.18%	16.50%	3.82%	0.01%	0.01%	0.01%	0.03%	0.03%	78.45%
phenanthrene	5.08E-04	0.19%	4.07%	2.40%	0.01%	0.01%	0.01%	0.02%	0.02%	93.30%
anthracene	3.28E-04	0.11%	5.68%	1.13%	0.00%	0.00%	0.01%	0.02%	0.02%	93.05%
fluoranthene	1.08E-03	0.02%	2.91%	0.76%	0.00%	0.00%	0.02%	0.06%	0.06%	96.23%
pyrene	3.97E-04	0.04%	6.70%	1.20%	0.00%	0.00%	0.02%	0.06%	0.06%	91.98%
benz[a]anthracene	6.09E-05	0.14%	26.92%	5.70%	0.00%	0.00%	0.81%	2.53%	2.53%	63.90%
benzo[a]pyrene	2.85E-05	0.00%	19.72%	0.19%	0.00%	0.00%	2.09%	6.55%	6.55%	71.45%

[†]equivalent to the fraction of total emission that will ultimately be taken in by the human population

or extrapolated from experimental test data. For freshwater ecotoxicity, USEtox relies upon median effective concentration (EC_{50}) data, which represent the chemical concentration that induces a response halfway between the baseline and maximal states for a given species population. One response that can be quantified in aquatic ecosystems is organism mortality, and this effect is incorporated into USEtox using median lethal concentration (LC_{50}) data. Other quantifiable responses include organism reproduction, growth, physiology, behavior, and biochemistry. An excellent resource for LC_{50} and other EC_{50} data is the U.S. EPA ECOTOX database⁴ (from “ecotoxicology” database), which contains records for over 350,000 aquatic tests with more than 8,500 chemicals and 5,700 species. In USEtox, ecotoxicological “effect factors” are calculated based on geometric means of single species EC_{50} test data. The geometric mean of EC_{50} values results in HC_{50} , the hazardous concentration of a chemical (units of kg/m^3 in USEtox) at which 50% of aquatic species are exposed to a concentration above their EC_{50} . Dividing the HC_{50} into the 50% potentially affected fraction of species (PAF) provides the ecotoxicological effect factor (units of $PAF \cdot m^3/kg$), which relates concentration of a dissolved chemical to aquatic ecotoxic impact for freshwater ecosystems.

Human toxicological effects may be divided into carcinogenic (causing cancer) and non-carcinogenic (causing, *e.g.*, cardiovascular, respiratory, congenital, neurological, or other disease). In USEtox, separate effect factors are derived for each of these effect types, and inhalation and ingestion exposure pathways are also addressed separately for each. Dose-response relationships come from animal tox-

⁴<http://www.epa.gov/ecotox>

icity testing, *in vitro* testing, and epidemiological studies (*e.g.*, occupational and clinical) in the form of effective dose data. There are many sources of such data, but the most comprehensive is the U.S. National Library of Medicine TOXNET⁵ (from Toxicology Data Network), which comprises “a group of databases covering chemicals and drugs, diseases and the environment, environmental health, occupational safety and health, poisoning, risk assessment and regulations, and toxicology.” Median effective dose (ED₅₀) values represent the daily dose that causes a disease probability of 50% in a subject, and they are dependent upon exposure pathway (inhalation or ingestion), exposure duration, and animal type. USEtox employs extrapolation factors from the work of Huijbregts *et al.* [158] to obtain chronic, human ED₅₀ values (units of kg/person/lifetime in USEtox) from non-chronic (*e.g.*, subacute or subchronic), non-human (*e.g.*, rat, mouse, pig, monkey, *etc.*), and/or non-ED₅₀ (*e.g.*, cancer slope factor or no observed adverse effect level [NOAEL]) data. Once these values have been obtained for carcinogenic oral, carcinogenic inhalatory, non-carcinogenic oral, and non-carcinogenic inhalatory pathways, dividing them into the 50% disease probability results in corresponding human toxicological effect factors (units of cases/kg), which relates lifetime human intake of a chemical to human toxic impact.

8.3.4 Characterization factors

Sections 8.3.1–8.3.3 provide the framework for calculating “characterization factors” relating environmental chemical emissions to ecotoxic and human toxic im-

⁵<http://toxnet.nlm.nih.gov>

pacts. Equation 8.1 defines the characterization factor, CF, as a simple product of the appropriate fate factor (FF), exposure factor (XF), and effect factor (EF).

$$CF = FF \cdot XF \cdot EF \quad (8.1)$$

Human toxicological characterization factors (whether carcinogenic or non-carcinogenic) incorporate a summation over both inhalation pathways and ingestion pathways. The units for ecotoxicological and human toxicological characterization factors are $\text{PAF} \cdot \text{m}^3 \cdot \text{day} / \text{kg}_{\text{emitted}}$ and $\text{cases} / \text{kg}_{\text{emitted}}$, respectively. In both cases, these units may be summarized as Comparative Toxic Units (abbrv. CTU, CTU_e , or CTU_h) in order to emphasize the comparative nature of characterization factors. Multiplying a characterization factor by an environmental emission (units of $\text{kg}_{\text{emitted}} / \text{day}$) quantitatively characterizes the emission's toxicological impact on freshwater ecosystems, in terms of potentially affected fraction of species for a given aquatic volume, or human beings, in terms of disease cases per day.

Table 8.4 presents characterization factors generated with USEtox for various byproducts from phenol SCWG when emitted into freshwater. Of the chemicals for which non-carcinogenic disease data are available, fluorene, fluoranthene, and pyrene (*c.f.* Table 8.1 for structures) exhibit the greatest toxic impact. The chemical with greatest carcinogenic impact is unsurprisingly benzo[a]pyrene (recall discussion of its carcinogenicity in Section 8.1). Finally, pyrene and benz[a]anthracene manifest the greatest ecotoxic impact on freshwater ecosystems.

Table 8.4: Toxicity characterization factors generated by USEtox for byproducts from phenol SCWG emitted into freshwater.

	Non-carcinogenic (cases/kg)	Carcinogenic (cases/kg)	Ecotoxic (PAF·m ³ ·day/kg)
benzene	6.14E-08	2.42E-07	6.60E+01
phenol	1.45E-07	0.00E+00	9.33E+02
naphthalene	3.02E-07	1.04E-06	1.87E+03
biphenyl	2.70E-07	0.00E+00	2.20E+03
acenaphthene	2.58E-07	-	4.12E+03
2-phenylphenol	1.98E-07	3.00E-07	8.57E+03
dibenzofuran	-	-	2.15E+03
fluorene	3.91E-06	-	9.58E+04
phenanthrene	-	-	1.65E+04
anthracene	1.48E-07	-	2.62E+05
fluoranthene	3.91E-06	-	9.58E+04
pyrene	2.39E-06	-	8.86E+05
benz[a]anthracene	-	-	7.94E+05
benzo[a]pyrene	-	3.42E-05	1.17E+04

“-” indicates the compound is non-toxic or toxicity information is unavailable.

8.4 Results and discussion

Instead of imagining a scaled up SCWG process with a hypothetical constant by-product emission stream to freshwater, it is simpler and equally illustrative to apply the characterization factors from Table 8.4 directly to mass yield data obtained from the experiments described in Section 8.2 (complete data are contained in Table A.2). Multiplying characterization factors by these mass yield values results in scale-independent metrics for toxic impact that are defined per kg of phenol processed. Complete toxic impact characterization results can be found in Table A.3 in Appendix A. These scale-independent values facilitate a better understanding of the relationship between process scale and toxic impact.

It should be noted that unconverted phenol has been excluded from the results analysis in this chapter in order to emphasize toxic impacts due to phenol SCWG

byproducts. Toxic impacts due to unconverted phenol are, however, included in Table A.3 in Appendix A. In general, unconverted phenol is only significant at 500 °C and, to a lesser extent, 550 °C, and such low conversions are undesirable from a gasification standpoint irrespective of any consideration of toxicity.

As mentioned in Section 8.1, obtaining byproduct toxicity information at different reaction conditions affords the opportunity to optimize the process with regard to toxic impacts. Figure 8.2 shows the effect of temperature on ecotoxic impact, broken down by chemical, due to an emission of phenol SCWG byproducts into freshwater. The general trend is increasing total ecotoxic impact with increasing temperature from 500 up to 650 °C, and then a rapid decrease in impact by a factor of 8 from 650 to 700 °C. The trend can be largely attributed to the PAH yield trends discussed in Section 8.2, in which highest yields are observed at intermediate temperatures. Pyrene is by far the greatest contributor toward total impact due to a combination of its intrinsic ecotoxic impact and its relatively high yields from phenol SCWG. Pyrene alone accounts for $3/4$ and $2/3$ of the total quantified ecotoxic impact at 600 and 650 °C, respectively.

Non-carcinogenic impact as a function of temperature is presented in Figure 8.2. The total impact trend tracks the general PAH yield trend, with greatest non-carcinogenic impact at 650 °C and a rapid decrease from 650 to 700 °C by a factor of 3. Fluoranthene and pyrene appear to be the greatest culprits with respect to non-carcinogenic impact, together accounting for over half of the total quantified impact at 650 °C.

The trends in carcinogenic impact with respect to temperature in Figure 8.4 are

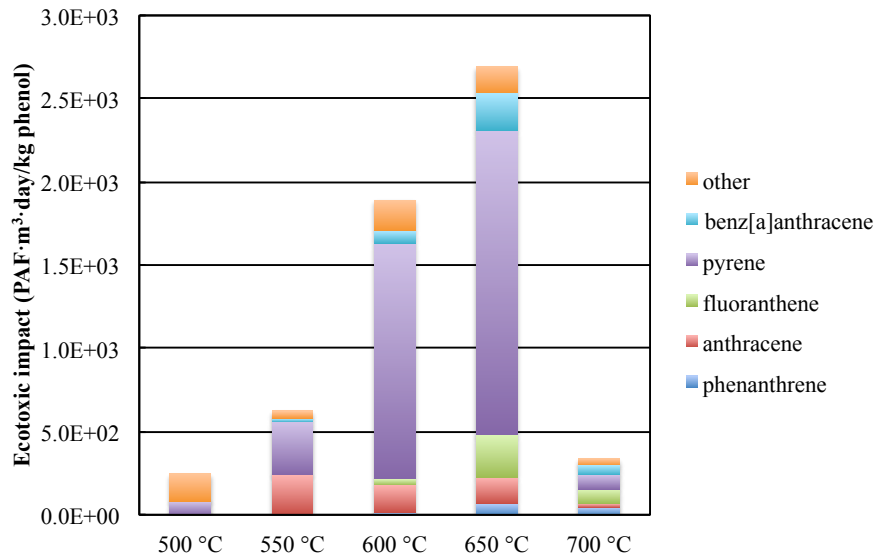


Figure 8.2: Effect of temperature on ecotoxic impact due to emission of byproducts into freshwater (60 min, 0.18 g/cm³ water density, 0.10 mol/L phenol concentration).

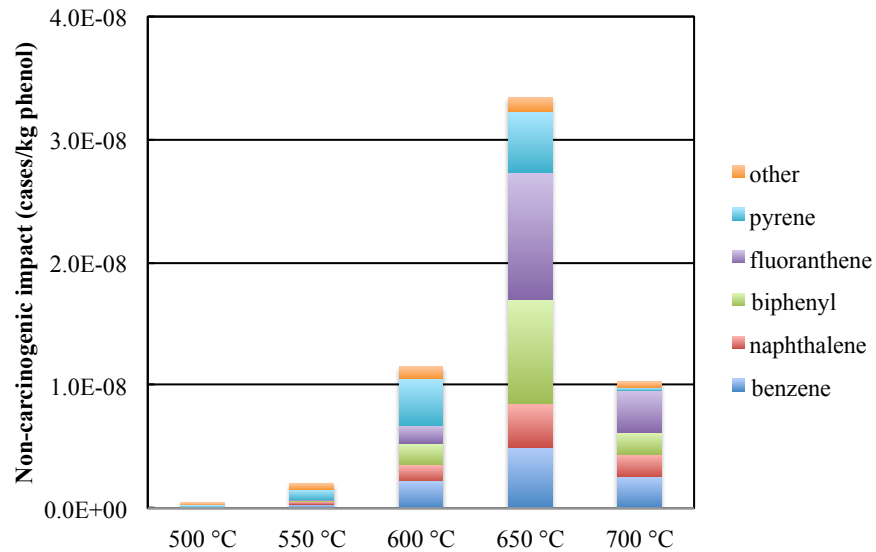


Figure 8.3: Effect of temperature on non-carcinogenic impact due to emission of byproducts into freshwater (60 min, 0.18 g/cm³ water density, 0.10 mol/L phenol concentration).

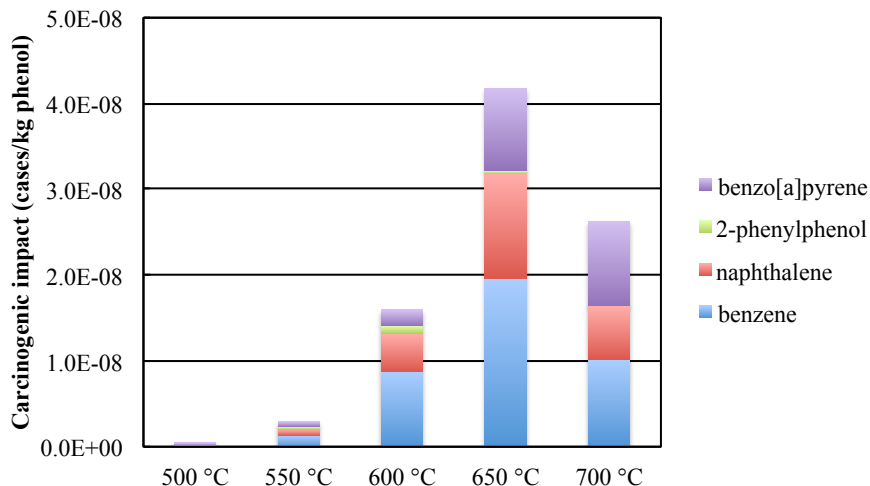


Figure 8.4: Effect of temperature on carcinogenic impact due to emission of byproducts into freshwater (60 min, 0.18 g/cm³ water density, 0.10 mol/L phenol concentration).

very similar to those for non-carcinogenic impact. Again, the reaction at 650 °C results in the greatest impact; however, the decrease in impact between 650 and 700 °C is smaller for carcinogenicity than non-carcinogenicity. Three chemicals—benzo[a]pyrene, naphthalene, and benzene—contribute substantially toward the carcinogenic impact despite having carcinogenic toxicity characterization factors of three different orders of magnitude. Benzo[a]pyrene is the most toxic when emitted into freshwater, followed by naphthalene, and then benzene, yet benzene was most abundant as a byproduct, followed by naphthalene, and finally benzo[a]pyrene in the lowest concentration. This illustrates how very toxic chemicals can have significant impact even in very small amounts.

The trends of all three USEtox impact metrics suggest the toxic impact from phenol SCWG byproducts can be minimized both as the temperature decreases below or increases above 650 °C. Since gasification yields increase with temperature

(*c.f.* Figure 4.3), operating the process at a temperature of 700 °C or higher is the best option for minimizing toxic impact while maximizing desired products. At—and above—700 °C, many of the priority pollutant PAHs from Table 8.1 become less stable and, hence, greater quantities of char form. This char is experimentally evidenced at high temperatures both by visual observation and by the simultaneous high conversions and low mass recoveries. There is a chance toxic impact may actually increase from 600 to 700 °C if the recovery procedure and analytical methods are insufficient to observe stabler, heavier, toxic compounds that hypothetically form when the compounds modeled here convert. However, substantial char formation at 700 °C (and, to a lesser extent, at 600 °C; *c.f.* Figure 4.1) and drastically decreasing carbon recoveries from 600 to 700 °C (*c.f.* Table 4.3) suggest that most, if not all, ungasified material may be accounted for as char. From a toxicity standpoint, char *qua* char (*i.e.*, black carbon) is harmless to human and aquatic life and is thus a desirable byproduct even though it can serve as an adsorbent for PAH and trace metal contaminants [159, 160]. From an environmental exposure standpoint, char and heavy char precursor compounds tend to be rapidly immobilized in the environment through sedimentation. As a general rule, PAH aqueous solubility decreases approximately one order in magnitude with each additional ring. Although char represents an effective net loss of gasification efficiency, it poses little toxic risk and is a desirable outcome environmentally. It can even provide beneficial fertilizing qualities as a soil amendment when it sediments.

CHAPTER 9

Conclusions and Future Work

9.1 Conclusions

The key findings of this work may be summarized as follows:

(1) In addition to the gases H_2 , CO , CH_4 , and CO_2 , supercritical water gasification of phenol leads to the formation of a swath of reaction intermediates, many of which were identified here for the first time. These intermediate compounds consist of decomposition products like benzene and dimerization products such as dibenzofuran and other dimers of phenol. Some of these products persist even when all of the phenol had been consumed. Thus, one might expect environmentally significant organic byproducts to reside in the aqueous stream emerging from an SCWG process.

(2) Higher temperatures promote gasification and result in greater fractions of H_2 and CH_4 , but the yields of ungasified intermediates and char also increase. These ungasified intermediates are precursors for char formation pathways, which can be driven by free radical polymerization at high temperatures. Dibenzofuran in particular is unstable at higher temperatures and represents a key gateway

molecule for such pathways.

(3) Increasing water density leads to a modest increase in gas yields, but water density has both an inhibitive and accelerative effect on conversion and intermediate formation. Conversion and intermediate yields are higher when the water density is 0.080 or 0.160 g/cm³ and lower at the densities in between these two extremes. An explanation for this is that one extreme (lower water density) reduces the availability of water molecules, which may permit phenol and its derivatives to react with each other more easily. The other extreme (higher water density) increases the frequency of reactions involving water, such as steam reforming and hydrothermolysis, and these reactions may also facilitate decomposition and dimerization *via* phenoxy radical formation.

(4) Increasing the initial phenol concentration leads to a decrease in the yields of CO and CO₂. As a consequence, the product gas is richer in H₂ and CH₄. Initial concentration, like water density, exhibits a dual effect on conversion and intermediate yields, and the implication is there are at least two competing pathways by which phenol is consumed. One path is less than first-order in phenol and dominates at lower phenol concentrations, and a second path is greater than first-order in phenol and dominates when phenol is more abundant.

(5) Analysis of the effects of temperature, water density, and phenol concentration informed the proposal of a reaction rate law to describe phenol disappearance by two competing pathways. Kinetic parameters were obtained by fitting this model to experimental data in a two-step process. One of the reaction rates is 1.73 order in phenol and -16.60 order in water and is inhibited by water, whereas the

second reaction rate is 0.92 order in phenol and 1.39 order in water and is therefore accelerated by water. This result indicates that phenol SCWG does not follow simple first-order kinetics, as previous studies assumed, but rather phenol participates in a combination of first-order and second-order reactions.

(6) Examining data for uncatalyzed phenol SCWG elucidated important reaction pathways responsible not only for gaseous products, but also for the liquid and solid phase products that detract from gas yields. Benzene and dibenzofuran are the sole primary products, and their direct formation accounts for all phenol consumption when only phenol and water are present.

(7) Dibenzofuran SCWG yielded many compounds familiar from phenol SCWG, such as 2-phenylphenol, biphenyl, benzene, PAHs, and char. The observation of phenol and benzene during dibenzofuran SCWG indicated there is a pathway by which dibenzofuran—itsself a dimerization product—decomposes. Gas yields and conversions from dibenzofuran closely resembled those observed in phenol SCWG when compared on an initial carbon basis. This resemblance suggested that, aside from benzene production, phenol SCWG and dibenzofuran SCWG are kinetically equivalent: the former just has an extra initial dimerization step.

(8) Benzene SCWG at 600 °C was dominated by dimerization reactions to form phenyl dimers and trimers and H₂ gas.

(9) A reaction network comprising 13 reaction pathways was elucidated, and the pathways are consistent with experimental data and free radical chemistry.

(10) A kinetic model based on the reaction network and experimental data highlighted that direct gasification is a major source of H₂ at short times and low tem-

peratures, although the water-gas shift reaction dominates for H₂ production at longer times as CO becomes available. Steam reforming also contributes H₂ as well as CO, and it is most influential at short times and high temperatures.

(11) The many byproducts that form from phenol SCWG tend to exhibit toxic characteristics toward both freshwater ecosystems and human health. Characterizing the toxic impacts of such compounds is important prior to scale up and commercialization so that information for an environmental impact assessment is available. Characterization studies carried out at different reaction conditions can lead to process optimization with regard to environmental impacts.

(12) The fate of phenol SCWG byproducts emitted into freshwater is primarily to remain there or flow into seawater. However, benzene and, to a lesser extent, biphenyl and dibenzofuran, manifest in large amounts in the atmosphere as a result of their volatility.

(13) Fish consumption is the major pathway by which the human population is exposed to phenol byproducts emitted into freshwater, followed by ingestion of drinking water. An exception to this is benzene, whose second most dominant exposure pathway is inhalation of air.

(14) The greatest contributor toward carcinogenic impact is benzo[a]pyrene. Fluorene, fluoranthene, and pyrene are the main instigators of non-carcinogenic impact. Finally, pyrene and benz[a]anthracene exhibit the greatest ecotoxic impact on freshwater ecosystems.

(15) Overall carcinogenic, non-carcinogenic, and ecotoxic impacts peaked at a temperature of 650 °C for 30 and 60 min reactions. Toxic byproducts became less

stable at 700 °C and were increasingly converted into carbonaceous solids. Although the formation of solids represents a net loss of gas, this outcome is the most preferable for minimizing overall environmental impact and maximizing total gas yield.

9.2 Future Work

This work is a prefiguration of the ultimate objective of developing a unified kinetic and environmental model for SCWG of more complex feedstocks. Working with model compounds is crucial for isolating the chemistry of particular molecular structures, but eventually the understanding of model compound chemistry must be reconstituted into a model for the chemistry of whole biomass. Likewise, being able to predict gasification yields under various conditions is necessary for process optimization, but potential environmental impacts must also be taken into account. The environmental impact modeling accomplished here for phenol SCWG needs to be extended to a broader range of reaction conditions and impact categories. Energy, land, and water use as well as greenhouse gas emissions could all be characterized in addition to human toxicity and ecotoxicity. An ideal model would accept reaction conditions and feedstock composition as inputs and provide product composition and environmental impacts as outputs. There remains much work to be done before this goal can be realized.

The immediate work remaining to be done with phenol SCWG is the assembly of a mechanistic kinetic model. This undertaking is not expected to be trivial. For

instance, the detailed free radical mechanism proposed for SCWO by Gopalan and Savage comprised 121 distinct elementary steps to account for primary dimerization pathways and secondary decomposition pathways [107]. Such a model for phenol SCWG would use the phenol pyrolysis and oxidation mechanisms in Sections 2.2.1 and 2.2.2 as a starting point and would incorporate additional mechanisms corresponding to hydrothermal reactions. Rate constants could be estimated from theory, obtained from literature, or elucidated from experiments. Developing a comprehensive mechanism for phenol SCWG would entail an extremely detailed understanding of intermediate product formation (*e.g.*, dimerization, ring-opening, dimer decomposition, *etc.*) and the free radical chemistry that drives SCWG.

APPENDIX A

Additional Experimental Data

This appendix contains tables of experimental data sets that were not included in their entirety in any of the main chapters. Table A.1 presents the raw data from dibenzofuran SCWG reactions described in Section 6.2. Table A.2 contains the yield data from the additional phenol SCWG experiments carried out for the toxic byproducts characterization in Chapter 8, and Table A.3 contains the complete toxic impact results from that characterization.

Table A.1: Experimental conditions, conversions, and major product yields from dibenzofuran SCWG (30 min, 0.18 g/cm³ water density, 0.10 mol/L dibenzofuran concentration).

T (°C)	500	550	600	650	700
Fractional Conversion	0.201 ± 0.119	0.311 ± 0.157	0.434 ± 0.171	0.849 ± 0.033	0.999 ± 0.000
Fractional Carbon Recovery	0.804 ± 0.121	0.696 ± 0.160	0.621 ± 0.154	0.314 ± 0.028	0.275 ± 0.059
Product Molar Yield					
Benzene	0.001 ± 0.000	0.001 ± 0.000	0.021 ± 0.016	0.109 ± 0.018	0.160 ± 0.033
Phenol	-	-	0.009 ± 0.006	0.025 ± 0.007	0.000
Naphthalene	-	-	0.001 ± 0.001	0.006 ± 0.001	0.008 ± 0.002
Biphenyl	0.000	0.000	0.008 ± 0.005	0.021 ± 0.001	0.011 ± 0.003
2-Phenylphenol	0.000	0.001 ± 0.002	0.013 ± 0.002	0.004 ± 0.002	-
H ₂	0.004 ± 0.003	0.007 ± 0.003	0.033 ± 0.018	0.180 ± 0.007	0.672 ± 0.095
CH ₄	0.000	0.001 ± 0.001	0.007 ± 0.005	0.150 ± 0.013	0.895 ± 0.223
CO ₂	0.030 ± 0.007	0.030 ± 0.008	0.025 ± 0.015	0.189 ± 0.023	0.963 ± 0.165

"0.000" indicates a minuscule finite value, whereas "-" indicates no peak was observed at all.

APPENDIX B

MATLAB Code

This appendix contains the MATLAB code written to accomplish the kinetic modeling of Section 7.3.

Code B.1 is a function called `ResidualSum` that calculates the objective function, Equation 7.15, which is the sum of relative squared errors between experimental values and values calculated from the model. `ResidualSum` first reads in a matrix of experimental concentration data from the external “data.csv” file. `ResidualSum` then passes its input vector of kinetic parameters (containing a number of pre-exponential factors, followed by a complementary number of activation energies) to the function `PointDiffSolver` denoted by Code B.2. `PointDiffSolver` calls the built-in numerical integration algorithm for solving stiff differential equations, `ode15s`, to solve a kinetic model comprising the system of differential mole balances listed in the function `myfun`, which is represented by Code B.3.

Code B.1: ResidualSum.m

```
1 %%%%%%%%%%%%%%%%%%%%%%%%%%%%%%%%%%%%%%%%%%%%%%%%%%%%%%%%%%%%%%%%%%%%%%%%%%
2 % The purpose of this function is to read in a parameter set that is the
3 % rate coefficients of the proposed mechanism. The solution this function
4 % returns is the residual between the predicted value and data value. This
5 % function can then be used in conjunction with the optimtool GUI to
6 % optimize the value of the rate coefficients (i.e. "fitting the data").
7 %
8 % PreF is a vector containing all Arrhenius coefficients in order followed
9 % by all activation energies in order
10 %
11 % Based on original code by Jacob Dickinson
12 %
13 % Revamped by Chad Huelsman in Spring 2012. The function now reads from a
14 % standardized input file ('data.csv'). Instead of a separate function
15 % for each experimental temperature, temperature info is now to be included
16 % in the input file. Information is now automatically determined from the
17 % input file and does not need to be updated manually in the code each time
18 % a new data set is modeled.
19 %
20 % Nothing in this function should need to be changed in order to adapt it
21 % to a new data set or model. All adaptations should be doable by editing
22 % the model function 'myfun.m' or the input file 'Data.csv'.
23 %%%%%%%%%%%%%%%%%%%%%%%%%%%%%%%%%%%%%%%%%%%%%%%%%%%%%%%%%%%%%%%%%%%%%%%%%%
24
25 function Soln = ResidualSum(PreF)
26
27 % Read in the data from a csv file in which the first column is time, the
28 % second column is temperature, then there is a column for each of the
29 % initial concentrations of each species, then an equal number of columns
30 % for the final concentrations of each species. There will be an even
31 % number of columns in total, and each row therefore corresponds to a
32 % distinct experimental data point. The first row is treated as a header
```

```

33 % row and will not be read in.
34 %
35 % Time [=] min
36 % Temp [=] C
37 % Conc [=] mol/L
38 %
39 % Check if data file has already been read into MATLAB (this is to minimize
40 % extra processing associated with opening an external file for every
41 % solution of the ODE system)
42 if exist('Data','var') == 0
43     Data = csvread('data.csv',1,0);
44 end
45
46 % Extract info from raw data
47 DataPoints = size(Data,1);
48 Time = transpose(Data(:,1));
49 T = transpose(Data(:,2));
50
51 NumSpecies = size(Data(:,3:end),2)/2;
52 C0 = Data(:,3:2+NumSpecies);
53 C = Data(:,3+NumSpecies:end);
54
55 % Number of rate coefficients
56 Numks = size(PreF,2)/2;
57
58 % The pre exponential factors
59 A = PreF(1:Numks);
60
61 % Or, if doing a partial fit, read in select pre exponential factors
62 %A=zeros(1,12);
63 %A(7:12)=PreF(1:6);
64
65 % The activation energies
66 Ea = abs(PreF(Numks+1:end));

```



```

67
68 % Or, if doing a partial fit , read in select activation energies
69 %Ea=zeros(1,12);
70 %Ea(7:12)=abs(PreF(7:12));
71
72 % Time needs to be in seconds not minutes
73 Time = Time * 60;
74
75 % T needs to be in Kelvin not Celsius
76 T = T + 273.15;
77
78 % The following nested loops calculate the concentration residuals of each
79 % species for each data point by calling the function PointDiffSolver which
80 % runs an ODE solver to the desired time using the model 'myfun.m' and
81 % returns an array SolvedODE with the time and predicted concentrations
82 SumResidual = 0;
83 R = 8.3144621;
84
85 % If doing a partial fit , some kinetic parameters can be set as constant
86 %k16=[0.533312007794326,0.373256761558587,0.867550375460470,1.32776150809647,
87 % 0.0653528757370801,0.909481084073873,0.528127906466394,1.34259392886207,
88 % 1.48527947606020,0.875069977838195,1.04661673434488,0.206935403987994,
89 % 1.42069111609294,1.15807453465943,1.97704076014653,2.91054593826208,
90 % 0.547419229738376,2.31847415318887,1.07398212836184,2.38059861670933,
91 % 2.44648596319937,1.54303649757482,1.81601742947857,0.962805274764412];
92 %A(1:6)=k16(1:6);
93 %Ea(1:6)=k16(13:18);
94
95
96 for i=1:1:DataPoints
97     SolveTime = Time(i);
98     SolveCini = C0(i,:);
99
100     % Calculating the rate coefficients for the temperature of this data point

```

```

101 % Units for Ea's are 100 kJ, and A's are in terms of log(SECONDS^-1)/10
102 k = 10.^(A*10).*exp(-Ea*100000/(R*T(i)));
103 ParameterSet = k;
104
105 % Solve the ODE system given the k values, initial conditions, and time
106 SolvedODE = PointDiffSolver(ParameterSet,SolveTime,SolveCini,T(i));
107
108 % Summing concentration residuals for each species
109 for j=1:1:NumSpecies
110     % This avoids fitting missing data (if there is no data for a
111     % concentration, this should be denoted using a negative value in
112     % the input, otherwise blank cells will become zeros and optimtool
113     % will try to fit these zero values)
114     if C(i,j) >= 0 && SolvedODE(j+1) ~= 0
115         % Using relative vs. absolute errors to calculate the residuals
116         %TempResidual=((SolvedODE(j+1)-C(i,j))/C(i,j))^2;
117         TempResidual=((SolvedODE(j+1)-C(i,j))/((SolvedODE(j+1)+C(i,j))/2))^2;
118         %TempResidual=(SolvedODE(j+1)-C(i,j))^2;
119         SumResidual = SumResidual + TempResidual;
120     end
121 end
122 end
123
124 Soln = SumResidual;

```

Code B.2: PointDiffSolver.m

```
1 function Soln = PointDiffSolver (ParamSet , PointTime , PointCini , Temp)
2
3 % Read in the initial concentrations
4 Co = PointCini;
5
6 % Set the solution length to integrate over
7 tspan = [0, PointTime];
8
9 % Solve the system of ODEs specified in function 'myfun' over the range 'span'
10 % using initial values 'Co', temperature 'Temp', and kinetic parameters 'ParamSet'
11 [t,C]=ode15s(@myfun,tspan,Co,[], ParamSet ,Temp);
12
13 % Create and populate 'Soln' matrix with output solution
14 SolnLength = size(t,1);
15 NumSpecies = size(C,2);
16 % or NumSpecies = size(Co,2);
17
18 Soln = zeros(1,NumSpecies+1);
19 Soln(1) = t(SolnLength,1);
20 for i=1:1:NumSpecies
21     Soln(i+1) = C(SolnLength,i);
22 end
23
24 % This file should not change.
```

Code B.3: myfun.m

```
1 function dC = myfun(t,C,param,T)
2
3 % phenol dimerizes to DBF, reversible
4 k1=param(1);
5 % DBF reacts to gasifiable dimers
6 k2=param(2);
7 % DBF decomposes to benzene and phenol
8 k3=param(3);
9 % phenol reacts with H2 to benzene
10 k4=param(4);
11 % benzene dimerizes to gasifiable dimers
12 k5=param(5);
13 % DBF decomposes to benzene and phenol
14 k6=param(6);
15 % gasify lumped intermediates to H2
16 k7=param(7);
17 % gasify lumped intermediates to CO
18 k8=param(8);
19 % gasify lumped intermediates to CH4
20 k9=param(9);
21 % gasify lumped intermediates to CO2
22 k10=param(10);
23 % gasifiable products reacts to ungasifiable products
24 k11=param(11);
25 % water-gas shift
26 k12=param(12);
27 K12 = exp( 2975.5 / T - 3.1376 );
28 k12r=k12/K12;
29 % steam reforming to CO
30 k13=param(13);
31
32 dC=zeros(10,1);
```

```

33 % mole balance on benzene
34 dC(1) = - k3*C(1)*C(2) + k4*C(2) - 2*k5*C(1)^2 + k6*C(3);
35 % mole balance on phenol
36 dC(2) = - 2*k1*C(2)^2 - k3*C(1)*C(2) + k6*C(3) - k4*C(2);
37 % mole balance on DBF
38 dC(3) = k1*C(2)^2 - k2*C(3) - k6*C(3);
39 % mole balance on gasifiable dimers
40 dC(4) = k2*C(3) + k3*C(1)*C(2) + k5*C(1)^2 - k11*C(4);
41 % mole balance on ungasifiable products
42 dC(5) = k11*C(4);
43 % mole balance on H2
44 dC(6) = k7*C(4) + k12*C(7)*C(10) - k12r*C(9)*C(6) + k13*C(4);
45 % mole balance on CO
46 dC(7) = k8*C(4) - k12*C(7)*C(10) + k12r*C(9)*C(6) + k13*C(4);
47 % mole balance on CH4
48 dC(8) = k9*C(4);
49 % mole balance on CO2
50 dC(9) = k10*C(4) + k12*C(7)*C(10) - k12r*C(9)*C(6);
51 % mole balance on water
52 dC(10) = -k12*C(7)*C(10) + k12r*C(9)*C(6);

```

BIBLIOGRAPHY

- [1] C. Organ, C. L. Nunn, Z. Machanda, and R. W. Wrangham, "Phylogenetic rate shifts in feeding time during the evolution of homo," *Proc Natl Acad Sci U S A*, vol. 108, no. 35, pp. 14 555–9, Aug 2011.
- [2] F. Berna, P. Goldberg, L. K. Horwitz, J. Brink, S. Holt, M. Bamford, and M. Chazan, "Microstratigraphic evidence of in situ fire in the acheulean strata of wonderwerk cave, northern cape province, south africa," *Proc Natl Acad Sci U S A*, vol. 109, no. 20, pp. E1215–20, May 2012.
- [3] *Annual Energy Review 2011*. U.S. Energy Information Administration, September 2012.
- [4] *Annual Energy Outlook 2014 Early Release Overview*. U.S. Energy Information Administration, December 16, 2013.
- [5] A. A. Peterson, F. Vogel, R. P. Lachance, M. Froeling, M. J. Antal, and J. W. Tester, "Thermochemical biofuel production in hydrothermal media: A review of sub- and supercritical water technologies," *Energy & Environmental Science*, vol. 1, no. 1, pp. 32–65, 2008.
- [6] N. Boukis, V. Diem, U. Galla, and E. Dinjus, "Methanol reforming in supercritical water for hydrogen production," *Combustion Science and Technology*, vol. 178, no. 1-3, pp. 467–485, January 2006.
- [7] A. Loppinet-Serani, C. Aymonier, and F. Cansell, "Current and foreseeable applications of supercritical water for energy and the environment," *ChemSuschem*, vol. 1, no. 6, pp. 486–503, 2008.
- [8] P. Savage, "Organic chemical reactions in supercritical water," *Chemical Reviews*, vol. 99, no. 2, pp. 603–621, February 1999.
- [9] N. Akiya and P. Savage, "Roles of water for chemical reactions in high-temperature water," *Chemical Reviews*, vol. 102, no. 8, pp. 2725–2750, August 2002.
- [10] I. Lee, M. Kim, and S. Ihm, "Gasification of glucose in supercritical water," *Industrial & Engineering Chemistry Research*, vol. 41, no. 5, pp. 1182–1188, March 6 2002.

- [11] Z. Fang, T. Minowa, R. Smith, T. Ogi, and J. Kozinski, "Liquefaction and gasification of cellulose with Na_2CO_3 and Ni in subcritical water at 350 degrees C," *Industrial & Engineering Chemistry Research*, vol. 43, no. 10, pp. 2454–2463, May 12 2004.
- [12] A. Kruse, T. Henningsen, A. Sinag, and J. Pfeiffer, "Biomass gasification in supercritical water: Influence of the dry matter content and the formation of phenols," *Industrial & Engineering Chemistry Research*, vol. 42, no. 16, pp. 3711–3717, August 6 2003.
- [13] O. Bobleter, "Hydrothermal degradation of polymers derived from plants," *Progress In Polymer Science*, vol. 19, no. 5, pp. 797–841, 1994.
- [14] A. Sinag, A. Kruse, and V. Schwarzkopf, "Key compounds of the hydrolysis of glucose in supercritical water in the presence of K_2CO_3 ," *Industrial & Engineering Chemistry Research*, vol. 42, no. 15, pp. 3516–3521, July 23 2003.
- [15] A. Sinag, A. Kruse, and J. Rathert, "Influence of the heating rate and the type of catalyst on the formation of key intermediates and on the generation of gases during hydrolysis of glucose in supercritical water in a batch reactor," *Industrial & Engineering Chemistry Research*, vol. 43, no. 2, pp. 502–508, Jan. 2004.
- [16] P. Williams and J. Onwudili, "Composition of products from the supercritical water gasification of glucose: A model biomass compound," *Industrial & Engineering Chemistry Research*, vol. 44, no. 23, pp. 8739–8749, Nov. 2005.
- [17] A. K. Goodwin and G. L. Rorrer, "Conversion of glucose to hydrogen-rich gas by supercritical water in a microchannel reactor," *Industrial & Engineering Chemistry Research*, vol. 47, no. 12, pp. 4106–4114, Jun. 2008.
- [18] A. Sinag, S. Gulbay, B. Uskan, and M. Gullu, "Comparative studies of intermediates produced from hydrothermal treatments of sawdust and cellulose," *Journal of Supercritical Fluids*, vol. 50, no. 2, pp. 121–127, Sep. 2009.
- [19] T. M. Brown, P. Duan, and P. E. Savage, "Hydrothermal liquefaction and gasification of *Nannochloropsis* sp.," *Energy & Fuels*, vol. 24, pp. 3639–3646, Jun. 2010.
- [20] P. Duan and P. E. Savage, "Hydrothermal liquefaction of a microalga with heterogeneous catalysts," *Industrial & Engineering Chemistry Research*, vol. 50, no. 1, pp. 52–61, Jan. 2011.
- [21] Q. Guan, P. E. Savage, and C. Wei, "Gasification of alga *Nannochloropsis* sp in supercritical water," *Journal of Supercritical Fluids*, vol. 61, pp. 139–145, Jan. 2012.

- [22] A. Kruse and A. Gawlik, "Biomass conversion in water at 330-410 degrees c and 30-50 mpa. identification of key compounds for indicating different chemical reaction pathways," *Industrial & Engineering Chemistry Research*, vol. 42, no. 2, pp. 267–279, January 22 2003.
- [23] W. Jablonski, K. R. Gaston, M. R. Nimlos, D. L. Carpenter, C. J. Feik, and S. D. Phillips, "Pilot-scale gasification of corn stover, switchgrass, wheat straw, and wood: 2. identification of global chemistry using multivariate curve resolution techniques," *Industrial & Engineering Chemistry Research*, vol. 48, no. 23, pp. 10 691–10 701, Dec. 2009.
- [24] A. Sinag, S. Gulbay, B. Uskan, and M. Canel, "Biomass decomposition in near critical water," *Energy Conversion and Management*, vol. 51, no. 3, pp. 612–620, Mar. 2010.
- [25] F. Melligan, R. Auccaise, E. H. Novotny, J. J. Leahy, M. H. B. Hayes, and W. Kwapinski, "Pressurised pyrolysis of miscanthus using a fixed bed reactor," *Bioresource Technology*, vol. 102, no. 3, pp. 3466–3470, Feb. 2011.
- [26] C. Martino and P. Savage, "Thermal decomposition of substituted phenols in supercritical water," *Industrial & Engineering Chemistry Research*, vol. 36, no. 5, pp. 1385–1390, May 1997.
- [27] K. Okuda, S. Ohara, M. Umetsu, S. Takami, and T. Adschiri, "Disassembly of lignin and chemical recovery in supercritical water and p-cresol mixture - studies on lignin model compounds," *Bioresource Technology*, vol. 99, no. 6, pp. 1846–1852, Apr. 2008.
- [28] Wahyudiono, M. Sasaki, and M. Goto, "Conversion of biomass model compound under hydrothermal conditions using batch reactor," *Fuel*, vol. 88, no. 9, pp. 1656–1664, Sep. 2009.
- [29] A. Kruse, P. Bernolle, N. Dahmen, E. Dinjus, and P. Maniam, "Hydrothermal gasification of biomass: consecutive reactions to long-living intermediates," *Energy & Environmental Science*, vol. 3, no. 1, pp. 136–143, 2010.
- [30] G. Busca, S. Berardinelli, C. Resini, and L. Arrighi, "Technologies for the removal of phenol from fluid streams: A short review of recent developments," *Journal of Hazardous Materials*, vol. 160, no. 2-3, pp. 265–288, Dec. 2008.
- [31] A. Kruse, "Supercritical water gasification," *Biofuels Bioproducts & Biorefining-Biofpr*, vol. 2, no. 5, pp. 415–437, September-October 2008.
- [32] T. Karayildirim, A. Sinag, and A. Kruse, "Char and coke formation as unwanted side reaction of the hydrothermal biomass gasification," *Chemical Engineering & Technology*, vol. 31, no. 11, pp. 1561–1568, Nov. 2008.

- [33] Y. Matsumura, "Evaluation of supercritical water gasification and biomethanation for wet biomass utilization in Japan," *Energy Conversion and Management*, vol. 43, no. 9-12, pp. 1301–1310, June-August 2002.
- [34] E. Gasafi, M.-Y. Reinecke, A. Kruse, and L. Schebek, "Economic analysis of sewage sludge gasification in supercritical water for hydrogen production," *Biomass & Bioenergy*, vol. 32, no. 12, pp. 1085–1096, Dec. 2008.
- [35] J. S. Luterbacher, M. Froling, F. Vogel, F. Marechal, and J. W. Tester, "Hydrothermal gasification of waste biomass: Process design and life cycle assessment," *Environmental Science & Technology*, vol. 43, no. 5, pp. 1578–1583, March 1 2009.
- [36] P. E. Savage, "A perspective on catalysis in sub- and supercritical water," *Journal of Supercritical Fluids*, vol. 47, no. 3, pp. 407–414, January 2009.
- [37] D. C. Elliott, "Catalytic hydrothermal gasification of biomass," *Biofuels Bio-products & Biorefining-Biofpr*, vol. 2, no. 3, pp. 254–265, May-June 2008.
- [38] A. Kruse, "Hydrothermal biomass gasification," *Journal of Supercritical Fluids*, vol. 47, no. 3, pp. 391–399, January 2009.
- [39] G. Brunner, "Near critical and supercritical water. part i. hydrolytic and hydrothermal processes," *Journal of Supercritical Fluids*, vol. 47, no. 3, pp. 373–381, Jan. 2009.
- [40] G. van Rossum, B. Potic, S. R. A. Kersten, and W. P. M. van Swaaij, "Catalytic gasification of dry and wet biomass," *Catalysis Today*, vol. 145, no. 1-2, pp. 10–18, Jul. 2009.
- [41] P. Basu and V. Mettananant, "Biomass gasification in supercritical water - a review," *International Journal of Chemical Reactor Engineering*, vol. 7, p. R3, 2009.
- [42] Y. Guo, S. Z. Wang, D. H. Xu, Y. M. Gong, H. H. Ma, and X. Y. Tang, "Review of catalytic supercritical water gasification for hydrogen production from biomass," *Renewable & Sustainable Energy Reviews*, vol. 14, no. 1, pp. 334–343, Jan. 2010.
- [43] Y. Bo and W. Chaohai, "Hydrogen production from organic compounds by supercritical water gasification," *Progress In Chemistry*, vol. 20, no. 10, pp. 1553–1561, October 2008.
- [44] P. E. Savage, R. B. Levine, and C. M. Huelsman, *Thermochemical Conversion of Biomass to Liquid Fuels and Chemicals*. Royal Society of Chemistry, 2010, ch. 8. Hydrothermal Processing of Biomass, pp. 192–221.

- [45] M. Modell, "Gasification and liquefaction of forest products in supercritical water," in *Fundamentals of Thermochemical Biomass Conversion*, R. Overend, T. Milne, and L. Mudge, Eds. Elsevier Appl. Sci. Publ., 1985, ch. 6, pp. 95–120.
- [46] F. L. P. Resende and P. E. Savage, "Kinetic model for noncatalytic supercritical water gasification of cellulose and lignin," *Aiche Journal*, vol. 56, no. 9, pp. 2412–2420, Sep. 2010.
- [47] H. Schmieder, J. Abeln, N. Boukis, E. Dinjus, A. Kruse, M. Kluth, G. Petrich, E. Sadri, and M. Schacht, "Hydrothermal gasification of biomass and organic wastes," *Journal of Supercritical Fluids*, vol. 17, no. 2, pp. 145–153, April 10 2000.
- [48] G. J. DiLeo and P. E. Savage, "Catalysis during methanol gasification in supercritical water," *Journal of Supercritical Fluids*, vol. 39, no. 2, pp. 228–232, December 2006.
- [49] G. J. DiLeo, M. E. Neff, and P. E. Savage, "Gasification of guaiacol and phenol in supercritical water," *Energy & Fuels*, vol. 21, no. 4, pp. 2340–2345, July-August 2007.
- [50] W. Buhler, E. Dinjus, H. Ederer, A. Kruse, and C. Mas, "Ionic reactions and pyrolysis of glycerol as competing reaction pathways in near- and supercritical water," *Journal of Supercritical Fluids*, vol. 22, no. 1, pp. 37–53, Jan. 2002.
- [51] G. J. DiLeo, M. E. Neff, S. Kim, and P. E. Savage, "Supercritical water gasification of phenol and glycine as models for plant and protein biomass," *Energy & Fuels*, vol. 22, no. 2, pp. 871–877, March-April 2008.
- [52] L. J. Guo, Y. J. Lu, X. M. Zhang, C. M. Ji, Y. Guan, and A. X. Pei, "Hydrogen production by biomass gasification in supercritical water: A systematic experimental and analytical study," *Catalysis Today*, vol. 129, no. 3-4, pp. 275–286, December 15 2007.
- [53] D. Elliott and J. Sealock, "Low temperature gasification of biomass under pressure," in *Fundamentals of Thermochemical Biomass Conversion*, R. P. Overend, T. A. Milne, and L. K. Mudge, Eds. Elsevier Appl. Sci. Publ., 1985, pp. 937–950.
- [54] D. Elliott, L. Sealock, and E. Baker, "Chemical-processing in high-pressure aqueous environments .2. development of catalysts for gasification," *Industrial & Engineering Chemistry Research*, vol. 32, no. 8, pp. 1542–1548, Aug. 1993.
- [55] D. Elliott, T. Hart, and G. Neuenschwander, "Chemical processing in high-pressure aqueous environments. 8. improved catalysts for hydrothermal gasification," *Industrial & Engineering Chemistry Research*, vol. 45, no. 11, pp. 3776–3781, May 2006.

- [56] T. Yoshida, Y. Oshima, and Y. Matsumura, "Gasification of biomass model compounds and real biomass in supercritical water," *Biomass & Bioenergy*, vol. 26, no. 1, pp. 71–78, 2004.
- [57] T. Minowa, F. Zhen, and T. Ogi, "Cellulose decomposition in hot-compressed water with alkali or nickel catalyst," *Journal of Supercritical Fluids*, vol. 13, no. 1-3, pp. 253–259, Jun. 1998.
- [58] A. Kruse and E. Dinjus, "Influence of salts during hydrothermal biomass gasification: The role of the catalysed water-gas shift reaction," *Zeitschrift Fur Physikalische Chemie-International Journal of Research In Physical Chemistry & Chemical Physics*, vol. 219, no. 3, pp. 341–366, 2005.
- [59] A. Kruse, H. Ederer, D. Ernst, and B. Seine, "Measurement of residence time in hot compressed water: 2. salts in a continuously stirred tank reactor," *Chemical Engineering & Technology*, vol. 32, no. 6, pp. 971–976, Jun. 2009.
- [60] A. Sinag, A. Kruse, and V. Schwarzkopf, "Formation and degradation pathways of intermediates formed in the hydrolysis of glucose as a model substance for wet biomass in a tubular reactor," *Chemie Ingenieur Technik*, vol. 75, no. 9, pp. 1351–1355, September 2003.
- [61] A. Kruse, P. Maniam, and F. Spieler, "Influence of proteins on the hydrothermal gasification and liquefaction of biomass. 2. model compounds," *Industrial & Engineering Chemistry Research*, vol. 46, no. 1, pp. 87–96, Jan. 2007.
- [62] A. Kruse, D. Meier, P. Rimbrecht, and M. Schacht, "Gasification of pyrocatechol in supercritical water in the presence of potassium hydroxide," *Industrial & Engineering Chemistry Research*, vol. 39, no. 12, pp. 4842–4848, Dec. 2000.
- [63] J. A. Onwudili and P. T. Williams, "Role of sodium hydroxide in the production of hydrogen gas from the hydrothermal gasification of biomass," *International Journal of Hydrogen Energy*, vol. 34, no. 14, pp. 5645–5656, Jul. 2009.
- [64] D. Elliott and L. Sealock, "Aqueous catalyst systems for the water gas shift reaction .1. comparative catalyst studies," *Industrial & Engineering Chemistry Product Research and Development*, vol. 22, no. 3, pp. 426–431, 1983.
- [65] Y. Matsumura, T. Minowa, B. Potic, S. Kersten, W. Prins, W. van Swaaij, B. van de Beld, D. Elliott, G. Neuenschwander, A. Kruse, and M. Antal, "Biomass gasification in near- and super-critical water: Status and prospects," *Biomass & Bioenergy*, vol. 29, no. 4, pp. 269–292, 2005.
- [66] M. Antal, S. Allen, D. Schulman, X. Xu, and R. Divilio, "Biomass gasification in supercritical water," *Industrial & Engineering Chemistry Research*, vol. 39, no. 11, pp. 4040–4053, November 2000.

- [67] X. Xu, Y. Matsumura, J. Stenberg, and M. Antal, "Carbon-catalyzed gasification of organic feedstocks in supercritical water," *Industrial & Engineering Chemistry Research*, vol. 35, no. 8, pp. 2522–2530, August 1996.
- [68] T. Yanagida, T. Minowa, Y. Shimizu, Y. Matsumura, and Y. Noda, "Recovery of activated carbon catalyst, calcium, nitrogen and phosphate from effluent following supercritical water gasification of poultry manure," *Bioresource Technology*, vol. 100, no. 20, pp. 4884–4886, Oct. 2009.
- [69] I.-G. Lee and S.-K. Ihm, "Catalytic gasification of glucose over ni/activated charcoal in supercritical water," *Industrial & Engineering Chemistry Research*, vol. 48, no. 3, pp. 1435–1442, February 4 2009.
- [70] F. L. P. Resende and P. E. Savage, "Expanded and updated results for supercritical water gasification of cellulose and lignin in metal-free reactors," *Energy & Fuels*, vol. 23, pp. 6213–6221, Dec. 2009.
- [71] M. Sasaki, B. Kabyemela, R. Malaluan, S. Hirose, N. Takeda, T. Adschiri, and K. Arai, "Cellulose hydrolysis in subcritical and supercritical water," *Journal of Supercritical Fluids, The*, vol. 13, no. 1-3, pp. 261 – 268, 1998.
- [72] M. Sasaki, Z. Fang, Y. Fukushima, T. Adschiri, and K. Arai, "Dissolution and hydrolysis of cellulose in subcritical and supercritical water," *Industrial & Engineering Chemistry Research*, vol. 39, no. 8, pp. 2883–2890, 2000.
- [73] M. Sasaki, T. Adschiri, and K. Arai, "Kinetics of cellulose conversion at 25 MPa in sub- and Supercritical water," *AIChE Journal*, vol. 50, no. 1, pp. 192–202, January 2004.
- [74] Y. Matsumura, M. Sasaki, K. Okuda, S. Takami, S. Ohara, M. Umetsu, and T. Adschiri, "Supercritical water treatment of biomass for energy and material recovery," *Combustion Science and Technology*, vol. 178, no. 1-3, pp. 509–536, January 2006.
- [75] M. Osada, T. Sato, M. Watanabe, M. Shirai, and K. Arai, "Catalytic gasification of wood biomass in subcritical and supercritical water," *Combustion Science and Technology*, vol. 178, no. 1-3, pp. 537–552, January 2006.
- [76] M. Saisu, T. Sato, M. Watanabe, T. Adschiri, and K. Arai, "Conversion of lignin with supercritical water-phenol mixtures," *Energy & Fuels*, vol. 17, no. 4, pp. 922–928, Jul-Aug 2003.
- [77] K. Okuda, M. Umetsu, S. Takami, and T. Adschiri, "Disassembly of lignin and chemical recovery - rapid depolymerization of lignin without char formation in water-phenol mixtures," *Fuel Processing Technology*, vol. 85, no. 8-10, pp. 803–813, Jul. 2004.

- [78] T. Sato, M. Osada, M. Watanabe, M. Shirai, and K. Arai, "Gasification of alkylphenols with supported noble metal catalysts in supercritical water," *Industrial & Engineering Chemistry Research*, vol. 42, no. 19, pp. 4277–4282, September 17 2003.
- [79] M. Watanabe, H. Inomata, M. Osada, T. Sato, T. Adschiri, and K. Arai, "Catalytic effects of naoh and zro2 for partial oxidative gasification of n-hexadecane and lignin in supercritical water," *Fuel*, vol. 82, no. 5, pp. 545–552, March 2003.
- [80] M. Osada, T. Sato, M. Watanabe, T. Adschiri, and K. Arai, "Low-Temperature catalytic gasification of lignin and cellulose with a ruthenium catalyst in supercritical water," *Energy & Fuels*, vol. 18, no. 2, pp. 327–333, Mar. 2004.
- [81] A. Kruse, A. Krupka, V. Schwarzkopf, C. Gamard, and T. Henningsen, "Influence of proteins on the hydrothermal gasification and liquefaction of biomass. 1. comparison of different feedstocks," *Industrial & Engineering Chemistry Research*, vol. 44, no. 9, pp. 3013–3020, Apr. 2005.
- [82] T. Yoshida and Y. Matsumura, "Gasification of cellulose, xylan, and lignin mixtures in supercritical water," *Industrial & Engineering Chemistry Research*, vol. 40, no. 23, pp. 5469–5474, November 14 2001.
- [83] A. K. Goodwin and G. L. Rorrer, "Conversion of xylose and xylose-phenol mixtures to hydrogen-rich gas by supercritical water in an isothermal micro-tube flow reactor," *Energy & Fuels*, vol. 23, no. 7, pp. 3818–3825, Jul. 2009.
- [84] E. Weiss-Hortala, A. Kruse, C. Ceccarelli, and R. Barna, "Influence of phenol on glucose degradation during supercritical water gasification," *The Journal of Supercritical Fluids*, vol. 53, no. 1-3, pp. 42–47, 2010, selected papers from the 9th International Symposium on Supercritical Fluids (ISSF 2009) - New Trends in Supercritical Fluids: Energy, Materials, Processing, Arcachon, France, May 18-20, 2009.
- [85] K. Tsukahara and S. Sawayama, "Liquid fuel production using microalgae," *Journal of the Japan Petroleum Institute*, vol. 48, no. 5, pp. 251–259, Sep. 2005.
- [86] T. Minowa and S. Sawayama, "A novel microalgal system for energy production with nitrogen cycling," *Fuel*, vol. 78, no. 10, pp. 1213 – 1215, 1999.
- [87] "Genifuel corporation," <http://www.genifuel.com/>, April 2014.
- [88] K. B. Cantrell, T. Ducey, K. S. Ro, and P. G. Hunt, "Livestock waste-to-bioenergy generation opportunities," *Bioresource Technology*, vol. 99, no. 17, pp. 7941 – 7953, 2008.
- [89] K. Tsukahara, T. Kimura, T. Minowa, S. Sawayama, T. Yagishita, S. Inoue, T. Hanaoka, and Y. Usui, "Microalgal cultivation in a solution recovered

- from the low-temperature catalytic gasification of the microalga," *Journal of Bioscience and Bioengineering*, vol. 91, no. 3, pp. 311–313, March 2001.
- [90] S. Stucki, F. Vogel, C. Ludwig, A. G. Haiduc, and M. Brandenberger, "Catalytic gasification of algae in supercritical water for biofuel production and carbon capture," *Energy & Environmental Science*, vol. 2, no. 5, pp. 535–541, 2009.
- [91] A. A. Peterson, P. Vontobel, F. Vogel, and J. W. Tester, "Normal-phase dynamic imaging of supercritical-water salt precipitation using neutron radiography," *Journal of Supercritical Fluids*, vol. 49, no. 1, pp. 71–78, May 2009.
- [92] A. Nakamura, E. Kiyonaga, Y. Yamamura, Y. Shimizu, T. Minowa, Y. Noda, and Y. Matsumura, "Gasification of catalyst-suspended chicken manure in supercritical water," *Journal of Chemical Engineering of Japan*, vol. 41, no. 5, pp. 433–440, 2008.
- [93] N. Boukis, U. Galla, H. Müller, E. Dinjus, and F. ITC-CPV, "Biomass gasification in supercritical water. experimental progress achieved with the verena pilot plant," *15th European Biomass Conference & Exhibition, Berlin, 2007*.
- [94] T. Yoshida and Y. Matsumura, "Reactor development for supercritical water gasification of 4.9 wt% glucose solution at 673 k by using computational fluid dynamics," *Industrial & Engineering Chemistry Research*, vol. 48, no. 18, pp. 8381–8386, Sep. 2009.
- [95] C. Horn, K. Roy, P. Frank, and T. Just, "Shock-tube study on the high-temperature pyrolysis of phenol," *Symposium (International) on Combustion*, vol. 27, no. 1, pp. 321–328, 1998, twenty-Seventh Symposium (International) on Combustion Volume One.
- [96] H. Richter and J. B. Howard, "Formation of polycyclic aromatic hydrocarbons and their growth to soot—a review of chemical reaction pathways," *Progress in Energy and Combustion Science*, vol. 26, no. 4-6, pp. 565 – 608, 2000.
- [97] L. Khachatryan, J. Adounkpe, and B. Dellinger, "Formation of phenoxy and cyclopentadienyl radicals from the gas-phase pyrolysis of phenol," *Journal of Physical Chemistry a*, vol. 112, no. 3, pp. 481–487, Jan. 2008.
- [98] K. Brezinsky, M. Pecullan, and I. Glassman, "Pyrolysis and oxidation of phenol," *Journal of Physical Chemistry a*, vol. 102, no. 44, pp. 8614–8619, Oct. 1998.
- [99] T. Thornton, "Phenol oxidation in supercritical water: Reaction kinetics, products, and pathways," Ph.D. dissertation, University of Michigan, 1991.
- [100] T. D. Thornton and P. E. Savage, "Phenol oxidation in supercritical water," *The Journal of Supercritical Fluids*, vol. 3, no. 4, pp. 240 – 248, 1990, symposium on Supercritical Fluids.

- [101] T. Thornton, D. Ladue, and P. Savage, "Phenol oxidation in supercritical water - formation of dibenzofuran, dibenzo-para-dioxin, and related-compounds," *Environmental Science & Technology*, vol. 25, no. 8, pp. 1507–1510, August 1991.
- [102] T. Thornton and P. Savage, "Phenol oxidation pathways in supercritical water," *Industrial & Engineering Chemistry Research*, vol. 31, no. 11, pp. 2451–2456, November 1992.
- [103] T. Thornton, D. Ladue, and P. Savage, "Phenol oxidation in supercritical water - formation of dibenzofuran, dibenzo-p-dioxin, and related-compounds - comment," *Environmental Science & Technology*, vol. 26, no. 9, pp. 1850–1850, September 1992.
- [104] T. Thornton and P. Savage, "Kinetics of phenol oxidation in supercritical water," *Aiche Journal*, vol. 38, no. 3, pp. 321–327, March 1992.
- [105] S. Gopalan and P. Savage, "A reaction network model for phenol oxidation in supercritical water," *Aiche Journal*, vol. 41, no. 8, pp. 1864–1873, August 1995.
- [106] —, "Reaction-mechanism for phenol oxidation in supercritical water," *Journal of Physical Chemistry*, vol. 98, no. 48, pp. 12 646–12 652, December 1994.
- [107] —, "Phenol oxidation in supercritical water - from global kinetics and product identities to an elementary reaction model," *Innovations In Supercritical Fluids*, vol. 608, pp. 217–231, 1995.
- [108] J. Born, R. Louw, and P. Mulder, "Formation of dibenzodioxins and dibenzofurans in homogenous gas-phase reactions of phenols," *Chemosphere*, vol. 19, no. 1-6, pp. 401–406, 1989.
- [109] D. Xu, S. Wang, Y. Guo, X. Tang, Y. Gong, and H. Ma, "Catalyzed partial oxidative gasification of phenol in supercritical water," *Industrial & Engineering Chemistry Research*, vol. 50, no. 8, pp. 4301–4307, 2011.
- [110] Q. Guan, C. Wei, H. Shi, C. Wu, and X.-S. Chai, "Partial oxidative gasification of phenol for hydrogen in supercritical water," *Applied Energy*, vol. 88, no. 8, pp. 2612–2616, Aug. 2011.
- [111] Q. Guan, C. Wei, and X.-S. Chai, "Pathways and kinetics of partial oxidation of phenol in supercritical water," *Chemical Engineering Journal*, vol. 175, pp. 201–206, Nov. 2011.
- [112] G. J. DiLeo, "Gasification of biomass model compounds in supercritical water," Ph.D. dissertation, University of Michigan, 2007.

- [113] R. Fournier and R. Potter, "An equation correlating the solubility of quartz in water from 25-degrees-c to 900-degrees-c at pressures up to 10,000 bars," *Geochimica Et Cosmochimica Acta*, vol. 46, no. 10, pp. 1969–1973, 1982.
- [114] A. Lovell, K. Brezinsky, and I. Glassman, "The gas-phase pyrolysis of phenol," *International Journal of Chemical Kinetics*, vol. 21, no. 7, pp. 547–560, Jul. 1989.
- [115] Y. He, W. Mallard, and W. Tsang, "Kinetics of hydrogen and hydroxyl radical attack on phenol at high-temperatures," *Journal of Physical Chemistry*, vol. 92, no. 8, pp. 2196–2201, Apr. 1988.
- [116] F. L. P. Resende, S. A. Fraley, M. J. Berger, and P. E. Savage, "Noncatalytic gasification of lignin in supercritical water," *Energy & Fuels*, vol. 22, no. 2, pp. 1328–1334, March-April 2008.
- [117] F. L. P. Resende, M. E. Neff, and P. E. Savage, "Noncatalytic gasification of cellulose in supercritical water," *Energy & Fuels*, vol. 21, no. 6, pp. 3637–3643, November-December 2007.
- [118] S. Rice, R. Steeper, and J. Aiken, "Water density effects on homogeneous water-gas shift reaction kinetics," *Journal of Physical Chemistry a*, vol. 102, no. 16, pp. 2673–2678, Apr. 1998.
- [119] J. Lawson and M. Klein, "Influence of water on guaiacol pyrolysis," *Industrial & Engineering Chemistry Fundamentals*, vol. 24, no. 2, pp. 203–208, 1985.
- [120] J. Henrikson, Z. Chen, and P. Savage, "Inhibition and acceleration of phenol oxidation by supercritical water," *Industrial & Engineering Chemistry Research*, vol. 42, no. 25, pp. 6303–6309, December 10 2003.
- [121] J. Henrikson and P. Savage, "Potential explanations for the inhibition and acceleration of phenol scwo by water," *Industrial & Engineering Chemistry Research*, vol. 43, no. 16, pp. 4841–4847, August 4 2004.
- [122] Y. Oshima, K. Hori, M. Toda, T. Chommanad, and S. Koda, "Phenol oxidation kinetics in supercritical water," *Journal of Supercritical Fluids*, vol. 13, no. 1-3, pp. 241–246, Jun. 1998.
- [123] J. Henrikson, C. Grice, and P. Savage, "Effect of water density on methanol oxidation kinetics in supercritical water," *Journal of Physical Chemistry a*, vol. 110, no. 10, pp. 3627–3632, March 16 2006.
- [124] T. Fujii, R. Hayashi, S.-i. Kawasaki, A. Suzuki, and Y. Oshima, "Water density effects on methanol oxidation in supercritical water at high pressure up to 100 mpa," *Journal of Supercritical Fluids*, vol. 58, no. 1, pp. 142–149, Aug. 2011.

- [125] P. Marrone, T. Arias, W. Peters, and J. Tester, "Solvation effects on kinetics of methylene chloride reactions in sub- and supercritical water: Theory, experiment, and ab initio calculations," *Journal of Physical Chemistry a*, vol. 102, pp. 7013–7028, 1998.
- [126] D. Salvatierra, J. Taylor, P. Marrone, and J. Tester, "Kinetic study of hydrolysis of methylene chloride from 100 to 500 degrees c," *Industrial & Engineering Chemistry Research*, vol. 38, pp. 4169–4174, 1999.
- [127] T. Adschiri, Y. Hakuta, K. Sue, and K. Arai, "Hydrothermal synthesis of metal oxide nanoparticles at supercritical conditions," *Journal of Nanoparticle Research*, vol. 3, pp. 227–235, 2001.
- [128] V. Anikeev, A. Yermakova, J. Manion, and R. Huie, "Kinetics and thermodynamics of 2-propanol dehydration in supercritical water," *Journal of Supercritical Fluids*, vol. 32, pp. 123–135, 2004.
- [129] G. Gonzalez and D. Montane, "Kinetics of dibenzylether hydrothermolysis in supercritical water," *Aiche Journal*, vol. 51, pp. 971–981, 2005.
- [130] W. L. Marshall, "Dielectric constant of water discovered to be simple function of density over extreme ranges from – 35 to + 600oc and to 1200 mpa (12000 atm.), believed universal," 2008, available from *Nature Precedings*, <http://dx.doi.org/10.1038/npre.2008.2472.1>.
- [131] W. Lamb, G. Hoffman, and J. Jonas, "Self-diffusion in compressed supercritical water," *Journal of Chemical Physics*, vol. 74, pp. 6875–6880, 1981.
- [132] A. Plugatyr and I. M. Svishchev, "Molecular diffusivity of phenol in sub- and supercritical water: Application of the split-flow taylor dispersion technique," *Journal of Physical Chemistry B*, vol. 115, pp. 2555–2562, 2011.
- [133] L. S. Lasdon, A. D. Waren, A. Jain, and M. Ratner, "Design and testing of a generalized reduced gradient code for nonlinear programming," *ACM Transactions on Mathematical Software*, vol. 4, no. 1, pp. 34–50, Mar. 1978.
- [134] Y. Matsumura, S. Yanachi, and T. Yoshida, "Glucose decomposition kinetics in water at 25 mpa in the temperature range of 448-673 k," *Industrial & Engineering Chemistry Research*, vol. 45, no. 6, pp. 1875–1879, Mar. 2006.
- [135] N. Bhore, M. Klein, and K. Bischoff, "The delplot technique - a new method for reaction pathway analysis," *Industrial & Engineering Chemistry Research*, vol. 29, no. 2, pp. 313–316, Feb. 1990.
- [136] I. Wiater, J. G. P. Born, and R. Louw, "Products, rates, and mechanism of the gas-phase condensation of phenoxy radicals between 500-840 k," *European Journal of Organic Chemistry*, vol. 2000, no. 6, pp. 921–928, 2000.

- [137] B. Shukla, A. Susa, A. Miyoshi, and M. Koshi, "Role of phenyl radicals in the growth of polycyclic aromatic hydrocarbons," *The Journal of Physical Chemistry A*, vol. 112, no. 11, pp. 2362–2369, 2008, pMID: 18298104.
- [138] Y. M. Alshammari and K. Hellgardt, "Thermodynamic analysis of hydrogen production via hydrothermal gasification of hexadecane," *International Journal of Hydrogen Energy*, vol. 37, no. 7, pp. 5656–5664, Apr. 2012.
- [139] S. Letellier, F. Marias, P. Cezac, and J. Serin, "Gasification of aqueous biomass in supercritical water: A thermodynamic equilibrium analysis," *The Journal of Supercritical Fluids*, vol. 51, no. 3, pp. 353 – 361, 2010.
- [140] F. A. P. Voll, C. C. R. S. Rossi, C. Silva, R. Guirardello, R. O. M. A. Souza, V. F. Cabral, and L. Cardozo-Filho, "Thermodynamic analysis of supercritical water gasification of methanol, ethanol, glycerol, glucose and cellulose," *International Journal of Hydrogen Energy*, vol. 34, no. 24, pp. 9737–9744, Dec. 2009.
- [141] H. Tang and K. Kitagawa, "Supercritical water gasification of biomass: thermodynamic analysis with direct gibbs free energy minimization," *Chemical Engineering Journal*, vol. 106, no. 3, pp. 261–267, Feb. 2005.
- [142] J. Lagarias, J. Reeds, M. Wright, and P. Wright, "Convergence properties of the nelder-mead simplex method in low dimensions," *Siam Journal On Optimization*, vol. 9, pp. 112–147, 1998.
- [143] Y. Yoshida, K. Dowaki, Y. Matsumura, R. Matsushashi, D. Li, H. Ishitani, and H. Komiyama, "Comprehensive comparison of efficiency and co2 emissions between biomass energy conversion technologies - position of supercritical water gasification in biomass technologies," *Biomass & Bioenergy*, vol. 25, no. 3, pp. 257–272, 2003.
- [144] P. Azadi, G. Brownbridge, S. Mosbach, A. Smallbone, A. Bhave, O. Inderwildi, and M. Kraft, "The carbon footprint and non-renewable energy demand of algae-derived biodiesel," *Applied Energy*, vol. 113, pp. 1632–1644, 2014.
- [145] Z. R. Xu, W. Zhu, M. Li, H. W. Zhang, and M. Gong, "Quantitative analysis of polycyclic aromatic hydrocarbons in solid residues from supercritical water gasification of wet sewage sludge," *Applied Energy*, vol. 102, pp. 476–483, 2013.
- [146] S. H. Aljbour and K. Kawamoto, "Bench-scale gasification of cedar wood - part ii: Effect of operational conditions on contaminant release," *Chemosphere*, vol. 90, pp. 1501–1507, 2013.

- [147] S. E. Hale, J. Lehmann, D. Rutherford, A. R. Zimmerman, R. T. Bachmann, V. Shitumbanuma, A. O'Toole, K. L. Sundqvist, H. P. H. Arp, and G. Cornelissen, "Quantifying the total and bioavailable polycyclic aromatic hydrocarbons and dioxins in biochars," *Environmental Science & Technology*, vol. 46, no. 5, pp. 2830–2838, Mar. 2012.
- [148] *Toxicological Profile for Polycyclic Aromatic Hydrocarbons*, Agency for Toxic Substances and Disease Registry (ATSDR), Public Health Service, U.S. Department of Health and Human Services, Atlanta, GA, December 1990.
- [149] C. E. Ridley, C. M. Clark, S. D. LeDuc, B. G. Bierwagen, B. B. Lin, A. Mehl, and D. A. Tobias, "Biofuels: Network analysis of the literature reveals key environmental and economic unknowns," *Environmental Science & Technology*, vol. 46, no. 3, pp. 1309–1315, Feb. 2012.
- [150] S. Y. Bircan, R. Kanamori, Y. Hasegawa, K. Ohba, K. Matsumoto, and K. Kitagawa, "Gc-ms ultra trace analysis of dioxins produced through hydrothermal gasification of biowastes," *Microchemical Journal*, vol. 99, no. 2, pp. 556–560, Nov. 2011.
- [151] *Office of Environmental Information, Emergency Planning and Community Right-to-Know Act – Section 313: Guidance for Reporting Toxic Chemicals: Polycyclic Aromatic Compounds Category*, EPA 260-B-01-03, United States Environmental Protection Agency (US-EPA), Washington, DC, August 2001.
- [152] *Polycyclic Aromatic Hydrocarbons (PAHs) Factsheet*, United States Environmental Protection Agency (US-EPA), Washington, DC, January 2008.
- [153] P. J. Valdez, M. C. Nelson, H. Y. Wang, X. N. Lin, and P. E. Savage, "Hydrothermal liquefaction of nannochloropsis sp.: Systematic study of process variables and analysis of the product fractions," *Biomass & Bioenergy*, vol. 46, pp. 317–331, 2012.
- [154] A. D. Henderson, M. Z. Hauschild, D. van de Meent, M. A. J. Huijbregts, H. F. Larsen, M. Margni, T. E. McKone, J. Payet, R. K. Rosenbaum, and O. Jolliet, "Usetox fate and ecotoxicity factors for comparative assessment of toxic emissions in life cycle analysis: sensitivity to key chemical properties," *International Journal of Life Cycle Assessment*, vol. 16, pp. 701–709, 2011.
- [155] R. K. Rosenbaum, M. A. J. Huijbregts, A. D. Henderson, M. Margni, T. E. McKone, D. van de Meent, M. Z. Hauschild, S. Shaked, D. S. Li, L. S. Gold, and O. Jolliet, "Usetox human exposure and toxicity factors for comparative assessment of toxic emissions in life cycle analysis: sensitivity to key chemical properties," *International Journal of Life Cycle Assessment*, vol. 16, pp. 710–727, 2011.
- [156] M. Z. Hauschild, M. Huijbregts, O. Jolliet, M. MacLeod, M. Margni, D. van de Meent, R. K. Rosenbaum, and T. E. McKone, "Building a model based on

scientific consensus for life cycle impact assessment of chemicals: The search for harmony and parsimony," *Environmental Science & Technology*, vol. 42, pp. 7032–7037, 2008.

- [157] R. K. Rosenbaum, T. M. Bachmann, L. S. Gold, M. A. J. Huijbregts, O. Jolliet, R. Juraske, A. Koehler, H. F. Larsen, M. MacLeod, M. Margni, T. E. McKone, J. Payet, M. Schuhmacher, D. van de Meent, and M. Z. Hauschild, "Usetox—the unep-setac toxicity model: recommended characterisation factors for human toxicity and freshwater ecotoxicity in life cycle impact assessment," *International Journal of Life Cycle Assessment*, vol. 13, pp. 532–546, 2008.
- [158] M. A. J. Huijbregts, L. J. A. Rombouts, A. M. J. Ragas, and D. van de Meent, "Human-toxicological effect and damage factors of carcinogenic and noncarcinogenic chemicals for life cycle impact assessment," *Integr Environ Assess Manag*, vol. 1, no. 3, pp. 181–244, Jul 2005.
- [159] D. Busch, A. Stark, C. I. Kammann, and B. Glaser, "Genotoxic and phytotoxic risk assessment of fresh and treated hydrochar from hydrothermal carbonization compared to biochar from pyrolysis," *Ecotoxicol Environ Saf*, vol. 97, pp. 59–66, Nov 2013.
- [160] P. Oleszczuk, I. Joško, and M. Kuśmierz, "Biochar properties regarding to contaminants content and ecotoxicological assessment," *J Hazard Mater*, vol. 260, pp. 375–82, Sep 2013.